National Defence / Défense nationale

MUTUAL COUPLING BETWEEN RECTANGULAR DIELECTRIC RESONATOR ANTENNA ELEMENTS

by

Bruce Henry, Aldo Petosa, Yahia M.M. Antar
and Gilbert A. Morin

Preceding Pages Blank

DEFENCE RESEARCH ESTABLISHMENT OTTAWA
REPORT NO. 1333

Canada

May 1998
Ottawa

National Defence / Défense nationale

MUTUAL COUPLING BETWEEN RECTANGULAR DIELECTRIC RESONATOR ANTENNA ELEMENTS

by

Bruce Henry
Department of National Defence

and

Aldo Petosa
Communications Research Center

and

Yahia M.M. Antar
Royal Military College of Canada

and

Gilbert A. Morin
Milsatcom Group
Space System & Technology Section

DEFENCE RESEARCH ESTABLISHMENT OTTAWA
REPORT NO. 1333

PROJECT
5CA12

May 1998
Ottawa

ABSTRACT

Dielectric resonator antennas (DRAs) have been suggested as potentially efficient antennas for use in Personal Communication Systems, Global Positioning Systems and wireless computer networks. They offer several advantages, such as high efficiency, large bandwidth, low profile, small size, ease of fabrication, and low production cost.

This paper examines characteristics of rectangular DRAs, both as individual radiating elements as well as elements in array environments. Numerical methods are used to obtain detailed information with respect to the resonant frequency, bandwidth, scattering parameters, input impedance, field structures and radiation patterns on which DRA design is based. This obtained information is then used to help in understanding and quantizing the interaction between elements in close proximity, i.e. mutual coupling. This coupling analysis provides important information for the array design process, as well as the necessary information required to positively exploit these coupling characteristics.

The simulation software provides data that very closely matches both experimentation and theoretical models. Mutual coupling measurements indicate that, beyond a spacing of $\lambda/2$, there is very little mutual interaction. However, this mutual coupling was exploited at lesser distances with parasitically coupled dielectric elements. These elements were used to create novel single-feed multi-element antennas with increased bandwidth and enhanced radiation patterns.

RÉSUMÉ

Les antennes à résonateur diélectrique (ARDs) ont été suggérées comme antennes efficaces dans les Services de communication personnelle (SCP), le Système de positionnement global (SPG), et les réseaux d'ordinateurs sans fil. Elles offrent plusieurs avantages, tel une haute efficacité, une grande largeur de bande, un profil réduit, de petites dimensions, une fabrication simple, et un coût réduit.

Ce rapport examine les caractéristiques des ARDs rectangulaires, tant du point de vue d'un élément isolé que d'un élément à l'intérieur d'une antenne réseau à commande de phase. Des méthodes numériques ont été utilisées pour obtenir de l'information détaillée sur la fréquence de résonance, la bande passante, les paramètres de dispersion S, l'impédance d'entrée, la structure des champs électromagnétiques, ainsi que les diagrammes de rayonnement. Cette information a permi de comprendre de façon quantitative le couplage mutuel entre les éléments d'ARDs. L'analyse du couplage a permis, non seulement, de comprendre l'interaction d'éléments dans un réseau, mais aussi d'exploiter le couplage de façon productive dans différents types d'antennes.

Le logiciel de simulation utilisé a fourni des données en concordance avec les modèles théoriques et les mesures de laboratoire. Les mesures de couplage mutuel indiquent qu'au delà d'un espacement d'une demi longueur d'onde entre les éléments, il y a très peu d'interaction mutuelle. Cependant, ce couplage a été exploité à des distances moindres avec de nouvelles antennes comprenant un élément actif couplé de façon parasite à plusieurs autres éléments. Comparé à une antenne à un seul élément, ces antennes multi-éléments possèdent une bande passante accrue et un diagramme de rayonnement à gain plus élevé.

EXECUTIVE SUMMARY

Personal Communication Systems such as cellular telephones, Global Positioning Systems, Local Multiport Communication Systems and wireless computer networks operating in the millimeter frequency band are becoming increasingly popular and are driving current research activities. Highly efficient, low profile antennas with large bandwidth capabilities are desired. Printed circuit technology has gained interest in this area due to its small size, conformal possibilities, ease of fabrication, and low production cost. The Microstrip Patch Antenna has seen the most research and practical design however, the Dielectric Resonator Antenna is also demonstrating a great deal of potential.

Rectangular shaped DRAs have been shown to achieve favourable results, however this shape is not easy to analyze, as there is no rigorous closed form solution. Analytical approximations have been used to form the modified dielectric model with mixed magnetic walls however, the capability limits of this model have been exhausted. Complete electromagnetic characterization is possible through the use of numerical methods, which have seen increased interest with the introduction of high speed, high power computers that are able to handle the vast amount of computations required.

The rectangular DRA is examined using the TLM numerical method in analyzing the characteristics of this specific shape. The specific parameters examined are input impedance, resonant frequency, bandwidth, scattering parameters, field structures, mutual coupling, and radiation patterns. Computer simulation results are compared with experimental data to help quantify the accuracy of TLM approximations.

The results show that the generally accepted magnetic dipole field structure is present and behaves as predicted. The simulation software provides data, which very closely match both experimentation and the theoretical models. Mutual coupling measurements indicate that beyond a spacing of $\lambda/2$ there is very little mutual interaction. This mutual coupling was exploited at lesser distances, with parasitically coupled elements used to create novel single feed multi-element antennas with altered resonant frequencies, increased bandwidth and enhanced radiation patterns, when compared to a single element.

TABLE OF CONTENTS

LIST OF FIGURES

ABBREVIATIONS

Ω	Ohms (Impedance)
ε	Dielectric permittivity
λ	wavelength
CAD	Computer Aided Design
CPU	Central Processing Unit
CRC	Communication Research Center
DRA	Dielectric Resonator Antenna
DREO	Defence Research Establishment Ottawa
DWM	Dielectric Waveguide Model
E	Electric Field
FEM	Finite Element Method
FDTD	Finite Difference Time Domain
GHz	Giga Hertz
H	Magnetic Field
HMCS	Her Majesty's Canadian Ship
L_L	Line - Line
M_M	MSDRA - MSDRA
M_L	MSDRA - Line
MHz	Mega Hertz
MIC	Microwave Integrated Circuit
MMW	Mixed Magnetic Walls
MOM	Method of Moments
MPA	Microstrip Patch Antenna
MSDRA	Multi-Segment Dielectric Resonator Antenna
MWGM	Modified WaveGuide Model
PEC	Perfect Electric Conductor
PMC	Perfect Magnetic Conductor
RMC	Royal Military College of Canada
TLM	Transmission Line Matrix
TM	Transverse Magnetic
TE	Transverse Electric

CHAPTER 1

1.1 Introduction

The proliferation of radio frequency devices that require unique frequency spectrum allocation as well as greater bandwidth has resulted in severe overcrowding of the electromagnetic spectrum. Personal Communication Systems, Global Positioning Systems, wireless computer networks and Local Multiport Communication Systems operating in the millimeter frequency band are becoming increasing popular and are driving current research activities into providing highly efficient, low profile antennas with relatively large bandwidth capabilities.

Printed circuit technology, and its application to antennas, has gained interest in this area due to its small size, conformal possibilities, ease of fabrication, and low production cost. Two techniques have been considered, the microstrip patch antenna, which has seen widespread use, and the dielectric resonator antenna, whose analysis and use is still in its infancy.

1.2 Microstrip Patch Antenna (MPA)

MPAs, consisting of an arbitrarily shaped metal layer mounted on a dielectric substrate backed by a metallic ground plane (Figure 1) have dominated antenna development since the 1970's and are widely in use today.

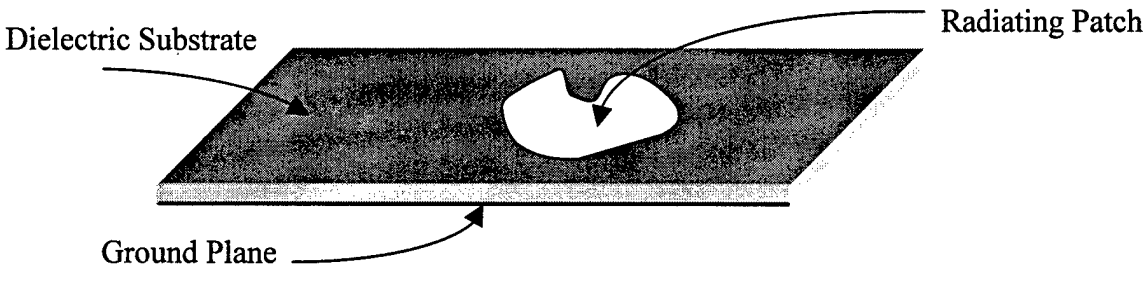

Figure 1: Microstrip Patch Antenna

The MPA is popular since it provides lightweight and conformal antennas for millimetre wave applications. They have the general advantages exhibited by MIC technology, including low cost, ease of integration with active components, as well as variety of design. There are, however, some well-known detrimental factors. These include; wide beamwidth, narrow bandwidth (1 to 6 %), surface wave excitation (which distorts the radiation pattern and increases power loss), and conductor losses (which increase dramatically with frequency). Attempts to reduce these negative effects have proven to achieve limited success, since an increase in one aspect usually comes with degradation in another factor. The largest detrimental effect at millimetre wave frequencies continues to be conductor losses, thus reduced radiation efficiency.

1.3 Dielectric Resonator Antenna (DRA)

DRAs are fabricated from low-loss dielectric material of various shapes, (figure 2) whose resonant frequencies are functions of the size, shape and permittivity of the material. The specifics of the theoretical electromagnetic characteristics are included in Chapter 2.

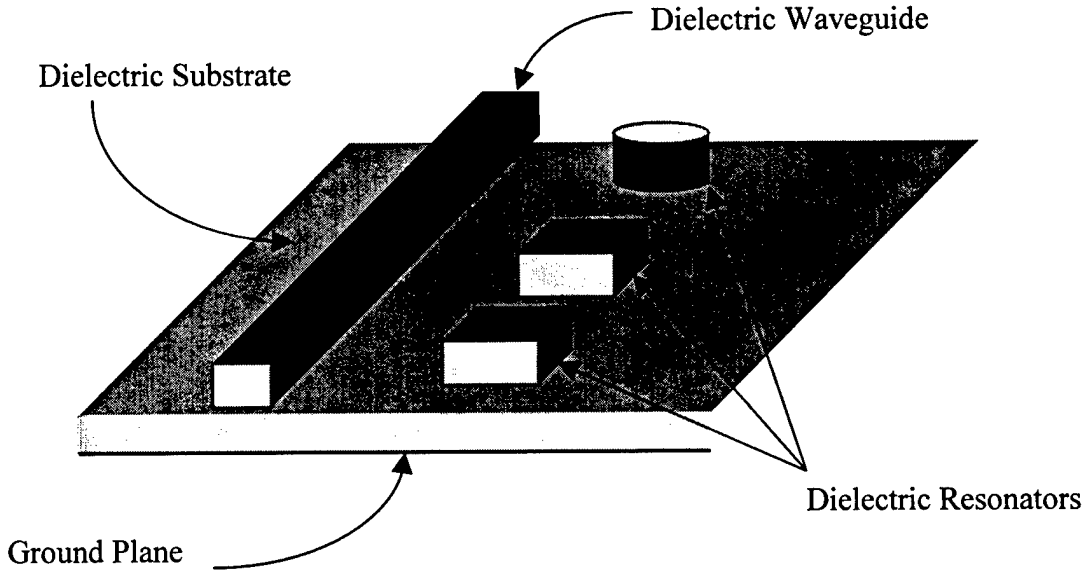

Figure 2: Dielectric Resonator Applications

The fact that dielectric resonators radiate energy was proven by Richtmyer in 1939, [Rich 39] however practical application did not take place until the 1960's [O&B 62] when suitable dielectric compounds became available. Initially there was very little interest in applying this technology at the then popular frequencies of interest. First antennas were in the MHz ranges, which were adequately handled with inefficient, bulky but simple rigid structures. Dielectric resonators were first popular as filter elements devices in microwave circuits [P&R 81] with the first reported use as a radiating element not until the early 1980's when the smaller size potential, and higher frequency applications boosted the research into the dielectric resonator antenna. [B&G 81]

The DRA offers several advantages over the MPA. Since the DRA is a non-metallic structure, there are no conduction or surface wave losses, therefore their radiation efficiency is very high (>98%) [M,I&C 94a]. They can be simply coupled to many types of transmission lines and are easily integrated with MICs. Various resonator shapes are possible (rectangular, cylindrical, hemispherical), and a variety of feed mechanisms can be utilised (probe, aperture, microstripline), which allows for great flexibility in the design process. The bandwidth is inherently larger than MPAs, and is controllable through the permittivity. Permittivity can also be used to control the relative size of the resonator, since the wavelength within the dielectric is shorter than that in free space. High permittivity allows for smaller resonators, while low permittivity results in higher bandwidth. Also, rectangular DRAs are not as susceptible to tolerance errors as are MPAs, especially at higher frequencies. [Mong 88]

DRA design requires accurate information on the basic antenna parameters, such as resonant frequency, bandwidth, radiation pattern and internal field distribution. To date, however, there is no comprehensive work published in order to assist in the design process. For the most part, much of the current work is hampered by the requirement for approximation methods, since many of the structures cannot be analytically determined through closed form solutions. Literature surveys indicate that considerable preliminary work is being conducted in determining resonant frequencies and Q factors, however since the intended application was usually as circuit elements there was little

consideration given to radiated fields or mode structures. This report provides some insight into these areas.

1.4 DRA Arrays

Single antenna elements are not always used in practical applications. Frequently, a number of elements will be combined into an array in order to enhance the radiation characteristics. However, certain aspects of this grouping of elements may have severe adverse effects on the radiation pattern. Antennas placed in close proximity to one another interact and change the current and field distributions that would normally be present in isolated elements. This phenomenon is known as mutual coupling, and its effect is usually detrimental. Large mutual coupling levels can degrade sidelobe levels, alter main beam shapes, or change the input impedance, which causes a mismatch at the antenna, and possibly causes array blindness. [Poza 83] On the other hand, if mutual coupling effects are known, they can be exploited to produce beneficial results. They can be used in creating a desired amplitude taper across an array, improving bandwidth, achieving dual frequency operation or adjusting the radiation pattern characteristics.

1.5 Present Research Activities

DRA technology is increasingly being employed in efforts to achieve more effective and less costly antenna systems. The Royal Military College of Canada, in collaboration with The Communications Research Center (CRC) initiated and are in the forefront of these research activities. A literature review indicates that the present state of the art is somewhat specific in nature, as research is being experimentally conducted on a trial and error basis, with specific frequencies and desired radiation patterns implicitly specified. Arrays have been designed without considering the effects of mutual coupling, with subsequent analysis showing discrepancies between measured results and common array prediction techniques. This indicates that elements in array environments behave differently than when isolated. Thus, there is a need to better understand this element interaction. There are no existing complete generic design equations, nor are there any

accurate analyses of the overall properties of the rectangular DRA. Analytical approximations have been developed [A&F 96], with the dielectric waveguide model (DWM) [M&I 97], and the modified waveguide model (MWGM) [Mong 92] being commonly used. The accuracy of these methods is good ($\approx$ 5 %) in determining return loss characteristics, however information about the field structures cannot be exactly determined. In order to progress the analysis of the rectangular DRA structure, more accurate and complete analysis techniques must be found. Some numerical modeling efforts using the FDTD and TLM methods have been pursued to provide this analysis, however most of these software packages are being developed in-house and are therefore very specific to certain needs, and are proprietary in nature. Although versatile and accurate, the development of these codes is often a cumbersome exercise, which could take considerable time and effort. Recently, a new extensive simulation package was developed by KCC Ltd. Micro-Stripes™, simulates 3-D structures using the numerical TLM method. [KCC 97] This package could be potentially useful in the analysis and characteristics of the rectangular DRA.

1.6 Objectives

The objective of this report is to numerically and experimentally investigate the rectangular DRA structure. This research is intended to accomplish two goals; the first is to study rectangular DRAs using numerical techniques, and compare simulation results with experimentation in order to evaluate the accuracy of the approximations used in characterizing the internal and external field structures. Numerical methods are used to obtain detailed information with respect to the resonant frequency, bandwidth, scattering parameters, input impedance, field structures and radiation patterns on which DRA design is based.

Secondly, the obtained information is used to understand and quantize the interaction between elements in close proximity, i.e. mutual coupling. This coupling analysis provides important information for the array design process, as well as the necessary information required to positively exploit these coupling characteristics.

1.7 Methodology

The organizational steps of the report are outlined as follows:

1.7.1 Single DRA Elements

a) A numerical analysis of antenna structures containing single DRA elements is conducted using Micro-Stripes ™, which is a software simulation package that provides three-dimensional electromagnetic analysis of arbitrary geometries utilising the Transmission Line Modelling (TLM) method. [KCC 97]. Results obtained from the simulations of rectangular DRAs fed by various coupling techniques are compared with published experimental results as well as to other simulation packages in order to confirm the validity of this software for the specific DRA structure used.

b) Once Micro-Stripes ™ is validated, the field structures of the dominant mode of the rectangular DRA at resonance are analyzed. Results are compared to the approximation methods currently being used. [O&B 62] [Mong 92]. As well, design information such as input impedance and coupling techniques are investigated to better classify their characteristics. Simple DRA structures as well as more complex structures such as Multi-Segment DRAs (MSDRAs) are examined to determine their electromagnetic characteristics and to confirm the validity of both the simulations as well as the approximation methods.

1.7.2 Array of several DRA Elements

a) Mutual Coupling effects are numerically analyzed and are also compared to experimental data. The initial analysis of mutual coupling focuses on determining relative coupling levels of two direct microstrip fed MSDRAs oriented individually in the E and H planes, as functions of spacing.

b) Mutual coupling is further exploited, in that a single microstrip fed MSDRA is parasitically coupled to several other DRAs in various configurations. The goal is to increase bandwidth, allow for dual or multiple frequency operation, or to alter the radiation pattern directivity in a desired squint direction, based on the total number and physical location of the DRAs.

1.8 Organization

This chapter has laid out the background as to why this research was carried out and outlined the expected goals and methodology. Chapter 2 details the theoretical analysis of dielectric resonators and focuses much of the information on the rectangular structure, as this is the configuration of interest for this research. The current analysis of this structure is through approximation methods, since there is no closed form analytical solution. It is for this reason that the simulations carried out in this report were closely examined for validity and accuracy. Chapter 3 outlines the more popular numerical modelling methods available and the specific TLM method is explained. Micro-Stripes™, a commercial software package using the TLM method, is explained in detail and validation experiments are carried out to confirm the accuracy of the specific application. Comparisons are made between simulated data and previously published experimentation and theoretical approximations. The fundamental mode of the rectangular DRA is closely examined through various element configurations and coupling methods. Both resonant frequency and radiation pattern comparisons are carried out. Chapter 4 deals with mutual coupling between two single elements oriented in the E and H planes respectively in order to quantify the levels of mutual coupling achieved. Experiments to examine mutual coupling are conducted and results are compared with simulations. The concept of coupling is examined further in Chapter 5. Parasitic coupling is applied to several configurations of DRA elements to determine the feasibility in producing broadband or multiple frequency band operation, or to achieve a desired radiation pattern. Finally, Chapter 6 presents concluding remarks as well as recommendations for further research.

CHAPTER 2

2.1 Theoretical Considerations

2.1.1 Dielectric Resonators

As previously mentioned, dielectric resonators have been known to radiate since the work conducted by Richtmyer in 1939, however, this information was not pursued as the then current application for dielectrics was as energy storage devices and not as radiators. In the 1980's, antenna research was being conducted at microwave and millimeter wave frequencies. Conductor losses limited the use of metallic structures, therefore research into dielectric materials became popular. Dielectric resonator antennas could be made smaller than their microstrip patch counterparts through the use of high permittivity materials, since the guided wavelength is inversely proportional to the permittivity of the dielectric material, $\lambda_{dielectric} = \lambda_o / \sqrt{\varepsilon_r}$.

2.1.1.1 Field Modes

All resonators have a series of resonant modes or field structures, which are determined by their electrical characteristics and the boundary conditions. Van Bladel [VanB 75a][VanB 75b] investigated DRAs of arbitrary shapes with very high permittivities, and concluded that there were two field modes in which the DRA could be classified. These are the confined and non-confined modes. The classification criteria are that at all interface boundaries the following conditions are met;

a. $E \bullet n = 0$, and

b. $n \times H = 0$.

Condition a., where E denotes the electric field intensity and n denotes the normal to the surface of the resonator, is satisfied for both confined and non-confined modes. This condition states that there is no electric field intensity normal to the boundary. Condition b., where H denotes the magnetic field intensity, is only satisfied for confined modes. This condition indicates that the magnetic field is normal to the boundary. He further states that the lowest order non-confined and confined modes act like magnetic and electric dipoles respectively. Finally, he has shown that confined modes can only be supported by dielectric elements exhibiting axial-symmetric properties.

These modes or field structures are often classified as H and E modes. The H modes, corresponding to the non-confined case above, have a large magnetic field perpendicular to the interface, with the lowest order mode resembling a magnetic dipole in field structure, as shown in Figure 3. The E modes, confined, do not have this large magnetic field and the lowest order mode resembles an electric dipole. Okaya and Barash first classified the H mode to belong to the transverse magnetic (TM) family and the E modes to the transverse electric (TE) family [O&B 62], however, later work by Yee [Yee 65] used the opposite notation. This second convention continues to be used today, with two or three subscripts to identify the specific mode order. The subscripts denote the field variations in the appropriate orthogonal component, dependent on the co-ordinate system used, spherical, cylindrical or rectangular. Cylindrical and spherical DRAs support both TE and TM modes, which, when combined together form an additional hybrid family of modes. These degenerate modes, in which two modes exhibit the same resonant frequency, and thus interact with each other, result in a lack of mode purity.

Various configurations of dielectric materials have been investigated [M&B 94], with the theoretical emphasis placed on cylindrical or hemispherical shapes. The reason for this is the ability to generate closed form analytical solutions for axial-symmetric shapes. Since the focus of this report is rectangular DRAs, the remainder of the discussion and analysis will deal solely with this geometric shape.

2.1.2 Rectangular DRAs

From Van Bladel's work, the rectangular DRA, since it is not axial-symmetric, can only support non-confined (TE or H) modes and the radiation pattern of the lowest order mode should resemble that produced by a magnetic dipole. Also, since the rectangular shape cannot be defined as a body of revolution, a closed form solution is impossible. Thus, approximation methods are required in order to analyze the rectangular DRA. Considerable experimental work has been conducted on rectangular DRAs, which further corroborate these finding [M,A,K,I&C 90], [Mong 92], [I,C,M,B&A 93], [K,R,A&I 95]. Although the rectangular DRA cannot be completely characterized analytically, they have an advantage over DRAs of other shapes. Since the rectangular DRA has three independent dimensions (vice two for cylindrical and one for spherical), the choice of these dimensions can be made to ensure that the resonant frequencies of the modes are separated apart from one another. Thus, rectangular DRAs need not suffer from the mode degeneracy problem exhibited by other shapes. TE^{x}, TE^{y}, and TE^{z} modes are possible. If we assume that the smallest dimension of the rectangular DRA is in the z direction, then the dominant lowest order mode will be the TE^{z}_{111} mode (a,b > d). Figure 3a provides the co-ordinate convention used in this report while Figure 3b and 3c show the directions associated with electric and magnetic fields expected of a rectangular DRA operating at this TE^{z}_{111} mode. The far field radiation pattern is shown in Figure 4, which is approximated as that of a magnetic dipole, with the E plane cut corresponding to the xy plane (E_θ) and the H plane cut to the zy plane (E_ϕ).

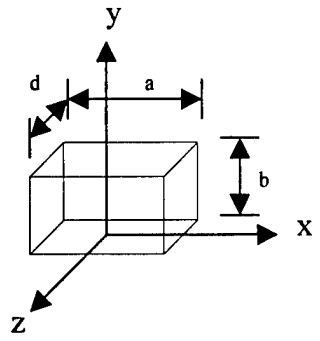

a) Co-ordinate System Convention

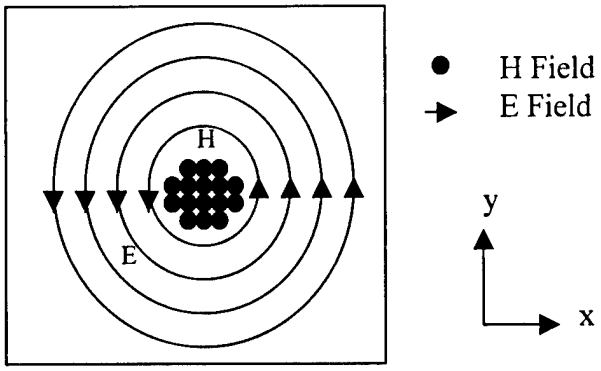

b) Field Distribution (Front View)

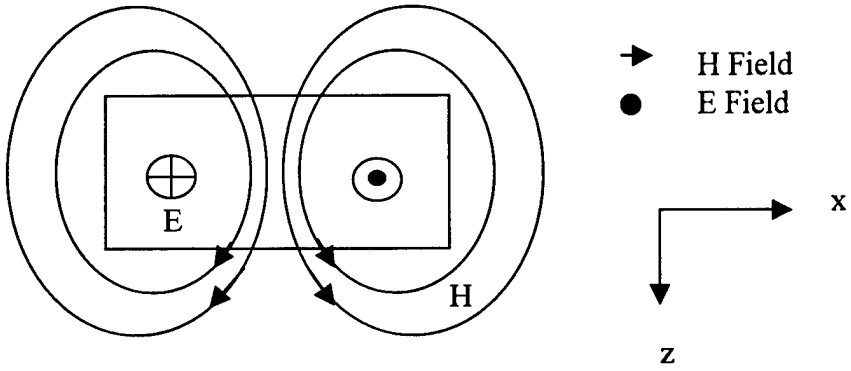

c) Field Distribution (Top View)

Figure 3: Co-ordinate Convention and Internal E and H Field Distribution

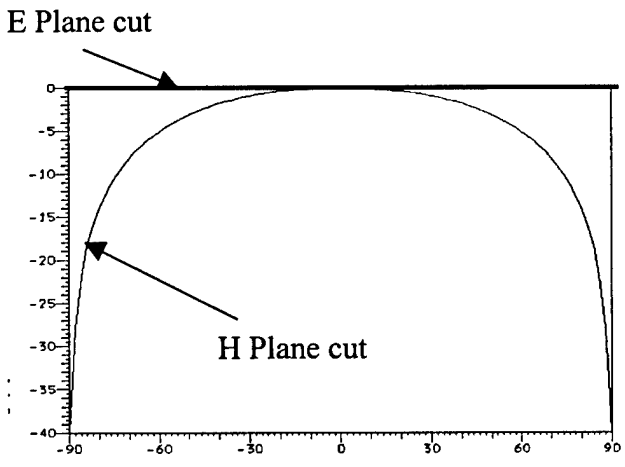

Figure 4: Far Field Radiation Pattern Cuts

2.2 Field Analysis Approximation Methods

The approximation techniques widely used are the magnetic wall model developed by Okaya and Barash [O&B 62], and the Dielectric Waveguide Model (DWM) introduced by Marcatili [Marc 69]. Okaya and Barash used first and second order approximations on a rectangular resonator with three unique dimensions. The first order approximations considered that all six surfaces of the DRA corresponded to a perfect magnetic conductor (PMC) boundary condition. This method provided relatively accurate results for higher order modes only. The second order approximation considered the four sidewalls as PMC and the two opposite end walls as imperfect boundaries. The continuity of the magnetic field was used to perform tangential field matching across the interface. This second order approximation was necessary in order to achieve accurate predictions for the lowest-order modes. This second order approximation is now commonly referred to as the mixed magnetic wall model (MMW). [O&B 69]

Marcatili approached his analysis from an integrated optics point of view. He applied some simplifying assumptions to solve for Maxwell's equations, and assumed continuous E and H fields across the four dielectric wall interfaces. He then used tangential field matching with exponentially decaying fields exterior to the dielectric boundary. This model forms the basis of the Dielectric Waveguide Model (DWM). [Marc 69].

Several authors [L,K,T&C 80] [Mong 92] [I,M,A,B&C 93a] [I,M,A,B&C 93b] [M,I,C&R 94] and [M&B 94] compared the DWM method with experimental results and achieved accuracy within 3% of experimentation.

2.3 Dielectric Waveguide Model with Mixed Magnetic Walls

This method uses results from Okaya and Barash's magnetic wall model as well as Marcatili's dielectric waveguide model. This method, like most others, assumes an isolated structure, while the resonators being investigated in this report are located over a ground plane. In order to account for this ground or image plane, image theory will be used to replace the resonator and ground plane with an isolated resonator of twice the height. [Balan 82] In order for us to accurately apply this image theory, the modes of interest in an isolated resonator must meet the criteria of a perfect electrical conductor (PEC) boundary condition along the line of symmetry at the center of the isolated resonator. In other words, if a plane of symmetry does not exist at the center of the isolated resonator, the model will not be valid. Examine, for example, figure 3, and note that the E field is normal to the x-axis along the centreline of the DRA. This condition must be met for the image theory to be valid.

An isolated rectangular DRA, shown in figure 5, is first considered to be an infinite dielectric waveguide with perfect magnetic walls, i.e. open circuit boundaries. In this way, the modal transverse fields can be determined from the DWM. The guide is then truncated in the z direction, to form the rectangular resonator, and the dominant transverse field components matched at this boundary with exponentially decaying fields external to the structure. Marcatili's approximation is used for this external field matching. The fields of the TE^{z}_{111} mode can be determined from the following:

$$H_z = A\cos(k_x x)\cos(k_y y)\cos(k_z z) \tag{2.3.1}$$

$$E_z = 0 \tag{2.3.2}$$

Where A is an arbitrary constant, and k_x, k_y, and k_z are the wave numbers inside the dielectric in the x, y and z directions respectively.

The other field components can be determined from these fields. As well, the wave numbers satisfy the following separation equation;

$$k_x^2+k_y^2+k_z^2 = \varepsilon_r k_o^2 \qquad (2.3.3)$$

ε_r is the dielectric constant of the DRA and k_o is the free space wavenumber corresponding to the resonant frequency.

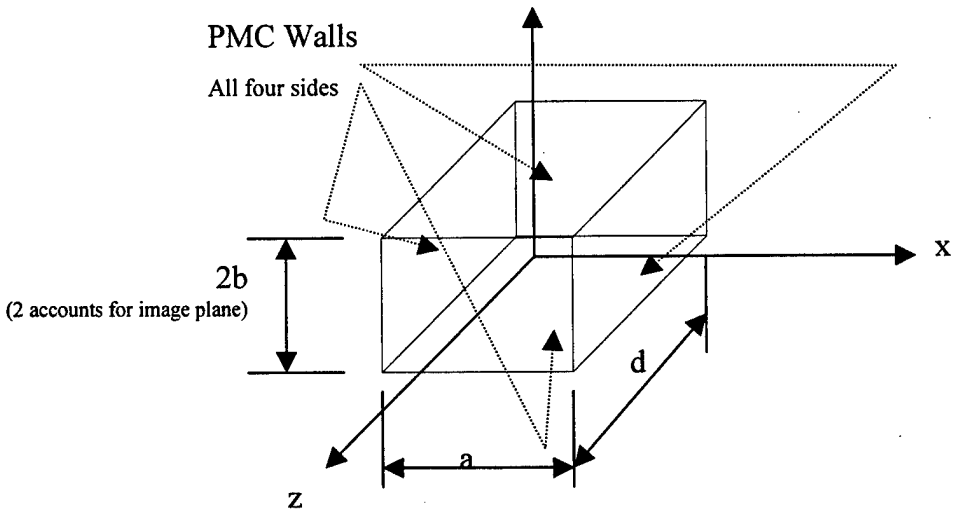

Figure 5: Isolated DRA represented as a section of infinite dielectric waveguide

The PMC approximations can now be used to find the transverse wave numbers;

$$k_x = \pi/a \qquad (2.3.4)$$

$$k_y = \pi/2b \qquad (2.3.5)$$

Truncating the waveguide at $z = \pm\ d/2$ with imperfect magnetic walls (IMW) will provide a standing wave, at resonance. Using the IMW allows the fields to propagate through the walls where they will decay exponentially. Thus, Marcatili's approximation can be applied to solve for k_z:

$$k_z d = \pi - 2\tan^{-1}(k_z/k_{zo}) \qquad (2.3.6)$$

Where $$k_{zo} = \sqrt{((\varepsilon_r - 1)k_o^2 - k_z^2)} \qquad (2.3.7)$$

Therefore, for a given resonant frequency f_o, and resonator parameters ε_r, a and b, the wavenumber k_z can be determined. The dimension d can then be determined. Conversely, for a given resonator with parameters ε_r and dimensions a, b, and d, the resonant frequency can be determined in an iterative manner.

These equations provide the basic analytical approximations, based on the model chosen, to characterize the electromagnetic properties of the rectangular DRA. Although not directly used in the remainder of this specific research, this analytical model is important in order to provide comparison values with which to validate the numerical simulation results. A more detailed and rigorous development of this model can be found in [Mong 92] or [M&I 97].

2.4 Field Excitation Techniques

The rectangular DRA can be excited in a variety of methods, with the most practical method being aperture coupling, while probes and microstripline are also capable of exciting the DRA. In the analysis presented in this report, two coupling methods have been explored. The aperture excitation method as well as the direct microstripline connection was examined. Both methods provide the proper excitation needed to elicit the magnetic dipole response from the DRA, however there are some precautions for each method.

2.4.1 Aperture (Slot) Coupling

Microstrip fed aperture coupled patch antennas were first used in 1985 [Poza 85]. This technique has seen extensive use for both microstrip patch and DRA applications, with the advantages of easy integration with MIC components and effective use at high frequencies making this method very popular. A simple representation of this technique is shown in Figure 6. Typically, a radiating element is placed over the slot, however this has been omitted to better visualize the coupling technique.

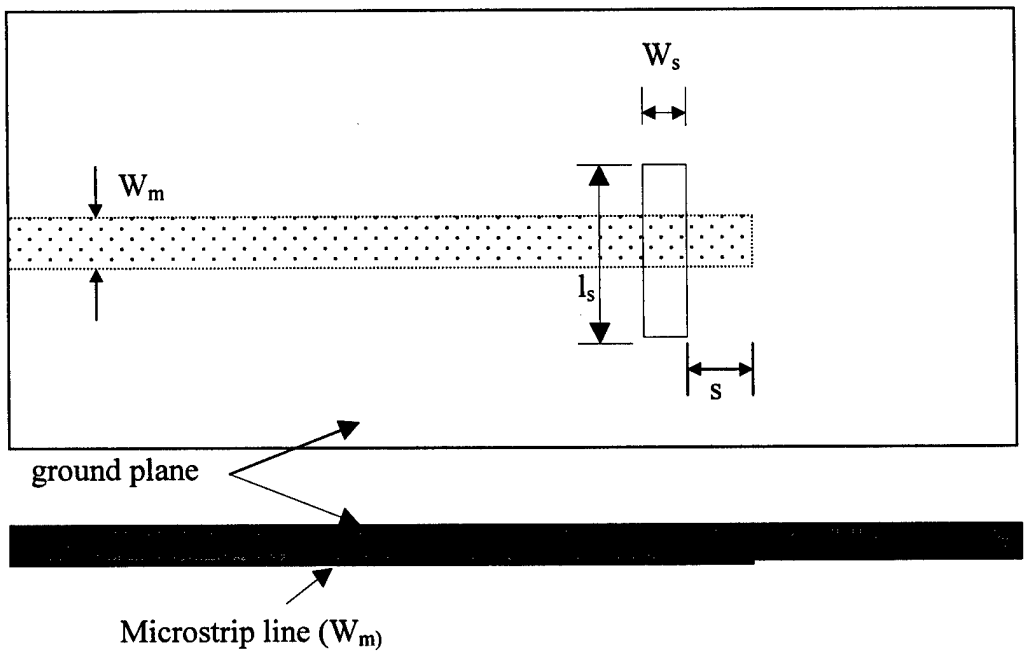

Figure 6: Aperture Coupling Technique

The width of the microstrip line (W_m) is chosen to provide a matched input impedance, normally 50 Ω. Additionally, the slot width (W_s) and slot length (l_s) are chosen to provide a matched impedance to the radiating structure. The stub length (s) is selected such that the slot is located at a maxima in the magnetic field strength created by the microstrip line. One advantage of this method of energy coupling, especially for DRAs, is that the coupling mechanism can be considered to represent a magnetic dipole, as shown in Figure 7. [Poza 90]

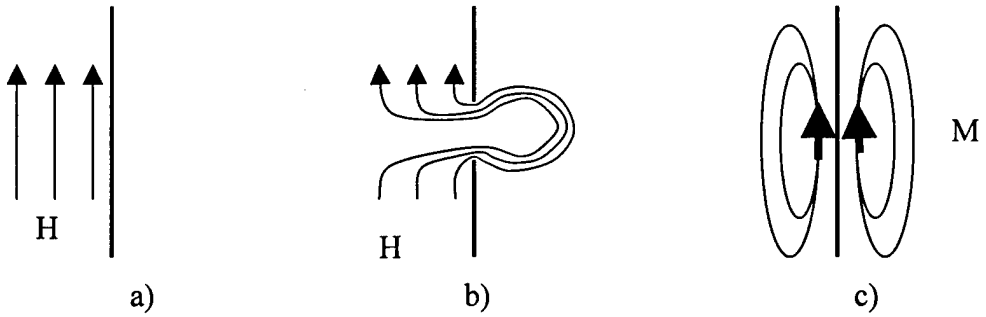

Figure 7: Magnetic Dipole Representation of Aperture

Figure 7a shows magnetic field lines tangential to the metallic wall. In the presence of an aperture, they fringe through the conducting wall (7b), An equivalent magnetic dipole moment (7c) exhibits the same field lines as that produced by the aperture, therefore it can be concluded that the aperture can be replaced by this magnetic dipole. These approximations are valid for small apertures only.

Another significant advantage that aperture coupling provides is the isolation between feed network components and radiating elements. The ground plane effectively isolates any fields or currents inherent in the feed network from affecting the radiation pattern of the radiating element. Conversely, the ground plane isolates the radiation effects from altering the characteristics of the feed network. There is also more real estate on which to locate the feed network, phase shifters or any other circuitry without the worry of radiation interference effects, since the two functions are located on opposite sides of the ground plane.

One disadvantage of this coupling mechanism is the requirement to etch both sides of the substrate, one side for the slot in the ground plane, and the second side for the feed network. This multilayer requirement is not overly onerous, however the second step is required.

2.4.2 Direct Microstrip Coupling

Simpler than aperture coupling, direct microstrip coupling is designed such that the radiating element, in this case the rectangular DRA, is placed directly onto the microstrip line. This method is attractive due to the low cost and ease of fabrication, since there is no requirement to etch two sides of the substrate, as required in the aperture coupling technique. Microstrip fed arrays of rectangular DRAs have been used to provide Taylor amplitude distributions as well as broadband impedance performance. [P,M,I&W 95],[P,I,C&R 96]

One disadvantage of direct microstrip coupling is that there is usually very little energy coupled to the resonator, thus a great number of radiators are required in order to provide sufficient radiation energy. The amount of coupling is dependent on the permittivity of the dielectric, the higher the permittivity the higher the coupling. However, the higher the permittivity, the lower the bandwidth.

To overcome some of these detrimental factors, a novel multi-segment DRA (MSDRA) has been developed. [P,M,S,I,&R 96]. Figure 8 shows the general configuration, which consists of a DRA of low permittivity stacked on top of one (or several) of higher permittivity. The low permittivity DRA provides the wide band radiation characteristics, while the high permittivity DRA insert(s) provide greater coupling to the microstrip line. A key point to note is that the thickness of the high permittivity insert(s) must be chosen sufficiently small so that they do not radiate.

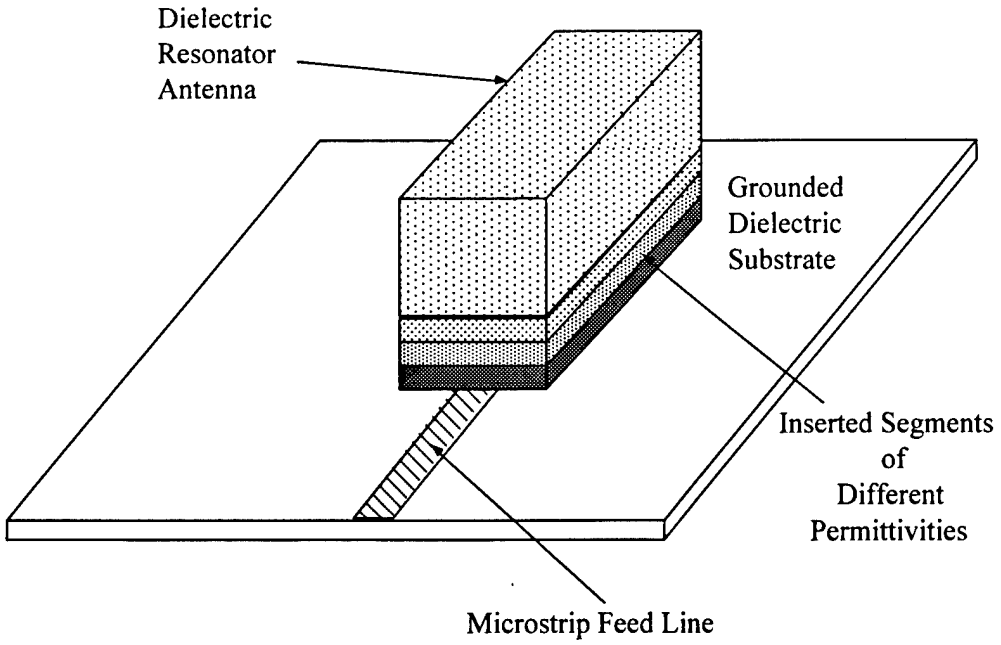

Figure 8: Multi-Segment DRA (MSDRA) geometry

The modified DWM model is used to predict resonant frequency, using the low permittivity DRA as the dimensional model. The effect of the insert will cause the actual resonant frequency to drop slightly with the frequency shift dependent on the thickness and permittivity of the insert. Therefore actual resonant frequency cannot be precisely determined until actual experimentation. Research is presently being conducted at CRC to introduce an effective dielectric permittivity, which takes in to account the combined permittivities of the DRA, inserts and substrate to better predict the resonant frequency of this novel element.

2.5 Radiating Mode Structures

As previously mentioned, the mode of interest for the rectangular DRA is the dominant TE_{111} mode. It is important in the design stage to ensure that the DRA dimensions are correctly chosen, to avoid degenerate modes, such that only this mode is excited at the desired frequency and that the coupling mechanisms are properly selected in order to excite that mode.

It has been stated already that the radiation pattern of this first order mode is said to resemble that of a magnetic dipole. Therefore, the expected pattern will resemble those shown in Figures 3 and 4. Second order modes have field patterns that resemble those due to quadrapoles, while for higher order modes multipole patterns are formed, which will be dependent on their mode indices.

2.6 Scattering Parameters

The characteristics of an antenna system, other than radiation pattern, can be determined experimentally through the use of a network analyzer, which measure the scattering [S] parameters. Generally, any network can be characterized through the use of these parameters which relate the voltage waves incident on the ports of the network to those reflected from the ports. A two port network is shown in Figure 9.

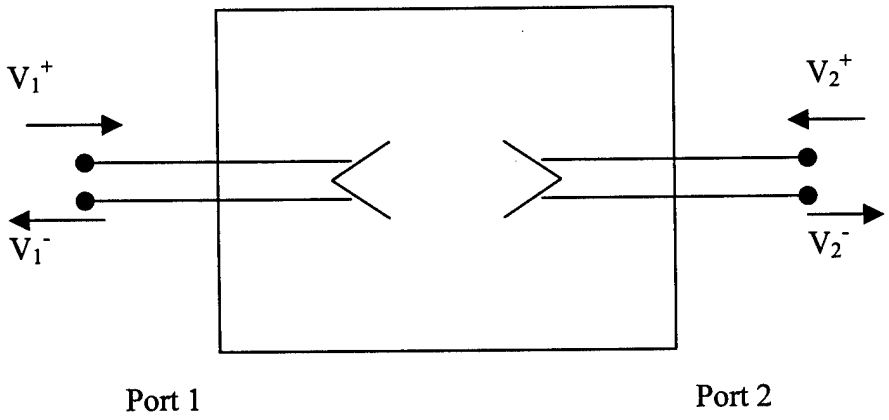

Figure 9: A Two Port Network for Scattering Parameter Determination

A specific element of the [S] matrix can be determined as

$$S_{ij} = V_i^-/V_j^+ \text{ given that } V_k^+ = 0 \text{ for } k \neq j$$

In words, this says that S_{ij} can be found by exciting port j with an incident wave V_j^+ and measuring the output V_i^- coming out of port i, with the remainder of the ports (if

more than two) match terminated in order to avoid reflections. Therefore S_{ii} is the reflection coefficient of port i, and S_{ij} is the transmission coefficient between ports i and j, when all other ports are match terminated.

The two-port antenna conceptual configuration shown in Figure 9 can thus be used to determine not only the reflection coefficient, S_{11}, and its associated characteristics, but also the transmission coefficient S_{21}. This second parameter will be used to determine mutual coupling levels, since this is a measure of the coupling interaction of the two antennas when the first antenna is excited, and the second antenna match terminated.

2.7 Mutual Coupling Considerations

Antenna elements located in close proximity to one another, as in the case of arrays, interact in a manner very different from when they are isolated from each other. This phenomena is known as mutual coupling, leading to the existence of mutual impedance, with the amount dependent primarily on:

a. mode configuration and radiation characteristics of each element,

b. relative spacing between elements, and

c. relative orientation between elements.

Large mutual coupling levels can degrade sidelobe levels, alter main beam shape, change elemental input impedances, and possibly cause array blindness. [Poza 83] Mutual coupling normally causes detrimental effects. However, it can be used to help create a desired amplitude taper across an array, or as will be further investigated in this report, can be used to create greater bandwidth and directional radiation characteristics.

Characterizing the effects of mutual coupling for DRAs has not been completely investigated to date. Until recently, DRs have been used strictly as circuit elements where their dominant characteristic was their ability to store energy. Thus the DR was normally "shielded", which resulted in minimal coupling to other elements. As well, since there are no closed form equations with which to analyze the electromagnetic fields of the isolated DRA, there are no equations or specific formulas to define the nature of mutual coupling.

2.8 Summary

Theoretical considerations, primarily with respect to the rectangular shape have been presented. The specific parameters of interest, and their effects on the resultant analysis are detailed. Mutual coupling is defined and explained. Due to the lack of closed form expressions for the particular rectangular shape, all research is through approximations, numerical modelling or experimentation. Chapter 3 outlines some of the various numerical modelling techniques available and details the method chosen for the theoretical investigation in this report.

CHAPTER 3

3.1 Numerical Methods

"Most Problems that can be solved formally (analytically) have been solved"

[P&H 69]

3.1.1 Overview

Numerical solutions became popular in the 1960's with the invention of high-speed digital computers. Today's modern technology has brought these methods more into the forefront, with some methods made more efficient, while others that originated in other disciplines are being applied to electromagnetic analysis. Until numerical methods became common, problems were solved through the classical separation of variables analytical method or through integral equation solutions. If these methods proved unwieldy, or closed form solutions were not possible, one of two outcomes was possible. The first was to make appropriate assumptions in order to bypass the gridlock, and the second was to halt any analytical analysis. The assumptions deemed adequate for previous low frequency applications do not meet the requirements of today's millimeter wave integrated circuits. The ability to tune or tweak the circuit characteristics after fabrication are virtually impossible, unlike that of the previous technology. This has increased the necessity of the computer-aided design (CAD) process, thus the reliance on these numerical methods.

Numerical solutions allow for the tedious, time consuming computations to be carried out by the computer. Accuracy, computer efficiency, memory requirements, analytical processing and versatility have been used as criteria to assess numerical method performances. The numerical computations are based on several well-known methods, as shown in Table 1, some of which will be briefly discussed in the following paragraphs.

Method	Storage Requirements	CPU Usage	Generality	Pre-processing Requirements
Transmission Line Matrix	Moderate to Large	Moderate to Large	Very Good	Small
Finite Element	Large	Moderate to Large	Very Good	Small
Finite Difference	Large	Large	Very Good	Nil
Method of Lines	Moderate	Small	Good	Moderate
Mode Matching	Moderate	Small to Moderate	Good	Moderate
Integral Equation	Small to Moderate	Small to Moderate	Good	Moderate
Spectral Domain	Small	Small	Marginal	Large

Table 1: Numerical Methods and their applicability [Itoh 89]

The first three methods from table 1 are useful in solving geometries with arbitrary shapes, while the remainders have applications in specific areas. The integral equation method, for example, is useful to solve DRA geometries exhibiting axial symmetric symmetry. The numerical method chosen for evaluating the electromagnetic characteristics in this report is the Transmission Line Method (TLM), which will be discussed in more detail. The TLM CAD simulation package, Micro-Stripes™, will be briefly explained, and some representative DRA examples presented for validation purposes.

3.1.2 Finite Difference Method

First developed in the 1920's by A. Thom under the title "method of Squares" it was used to solve hydrodynamic equations. Finite difference techniques are based on discretization approximations, which allow for the replacement of differential equations by finite difference equations, hence the name. These approximations relate the value of the dependent variable at a point in the solution region to the values at some neighbouring point. A finite difference solution process consists of dividing the solution region into a grid of nodes, and applying the approximations to each point in the grid. The differential equations are then solved subject to the boundary and/or initial conditions of the structure. The finite difference approximations are essentially numerical estimates of the derivatives. The finite difference time domain (FDTD) is a common technique that uses this method, approximating the differential equations in the time domain.

This method is well known to be the least analytical. Mathematical pre-processing is minimal, and the method can be applied to a wide variety of structures, even those with odd shapes. Numerical efficiency however, is not good. Open region problems truncated to a finite size can produce problems and mesh points must lie on boundary regions for accurate solutions.

3.1.3 Variational Methods

This method allows a problem of integrating a differential equation to be reduced to an equivalent variational problem. The variational problem finds a function that gives a minimum value for some integral. This method forms the basis for the Method of Moments (MOM) and Finite Element Method (FEM).

3.1.3.1 Method of Moments (MOM)

MOM is a method of weighted residuals applicable for solving both integral and differential equations. The procedure usually involves four steps.

1. The appropriate integral or differential equation is derived.
2. This equation is discretized into a matrix equation using basis (or expansions) functions and weighting (or testing) functions.
3. The matrix elements are evaluated.
4. The matrix equation is solved and the parameters of interest obtained.

This method owes its name to the process of taking moments by multiplying by appropriate weighting functions, and integrating. Its use has been successfully applied to a wide variety of EM problems.

3.1.3.2 Finite Element Method (FEM)

Finite element analysis consists of discretizing the solution region into a finite number of sub-regions or elements. Governing equations are then derived for a typical element. All elements in the solution region are assembled and the system of equations solved for. The finite difference and moment methods are conceptually simpler and easier to program than the finite element method, however the FEM is more powerful and versatile for handling complex geometries and inhomogeneous media. General-purpose computer programs can be created to solve a wide range of problems, due to the systematic nature of this method. Care must be taken at the truncation points when this method is applied to open region problems.

3.1.4 Method of Lines

This method solves three-dimensional problems by reducing the problem to a single dimension through the use of discretization in two of the three dimensions. Analytical solutions are then sought for the remaining dimension. Similar to the mode-

matching technique and the finite difference method, the biggest difference is the simplification in that all but one independent variables are discretized to obtain a system of ordinary differential equations.

3.1.5 Spectral Domain Approach

This is a Fourier-transformed version of the integral equation method, which is applied to microstrip or printed line structures. An efficient but restricted method, it can only handle well shaped structures that involve infinitely thin conductors.

3.1.6 Mode Matching Method

Typically applied to the problem of determining the scattering characteristics in a waveguide structure on both sides of any discontinuity, the fields on both sides of the discontinuity are expanded with respect to their various modes. Boundary conditions are applied along with the concept of field continuity in achieving the desired solution.

3.1.7 Transmission Line Method

This method is used for solving field problems using circuit equivalents. It is based on the equivalence between Maxwell's equations and the equations for voltages and currents on a mesh of continuous two-wire transmission lines. The main feature of this method is the simplicity of formulation and programming for a wide range of applications.

Originally proposed by Johns and Beurle in 1971 in order to analyze 2-D field problems [J&B 71], the model is based on Huygen's principle, which states that "each particle in any wave front acts as a new source of disturbance, sending out secondary waves combined to form a new wave front". [J&B 68] In 1975 Ahtarzad and Johns expanded the 2-D analysis to 3-D. [A&J 75] This increases the complexity, however not

the general procedure. Complexity is increased since the 3-D node consists of 12 transmission line sections while the 2-D node encompassed only 4 transmission lines.

Waves propagate on a mesh of transmission lines interconnected at nodal points spaced a distance Δl apart. At each node, the incident fields are redirected outward based on the impedance seen on the respective transmission lines. The disturbance then propagates outward, joining together to form a secondary wavefront as Huygen's theory stipulates. This procedure continues through the structure, repeating the process at each and every node.

3.1.7.1 Micro-Stripes ™

MicroStripes™ is a 3-D Electromagnetic Field Simulation package that provides three-dimensional analysis of arbitrary geometries utilizing the TLM method. This allows a full-wave analysis that takes into account all possible radiation losses, dielectric losses, surface waves, coupling mechanisms and arbitrary geometric structures. The method uses a volume meshing structure, which allows complete 3-D solutions to be developed for the fields and currents with respect to time, and at any user defined frequency [KCC 97]. This method is therefore considered ideal for solving multilayer coupling schemes as well as analysing radiation from 3-D structures such as the dielectric resonator antenna. The software is based on the Transmission Line Modelling Method (TLM) and provides results in both the time and frequency domains.

3.2 Validation of Simulation Software

Since closed form analytical methods for determining resonant frequencies and radiation characteristics are not available for the geometries used in this report, numerical simulations using Micro-Stripes™ will form the basis of the analysis.

The selection of a commercially available simulation package, instead of the rigorous development of the numerical method, was made for purposes of the insights to be gained as well as expediency. The desire in the research presented in this report was to examine and characterize the nature of the rectangular DRA, rather than devise a code with which to apply the TLM method. The physics of the simulation problem has already been solved for with the development of MicroStripes™; therefore, instead of re-inventing the wheel this tool was used to achieve the desired goal of analyzing the nature of element and field interactions within the specific structure.

The first step then in the analysis process will be to confirm that the results provided by this software agrees with actual measured results. Comparing results previously published, both experimental and modified DWM approximations, with the Micro-Stripes generated characteristics will help achieve this.

The chosen configuration for comparison purposes was provided by Mongia, Ittipiboon and Cuhaci, in their analysis of rectangular dielectric resonators fed through an aperture in the microstrip ground plane [M&I 97] and [M,I&C 94b]. These experimental results were selected as they provide comparisons of the DWM model with experimental data, as well as all dimensional data with which to build the geometric TLM model.

3.2.1 Resonant Frequency Validation

Figure 10 shows the geometry of the structure being analyzed. The DRA is shown centred over the slot, however in actual fact, it had to be offset in the z direction to varying degrees in order to provide an appropriate impedance match, thereby achieving critical coupling [K&L 88], [M&I 97]. The dimensions of the aperture and substrate are w_m = 0.6 mm, l = 6.1 mm, s = 3.1 mm, w_s = 3.1 mm, substrate thickness t = 0.635 mm and ε_{rs} =10.2. The geometric file used to simulate the DRA for Sample A is included in Annex A-3 as a representative example for the analysis.

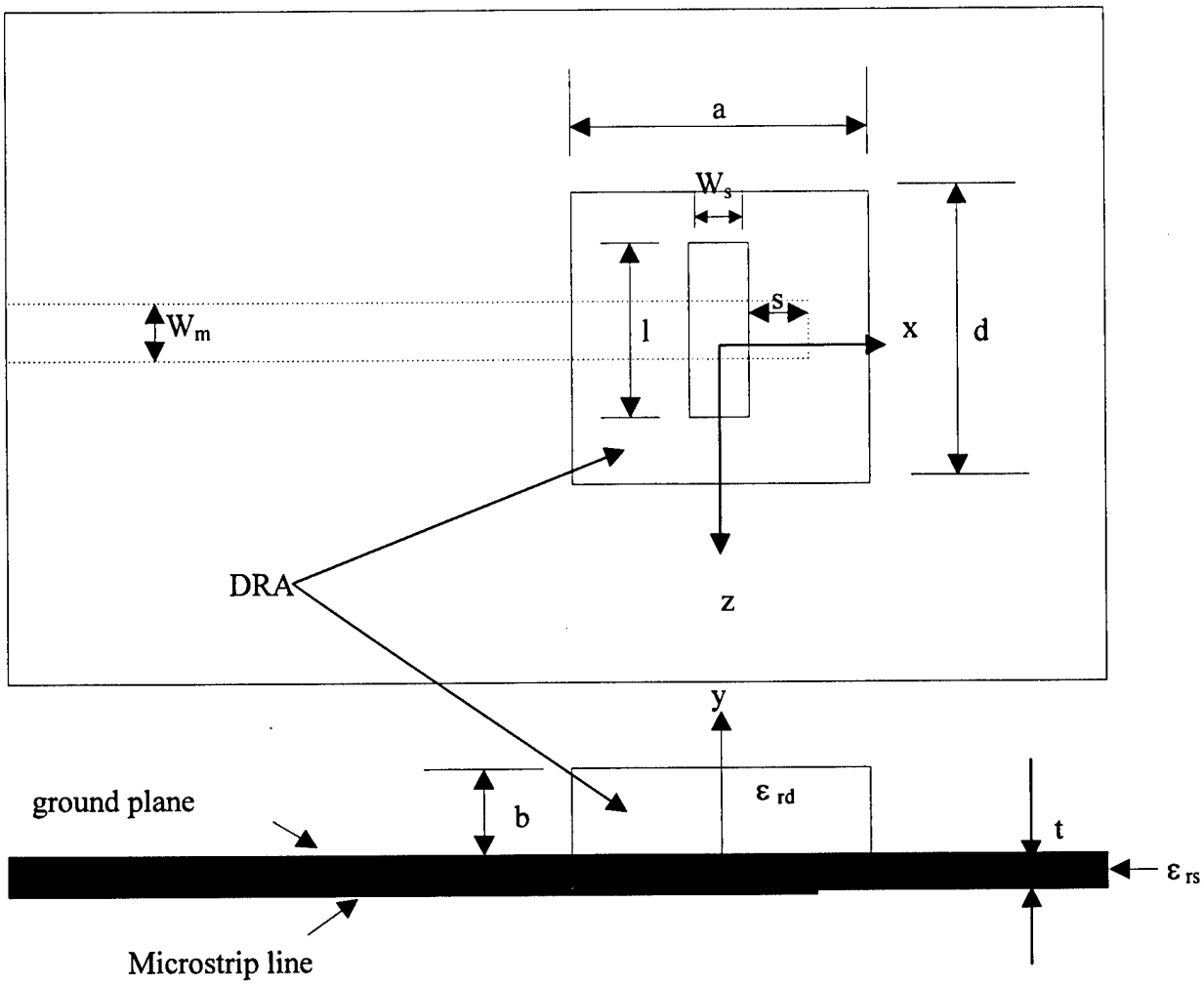

Figure 10: Top and side views of aperture coupled rectangular DRA.

Resonant frequencies for each of the DRAs were determined through examinations of the S_{11} simulations. Comparisons of simulations to experimentation, as well as the DWM calculations using equations (2.3.4) to (2.3.7) are provided in Table 2.

Sample	ε_r	a (mm)	b (mm)	d (mm)	Resonant Frequency (GHz)			% Error	
					Meas.	Micro-Stripes	DWM Model	Micro-Stripes	DWM Model
A	37.84	8.77	3.51	8.77	5.34	5.24	4.89	1.9	8.5
B	37.84	9.31	4.60	9.31	4.59	4.34	4.16	5.5	9.4
C	37.84	8.6	8.6	2.58	5.34	5.10	5.07	4.5	5.1
D	37.84	8.77	8.77	3.51	4.79	4.52	4.52	5.6	5.7
E	37.84	9.31	9.31	4.6	4.11	3.77	4.00	8.3	2.7
F	100	10	2	10	4.57	4.25	4.22	7.1	7.7
G	100	10	1	10	7.97	7.93	7.78	0.5	2.4
H	100	12.7	1	12.7	7.72	7.70	7.67	0.3	0.7
I	100	5	1	10	8.85	8.68	8.19	1.9	7.5
J	100	10	1	5	8.5	8.70	8.02	2.3	5.6

Table 2: Resonant Frequency Comparisons

The simulations conducted in this research were all carried out on a Compaq Deskpro PC (Intel P200 MHz CPU with 256 Mbytes of RAM). Simulations for the single element aperture coupled DRAs presented above required run times of approximately 5 hours, utilizing 95 – 100% of the CPU time during this period. RAM usage was in the order of 50 MBytes. Simulation times of up to 100 hours were required for some of the more complex antenna elements presented in chapters 4 and 5. Computing times could be shortened, if only the scattering parameters were desired, as the computation of the field characteristics were extremely time and memory intensive.

From these resonant frequency comparisons, it can be seen that there is close agreement between the simulated results and experimental data. Also, in almost all cases, the simulated data is closer to the experimental results than that achieved through the DWM calculations.

A second configuration was chosen to compare higher order mode simulation results with experimental work. [Loos 94] The configuration is again similar to that of Figure 10, however the dimensional data is different. Using an aperture coupled DRA

with ε_{rd} =10.8, and dimensions; a = 15 mm, b = 7.5 mm, and d = 3.1 mm, on a substrate with w_m = 0.6 mm, l = 6.1 mm, s = 2.2 mm, w_s = 1.2 mm, substrate thickness = 0.762 mm and ε_{rs} =10.2, the experimental modal frequencies obtained are 6.96 GHz, 12.1 GHz and 17.8 GHz. The simulation predicted resonant frequencies of 7.51 GHz, 13.24 GHz and 15.82 GHz, which are within 7.9, 9.4, and 12.5 % respectively. Agreement is good at the lowest order mode, which is of the most concern to this research. The higher order modes agree fairly well, however these modes were not closely explored, nor is there any specific knowledge as to the mode structures or behaviour at these frequencies.

3.2.2 Field Pattern Validation

The rectangular DRA is expected to exhibit radiation characteristics of a simple magnetic dipole. In order to confirm the simulation capabilities, the same dimensional data as the second configuration above was used and appropriate field patterns generated. Figure 11 shows the simulated far field pattern cuts, which closely resemble that expected of a magnetic dipole, and also accurately represent the patterns obtained by Loos.

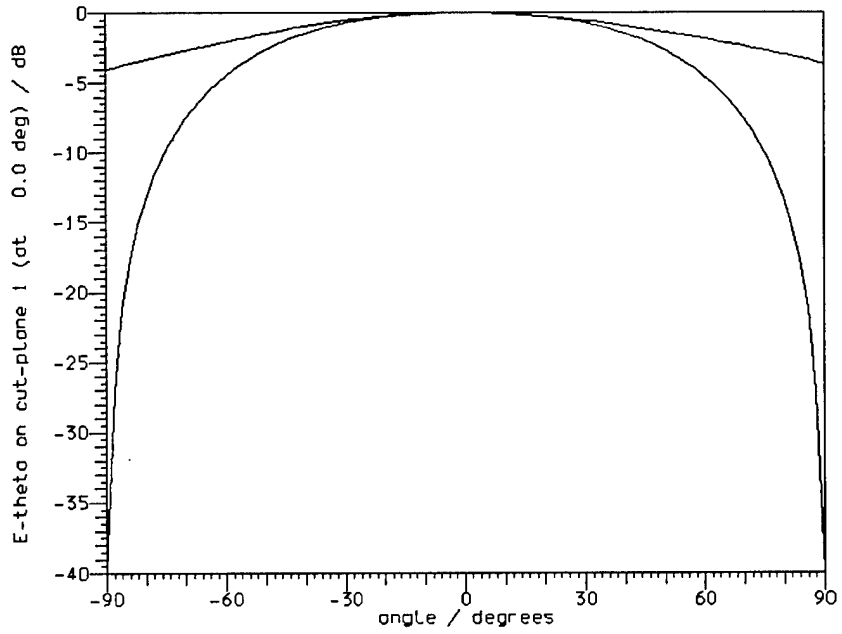

Figure 11: Far Field E and H Plane Radiation Patterns

Figure 12 is a representation of the internal field magnetic and electric field structures. This representation of the field direction and strength was obtained through the simulation of the physical structure. It is comforting to note that the field patterns determined agree with the structure expected of the magnetic dipole. This field distribution is further analyzed in the next section in order to better understand the relationships obtained.

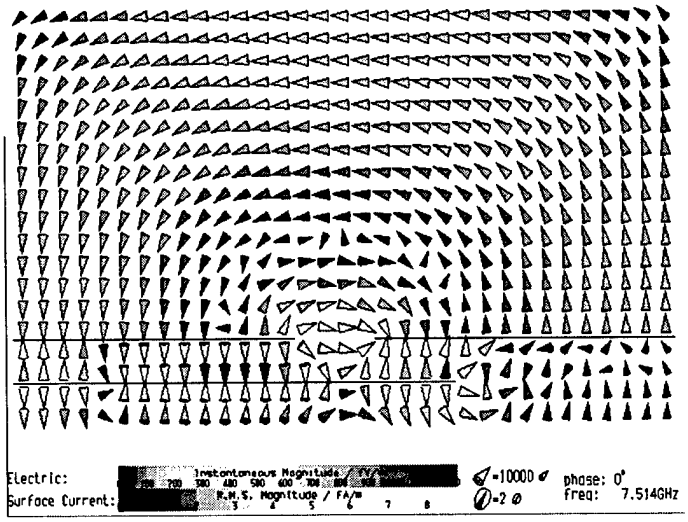

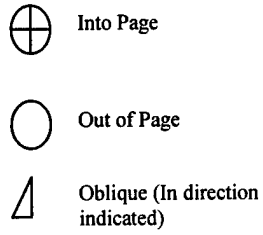

Figure 12a) Internal Electric Field Distribution

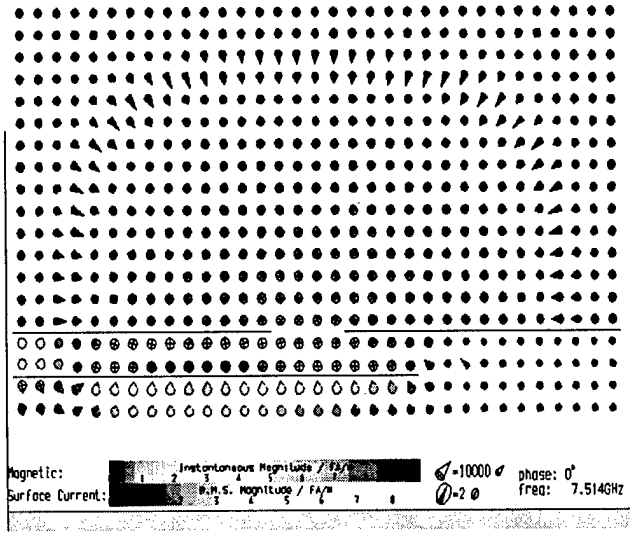

Figure 12b) Internal Magnetic Field Distribution

3.2.3 Effective Wavelength

Further, the internal magnetic field pattern was investigated closely to determine if the field pattern at resonance could provide any assistance in calculating the effective wavelength within the DRA. Figure 13 is a plot in the xy plane of the internal magnetic field intensity of the Loos model aperture coupled DRA at resonance. The intent here was to measure the width of the magnetic field, and work backward to determine if this corresponds to the expected effective wavelength within the dielectric structure. Recall, that the wavelength inside the dielectric is given by $\lambda_{dielectric} = \lambda_o / \sqrt{\varepsilon_r}$.

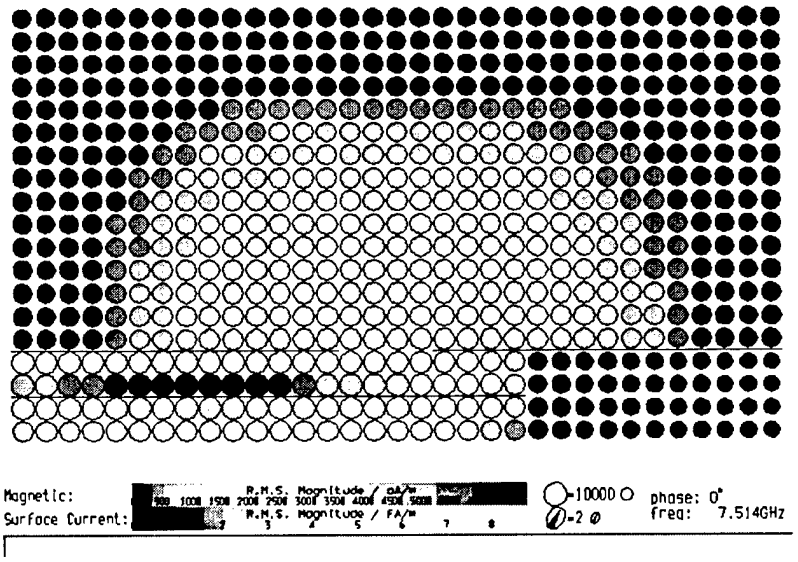

Figure 13: Internal Magnetic Field Intensity

Each circle within Figure 13 represents one cell of the mesh structure, which are all drawn the same size, regardless of the actual mesh sizes used. In order to determine the effective length, the cells within the chosen area must be correlated to their dimensional widths and these widths added together. This TLM method does not reproduce the actual physical structures in the field plots, therefore careful analysis is required to determine structure boundaries, cell sizes, and thus total dimensions.

The selection of the edge of the magnetic field boundary was difficult to decipher graphically, but by examining the entire shape and selecting the cell at which there was little or no colour change beyond it made the best selection. This method led to results which fairly closely matched the expected half wavelength. The outcome of this observation is that the internal fields of an isolated element are well behaved and that the TLM simulations provide a very good model with which to conduct full field analysis. Although the selection of the magnetic field edge may seem somewhat arbitrary, close agreement was obtained throughout the different DRA shapes examined.

Additional work was conducted on this premise of smaller effective dimensions [A,C,S,H&K 98] with comparisons made between the conventional dielectric waveguide model, the TLM simulations and a newly introduced modified waveguide model (MWGM). This new MWGM which proposes effective dimensions to be used in the equations of the DWM achieves results closer than that of the DWM, however, not quite as good as the computer simulations. This method calculates dimensions that are smaller than the true dimensions, and are permittivity dependent. The advantage of the MWGM however is that the computation time is in the order of minutes instead of hours for the TLM. The TLM results however, show the internal field structure, as presented in Figure 13, which allows for a visual representation and thus effective length determination. Exact values are not presented for these comparisons, nor is further analysis of the internal field structure. Time constraints left this for future work.

3.2.3 MSDRA Validation

A final validation of the simulation capabilities is conducted on a direct microstrip coupled MSDRA, since this geometry will be the focus of a major part of the work in this report. The geometry shown in Figure 8 was simulated using the following dimensional data:

DRA; $\varepsilon_{rd} = 10$, a = 7.875 mm, b = 3.175 mm, d = 1.9 mm,

Insert; $\varepsilon_{rd} = 20$, a = 7.875 mm , b = 0.635mm , d = 1.9 mm,

Microstrip and substrate; $w_m = 1.9$ mm, $\varepsilon_{rs} = 3$, h =0.762 mm .

The return loss of the simulated structure is compared to experimental results in Figure 14. Also included for comparison purposes are plots obtained from an FDTD analysis as well as a second TLM analysis [P,S,S,I&C 98].

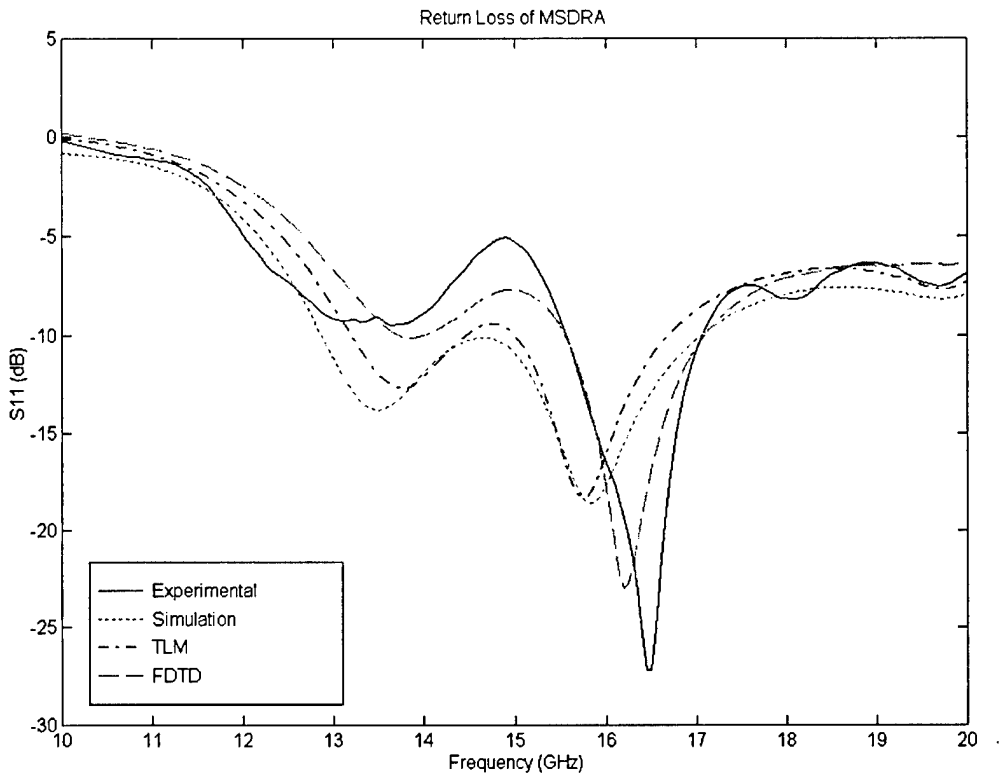

Figure 14: Return Loss Comparisons for MSDRA

The return loss characteristics agree very well with experimental data as well as with the other simulation techniques. All three simulation methods predict a lower resonant frequency than experimentally determined. Knowing this fact in advance will help the designer in the initial choice of dimensions, where designs for a slightly higher frequency than required can be made. Conversely, if exact frequency selection is not a priority, this downward shift is not significant.

3.3 Summary

The above analysis of the Micro-Stripes simulation process using a variety of DRA structures, although not exhaustive, confirms the validity of the approximation methods and also confirms the accuracy of the simulation technique. The return loss characteristics indicate the resonant frequency and impedance bandwidth are also closely matched, with the resonant frequency predicted within 5 % and usually much closer than that. The predictions of the higher order modes are less closely matched, although this is a limited comparison with only one case examined.

In general, field patterns are predicted with very close agreement to both theoretical approximations and experimental results. The results of this field pattern comparison, although general in nature, help confirm the existence of the expected modal structure. Good agreement is achieved in determining the effective wavelength and thus effective permittivity or resonant frequency.

These findings, with respect to single radiating elements, provide additional confidence in the accuracy of the approximation techniques widely used, as well as the capabilities of the simulation software. The close agreement achieved in these comparisons set the stage for continued analysis into the electromagnetic characteristics of elements when placed in close proximity, ie mutual coupling considerations.

CHAPTER 4

4.1 Mutual Coupling Analysis

DRAs have been previously investigated as isolated elements with little consideration given to determining their coupling interrelationships in array environments. This is due to the inability to form closed form equations with which to develop analytical solutions, the same reason that the electromagnetic characteristics are not fully known. Therefore numerical simulations will be performed and compared to experimental data in order to provide some insight into these coupling characteristics.

[Loos 94] and [L&A 94] did some related earlier experimental investigation into mutual coupling. While they examined aperture coupled DRA elements in their investigation, the same general steps are continued in this report using direct microstrip coupled MSDRAs. Two independently fed dielectric elements were positioned on a substrate over a ground plane at sequentially larger distances and the scattering parameters determined. Loos started at the largest spacing distance and cut out the middle section of the ground plane to achieve the desired spacing, using copper tape to join the two elements' ground planes. The experimental data for the results presented here were obtained using both elements attached to the same ground plane, which required 20 unique test pieces to be fabricated, as opposed to his single apparatus joined by copper tape. Errors could result during the fabrication of individual test pieces, however, it is expected that the level of error was less than that experienced by Loos with his non-continuous ground plane. Simulations of the experimental test pieces were carried out, as were other spacing values in order to compare results and obtain a smooth spacing distance curve.

4.2 Experimental Configuration

Figure 15 outlines the dimensional data of the test pieces. Throughout both the experimental analysis and the simulations, all dimensions were maintained constant with the exception of the spacing (S) between elements. The spacings used are summarized in Table 3.

	ε_r	x (mm)	y (mm)	z (mm)
DRA	10	7.875	3.175	1.9
Insert	40	7.875	0.635	1.9
Substrate	3	na	0.762	na

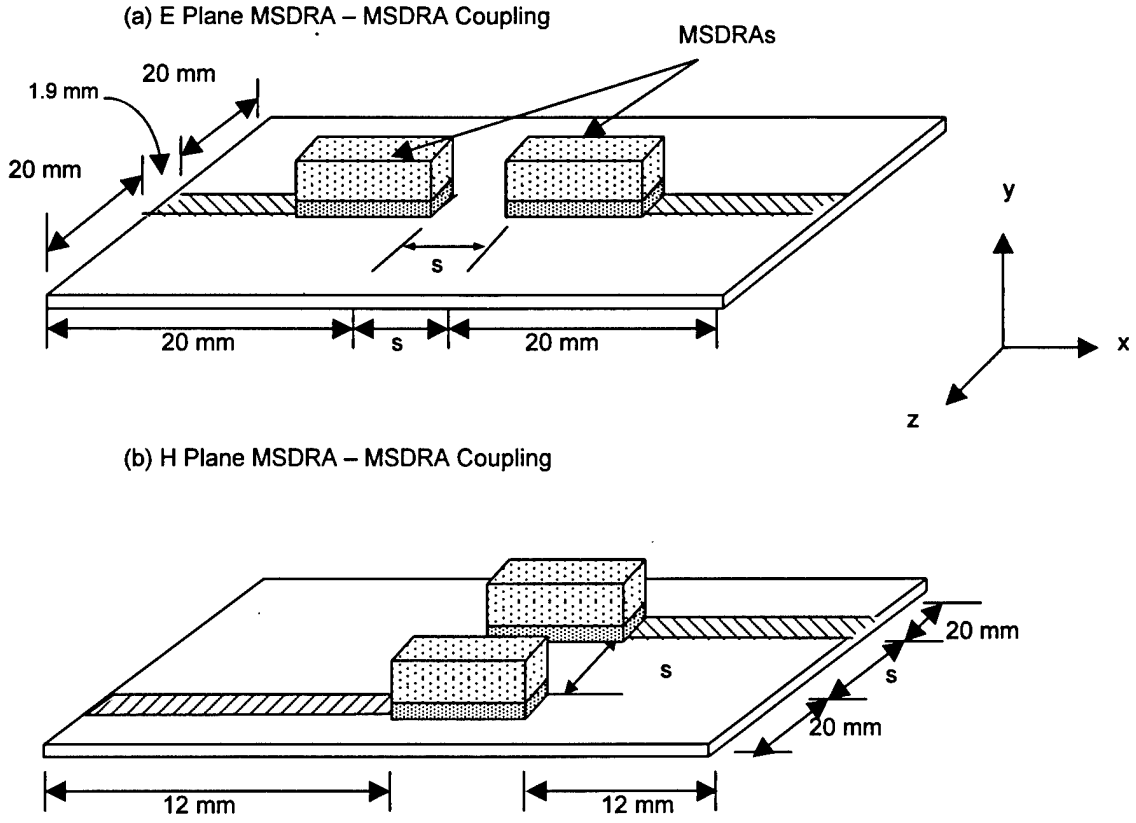

Figure 15: Experimental Design Layout; MSDRA – MSDRA Coupling

The direct microstrip coupling mechanism was chosen to excite the DRA for two reasons. Firstly, since Loos had provided a qualitative experimental assessment of mutual coupling between DRAs that were excited through aperture feeds, experimental data was readily available with which to compare coupling with respect to feed arrangements. Secondly, direct microstrip feed mechanisms are being experimentally investigated for large planar rectangular arrays [P,L,I&C 97]. Therefore, this already available information could be beneficial and would have a direct application in such investigations.

The characteristics to be compared in this analysis are the return loss, S_{11}, and the coupling, S_{21}. The specific configurations examined are coupling between:

a. DRAs on top of each microstrip line, as shown in Figure 15
b. one DRA on top of one microstrip line and the second strip line, as shown in Figure 16, and
c. the microstrip feed lines themselves, as shown in Figure 17.

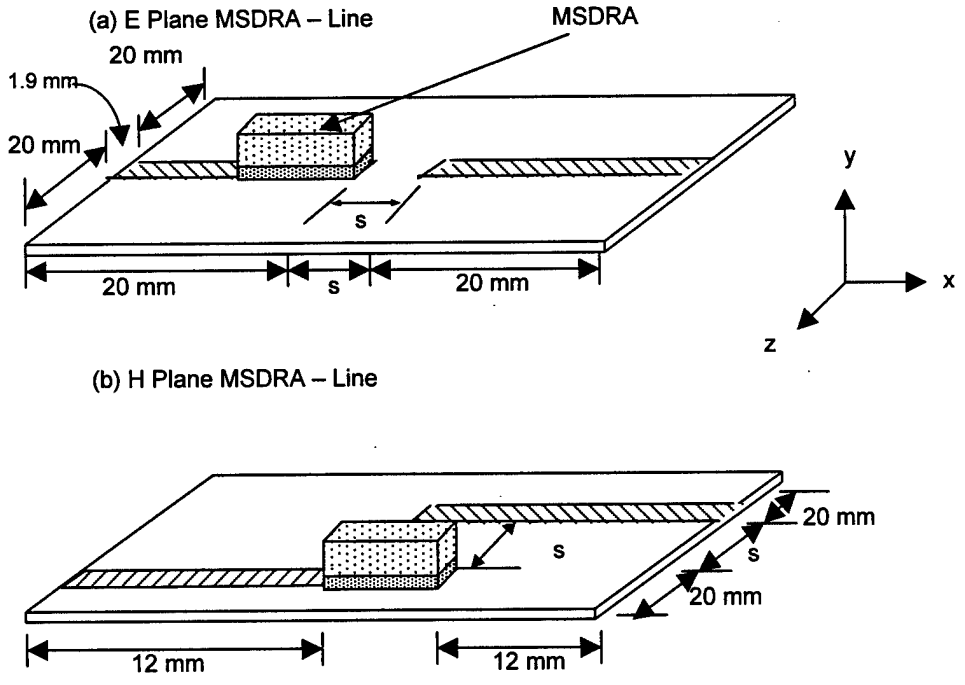

Figure 16: Experimental Design Layout; MSDRA – Line Coupling

(a) E Plane Line – Line Coupling

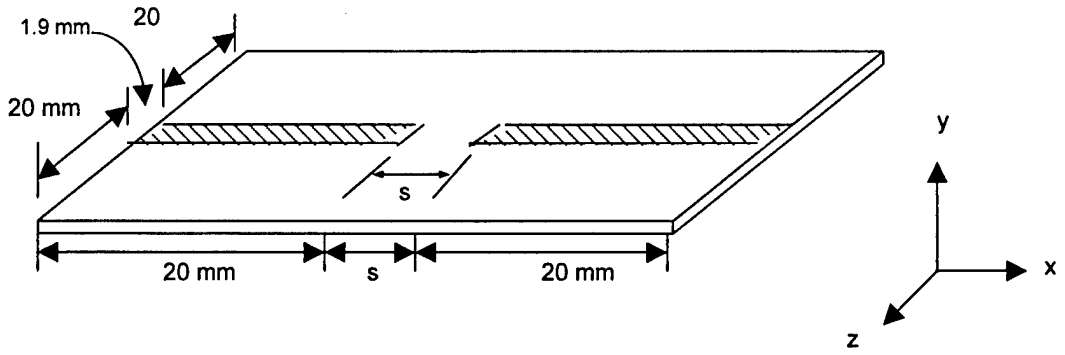

(b) H Plane Line – Line Coupling

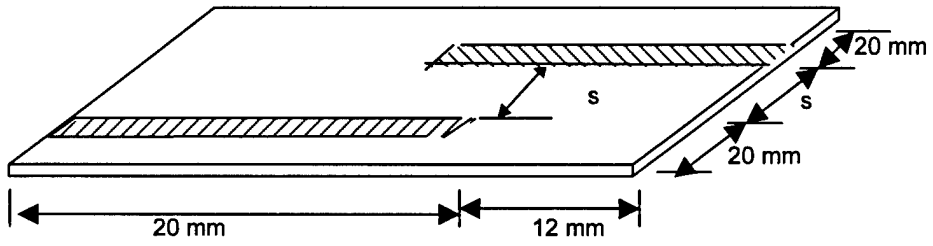

Figure 17: Experimental Design Layout; Line – Line Coupling

The DRAs were fastened to the microstrip using a very thin layer (≈0.02 mm) of non-conductive silicon epoxy with a dielectric constant of approximately 2 to 4. This may have an effect on the measurement results as will be explained in a later section on sources of error. The placing of the DRAs onto the line was not absolutely critical, however care was taken to ensure the DRA was aligned with the microstrip line to avoid any chance of exciting other modes [M&I 97]. The experimental process was to conduct configuration a. measurements first, and then remove one DRA to conduct configuration b. measurements before removing the second DRA and proceeding with measurements of configuration c. Considerable care was taken in ensuring accurate measurements were conducted, since the removal of the DRAs would result in the loss of configuration integrity, and could thus minimize results reproducibility.

4.3 Experimental Measurements

Experimental measurements were conducted at CRC. The scattering parameters were determined using a Wiltron 360 Network analyzer that had been calibrated up to the 50 ohm extension. The actual connectors on the antenna device were not included in the calibration process, and could introduce some errors as will be discussed in the section on sources of error. The experimental set-up to determine the scattering parameters is shown in Figure 18.

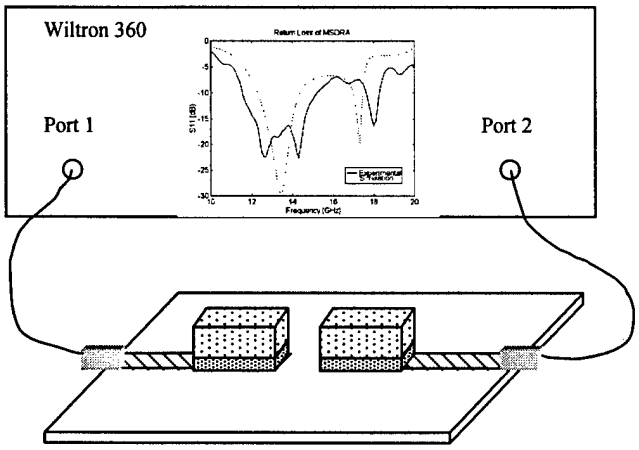

Figure 18: Experimental Configuration for Scattering Parameter Determination

4.4 Simulation Protocol

The simulations were conducted using the same spacings and configuration data as the experimental case. The Micro-Stripes geometric code for the E plane and H plane measurements at 5 mm is included in Annexes A-1 and A-2 as representative examples. Table 3 outlines the spacing distances for which simulation and experimentation were conducted. Line to Line (L_L) and MSDRA to Line (M_L) experimental measurement was ceased at a spacing of 50 mm due to the low coupling levels achieved. MSDRA to MSDRA (M_M) coupling measurements were continued to the largest spacing of 100

mm in order to provide enough data with which to predict any trends, as well as to ensure the coupling behaviour was consistent throughout these distances. The simulated measurements at 35, 65 and 80 mm were conducted to ensure enough data points were available to plot smooth prediction curves. Table 3 is applicable to both E and H plane coupling.

Spacing (S) mm	Experimentation			Simulation		
	L_L	M_L	M_M	L_L	M_L	M_M
1	Yes	Yes	Yes	Yes	Yes	Yes
2	Yes	Yes	Yes	Yes	Yes	Yes
3	Yes	Yes	Yes	Yes	Yes	Yes
4	Yes	Yes	Yes	Yes	Yes	Yes
5	Yes	Yes	Yes	Yes	Yes	Yes
10	Yes	Yes	Yes	Yes	Yes	Yes
15	Yes	Yes	Yes	Yes	Yes	Yes
20	Yes	Yes	Yes	Yes	Yes	Yes
35	No	No	No	Yes	Yes	Yes
50	Yes	Yes	Yes	Yes	Yes	Yes
65	No	No	No	No	No	Yes
80	No	No	No	No	No	Yes
100	No	No	Yes	No	No	Yes

Table 3: Spacing Distance (S) Sample Points

4.5 Simulation and Experimentation Comparisons

The raw data obtained was extensive, with the ability to make comparisons between experimentation and simulation possible for all aspects of the scattering parameters. The ultimate goal of this analysis was to determine the accuracy of the simulation results as well as to characterize the effect that the distance between elements caused in the MSDRA coupling levels. In order to satisfy the first goal, comparisons

between experimental and simulation results were made on a direct spacing-spacing basis. The second goal was satisfied through examining the cumulative data with the creation of coupling versus spacing distances as functions of frequency. The first step however, is to determine the response of a single element.

4.5.1 Single Microstrip Fed MSDRA

Return Loss results (S_{11}) for a single microstrip fed MSDRA were obtained both experimentally and through simulations in order to provide a strong confidence level that the coupling measurements would agree. The return loss response for a single microstrip fed MSDRA with the same dimensions as that used for the coupling experiment is shown in Figure 19. Since the simulations adequately match the experimental measurements, this should provide confidence in the coupling analysis to follow.

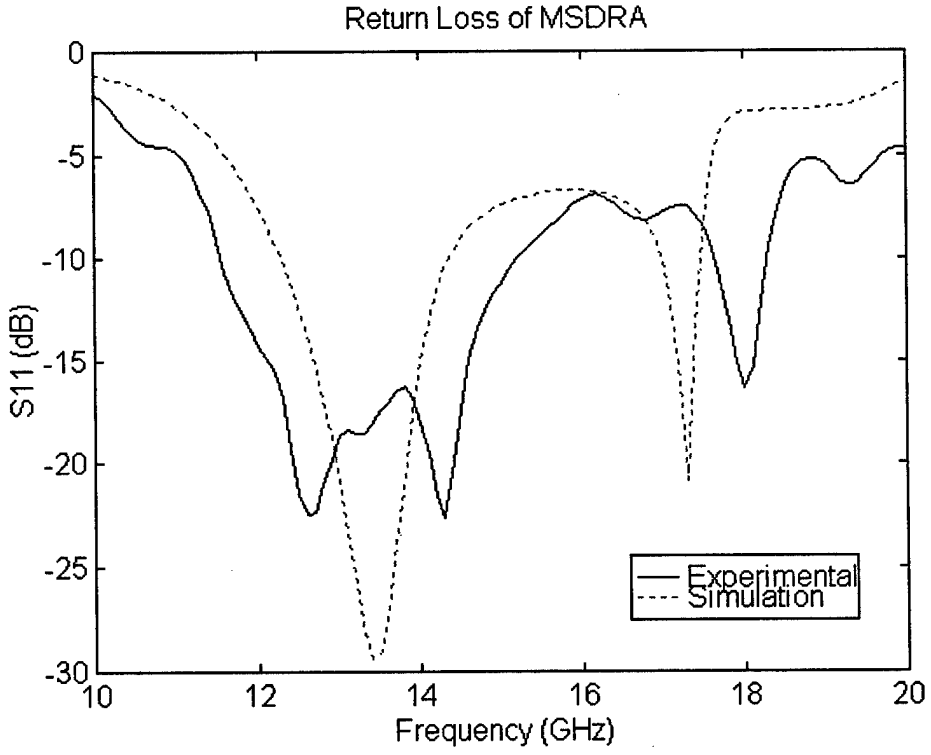

Figure 19: Return Loss for a Single Element Microstrip Fed MSDRA

4.5.2 Transmission Coefficient Determination (S_{21})

The comparisons between experimentation and simulation were made at a variety of spacings and included all three configurations. Figures 16 through 18 show these comparison for all three configurations in the E plane and H Planes. The remainder of the comparisons are provided in Annex B. Annex C contains all the simulated S_{21} plots.

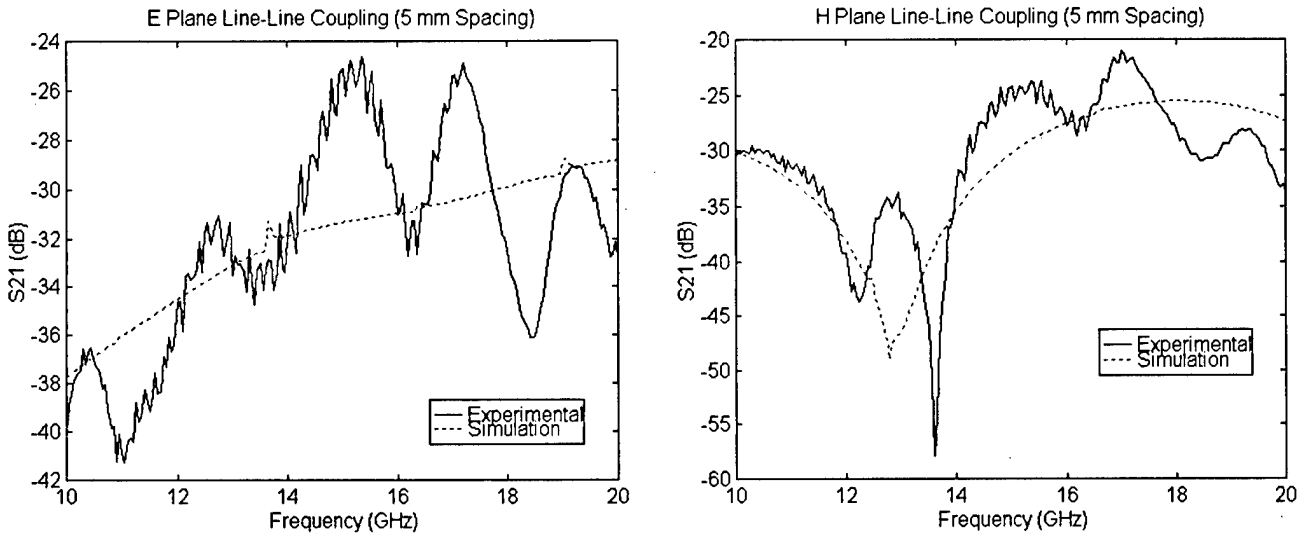

Figure 20: E and H Plane Line-Line Coupling Comparisons (5 mm)

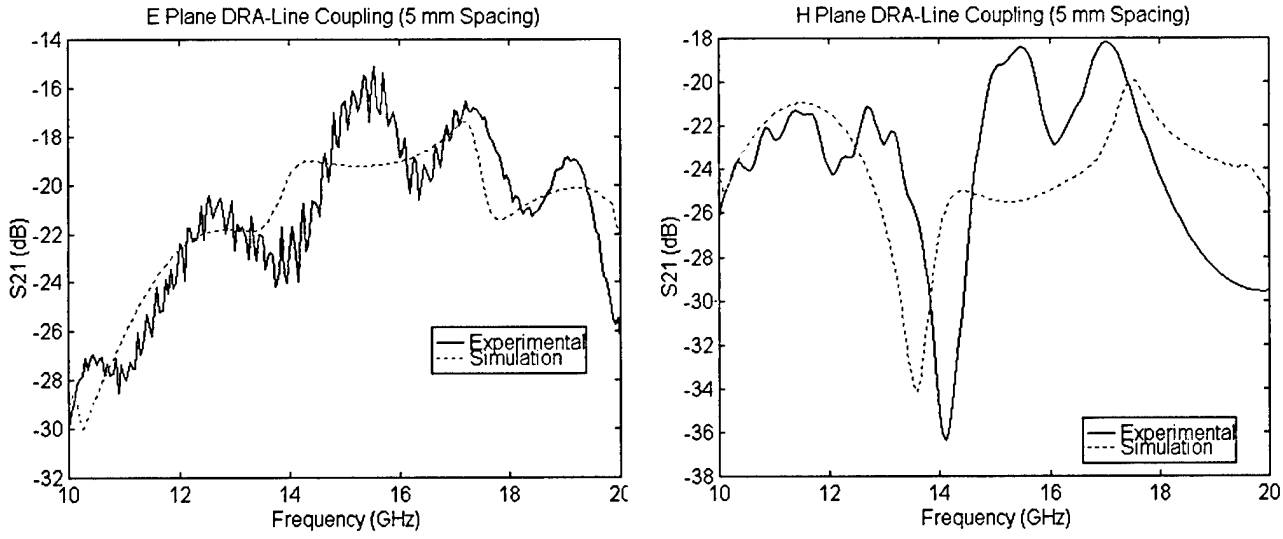

Figure 21: E and H Plane MSDRA-Line Coupling Comparisons (5 mm)

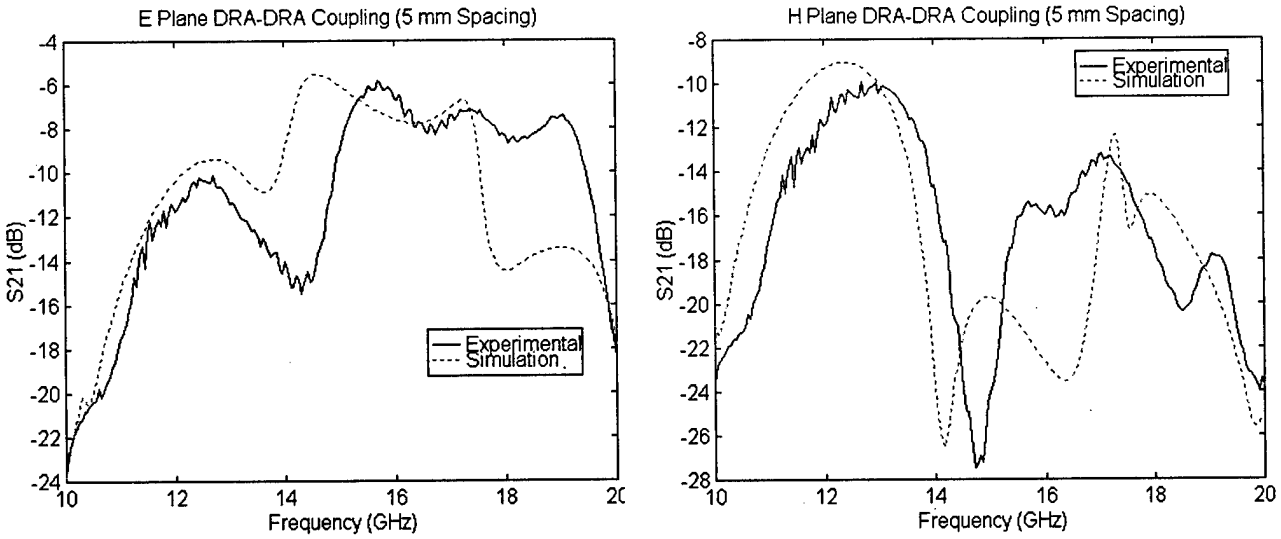

Figure 22: E and H Plane MSDRA-MSDRA Coupling Comparisons (5 mm)

4.5.3 Reflection Coefficient Determination (S_{11})

The return loss parameter, S_{11}, also provides some insight into the effect that coupling has in an antenna array environment. If we consider that the two DRAs and their associated feed systems are two elements in an antenna array, comparison of the S_{11} parameter with respect to the spacing distance will provide a measure of the input impedance changes. This "loading" will have an effect on antenna bandwidth as well as resonant frequency, since the effective impedance of the antenna will no longer be matched to the feed system. Figures 23 and 24 show the reflection coefficient (return loss) curves for the simulated data at a spacing of 5 mm. The Line-Line plot is not presented for either plane since there is virtually 100% reflection without any DRA on the line. The simulated S_{11} data at the remainder of the spacing intervals is included in Annex C.

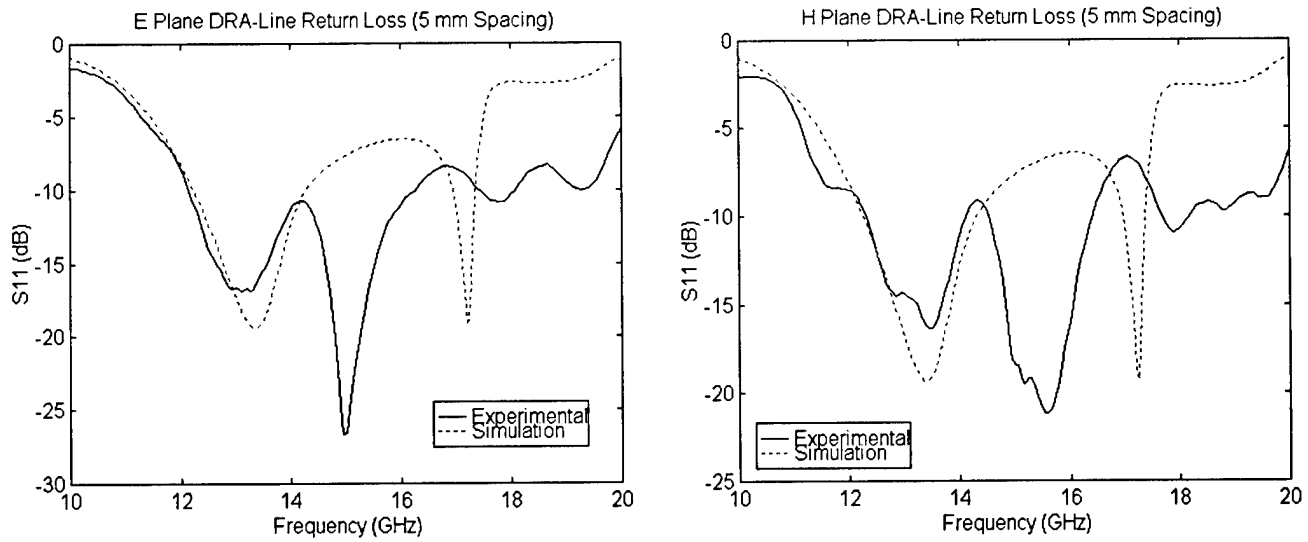

Figure 23: E and H Plane MSDRA-Line Return Loss (5 mm)

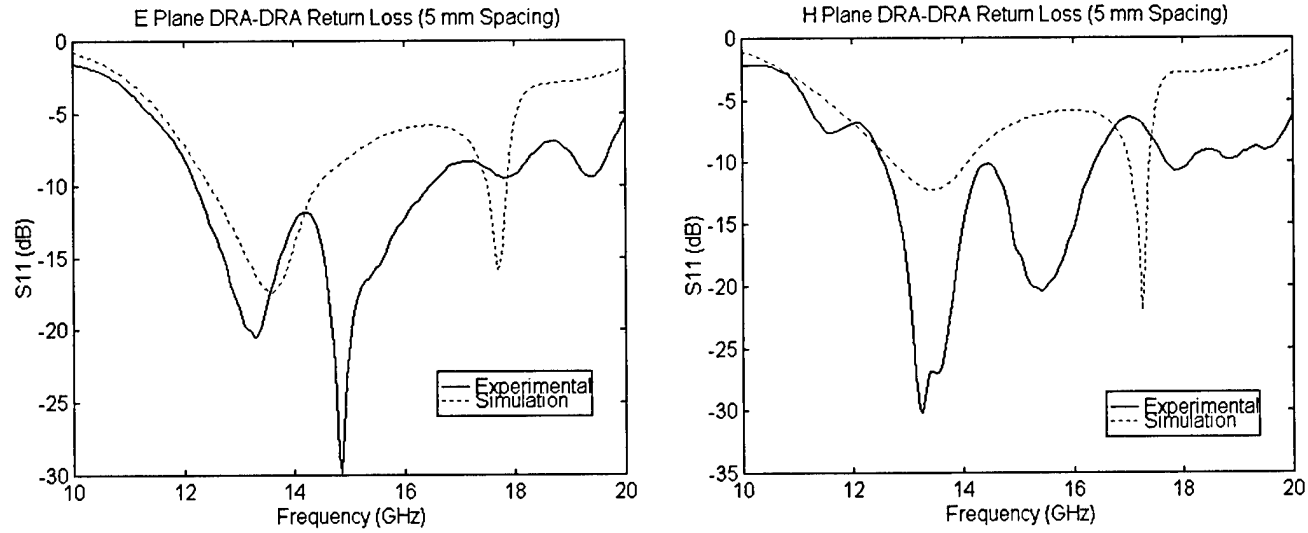

Figure 24: E and H Plane MSDRA-MSDRA Return Loss (5 mm)

4.6 Simulation and Experimental Discussion

The initial goal of this study was to gain confidence in the simulation capabilities of the software used. With the exception of the previously stated discrepancies at higher frequencies, the simulation results agree very well with those experimentally obtained. The downward frequency shift of approximately 0.5 GHz (4%) as well as the disagreement at higher frequencies is presented in the following section on sources of

error. The reason for the duplication in data collection at this stage was the initial uncertainty of the validity of the simulation process, since there was no previous knowledge on the capabilities of the simulation software using the DRA configuration. With the confidence now instilled in the capabilities of Micro-Stripes, simulation could be confidently used for further electromagnetic analysis, with final confirmation obtained through an experimental test of the final Micro-Stripes designed prototype.

4.6.1 Coupling Results and Analysis

With all the data available for each individual spacing, a MATLAB program was written to bring the information together in order to plot the scattering parameter characteristics with respect to frequency. The raw data was available for spacings out to almost 5 λ (100 mm), however the curves for both planes were virtual straight lines beyond 2 λ with the slopes unchanged from that at 2 λ. Thus there is no further relevant information to be gained from including these distances in the coupling plots or subsequent analysis.

Limits were also put on the frequencies presented. Since the analysis was focused on the dominant first order TE^{z}_{111} mode, which exhibits a resonant frequency of 13.5 GHz when in an isolated setting, the coupling relationship was centred on this frequency. The frequency range of 13 – 14.5 GHz was chosen for the analysis due to three main factors. Firstly, this range covers a sufficient bandwidth around the resonant frequency in which to make an analysis of the coupling behaviour at resonance. Secondly, the behaviour of the coupling below 13 GHz is well represented by that at 13 GHz. Finally, as will be further discussed in the section dealing with potential error sources, the agreement between simulation and experimentation begins to differ significantly at frequencies above 15 GHz, as can be readily seen from Figures 20 through 24. The difference is more pronounced in the H plane, with significant curve disagreement, however the E plane is also affected, with frequency discrepancies that appear to increase with frequency.

The MSDRA-MSDRA coupling relationships are presented in Figure 25a & 25b for E and H plane coupling respectively, with the interpretation of the results presented in the following paragraphs.

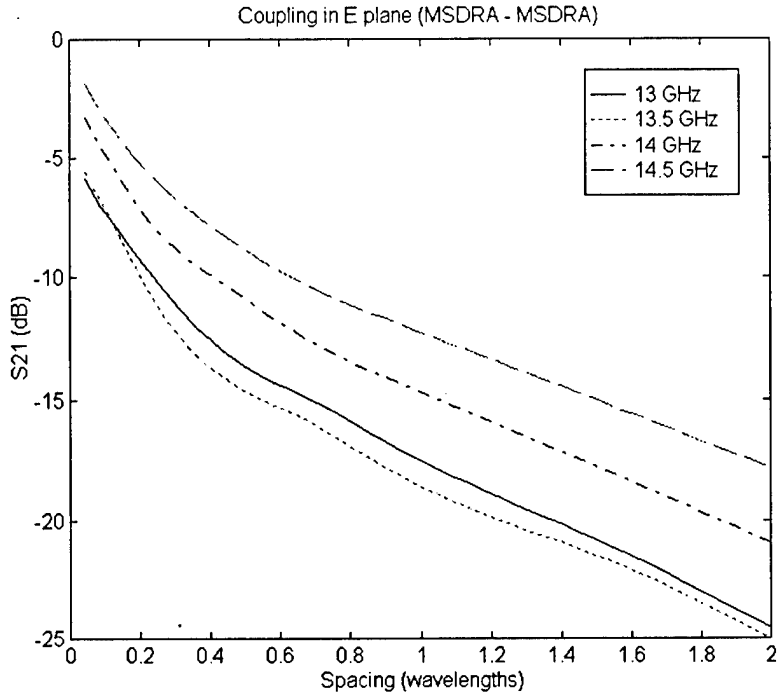

Figure 25a: E Plane Coupling Levels versus Spacing for Various Frequencies

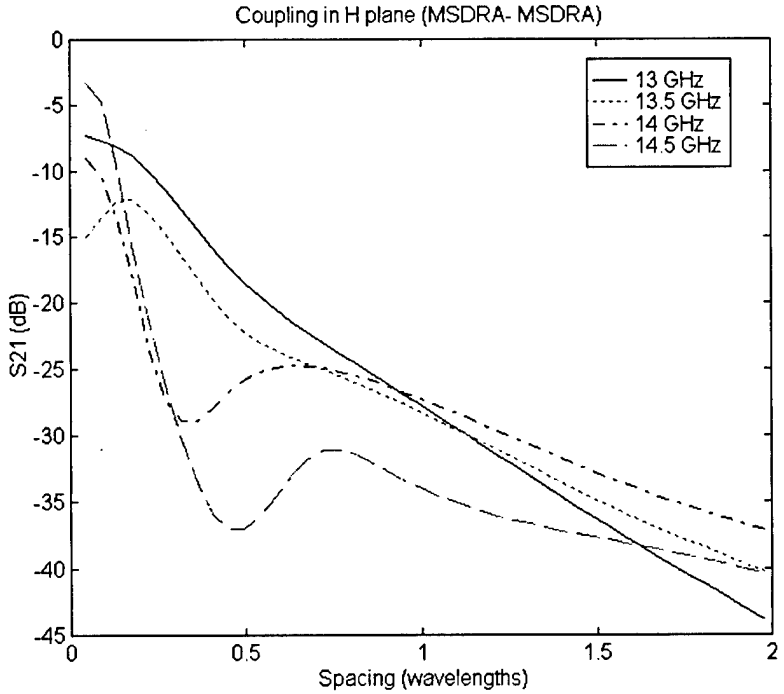

Figure 25b: H Plane Coupling Levels versus Spacing for Various Frequencies

Examinations of the curves shown in Figure 25 quickly show the expected trend of decreasing coupling levels with an increase in spacing. The coupling levels at larger spacing distances, (greater than 1 λ) decrease linearly, which, in this semilogarithmic representation, indicate exponential decay. This is demonstrative of the levels expected from a leaky decaying surface wave. At spacings closer than $\lambda/2$, the coupling is obviously influenced by additional factors. This is the loading effect caused by the proximity of the two elements. Although these cannot be explicitly characterized, several general trends are noticeable:

a. E Plane coupling levels are higher than H Plane levels at the same spacing interval. This is due to the nature of the field strengths in their respective planes. Recall that a magnetic dipole has an omnidirectional radiation pattern in the E plane, while exhibiting a null at low elevation angles in the H plane. (See figure 3)

b. The shape of the coupling curve remains constant in the E plane case, with increasing spacing distances simply showing a uniform drop in coupling intensity. Examinations of the S_{11} and S_{21} curves at each of the spacing intervals indicate that the resonant frequency remains stable at 13.5 GHz. This helps explain the stable nature of the coupling curves at resonance. In the H plane however, similar comparisons show the resonant frequency to be spacing dependent up to approximately $\lambda/4$. This results in the erratic behaviour of the coupling levels seen in Figure 25b. Once the resonant frequency stabilizes to 13.5 GHz the expected monotonic trend continues.

c. When the spacing distance approaches $\lambda/2$, which is considered the minimum spacing for element placement in a typical array environment, the coupling levels are down to –14 dB in the E plane and –22 dB in the H plane. Thus the effect on the radiation pattern of an array should be minimal, however mutual coupling should not be ignored.

d. Line – Line and MSDRA – Line coupling levels are significant at small spacings (up to 5 mm). This indicates that care must be taken in designing the feed network of multi element arrays so as to ensure that adjacent elements or feed lines are kept at least this far away from each other. Once again, this is more pronounced in the E Plane. Figure 26 shows the relationships between the 3 configurations for each of the planes.

Of particular notice in Figure 26 is the similar behaviour exhibited by each of the configurations in the E plane, while the H plane Line-Line and Line–MSDRA coupling quickly fall off.

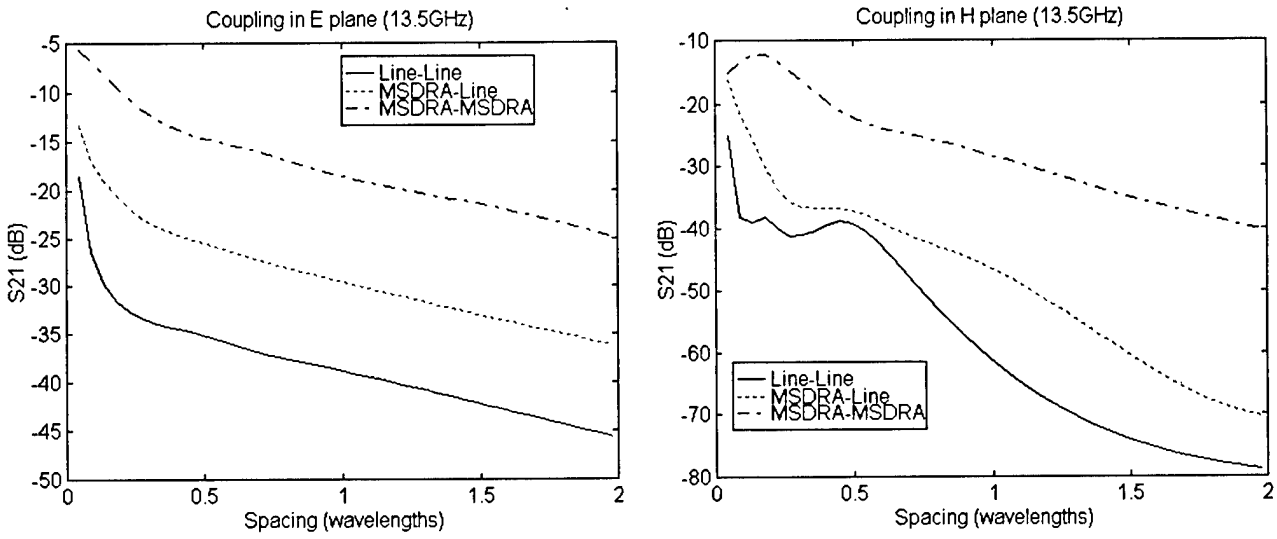

Figure 26: Coupling Comparisons at resonance

e. Coupling level comparisons with the aperture coupled DRA [Loos 94] indicate close agreement at $\lambda/2$ spacing, with his levels being –13 and –15 dB for the E and H plane cases respectively. The E plane values agree closely, however the H plane coupling is 7 dB stronger for the aperture coupled case. This could indicate that either the ground plane or the aperture significantly affects coupling levels. Comparisons at smaller distances could not be made as his experiment did not consider any spacing closer than $\lambda/2$.

f. Comparisons to mutual coupling levels in probe fed hemispherical DRAs [L,L&L 94] show the same general trends with the H plane coupling levels falling off much more quickly than the E plane levels. Once again, they used a minimum distance of $\lambda/2$, so comparisons could not be made at close spacings. At $\lambda/2$ they measured coupling levels of – 13 dB in both planes, which coincide well with a theoretical model they reported.

g. Compared to microstrip patch antennas, 'typical spacing distances' exhibit –20 and –25 dB in the E and H planes respectively [J,P&C 81]. This comparison cannot be objectively qualified since there is no reference given to what the 'typical' spacing distance is. Intuitively however, it seems probable that DRAs exhibit greater coupling levels than MPAs due to the nature of their field configurations.

4.6.2 Reflection (Return Loss) Results and Analysis

Other information can be retrieved through examinations of the S_{11} plots, with the key factor being the changes in input impedance as a result of the antenna being "loaded" with the second element in close proximity. This relationship is presented in Figure 27.

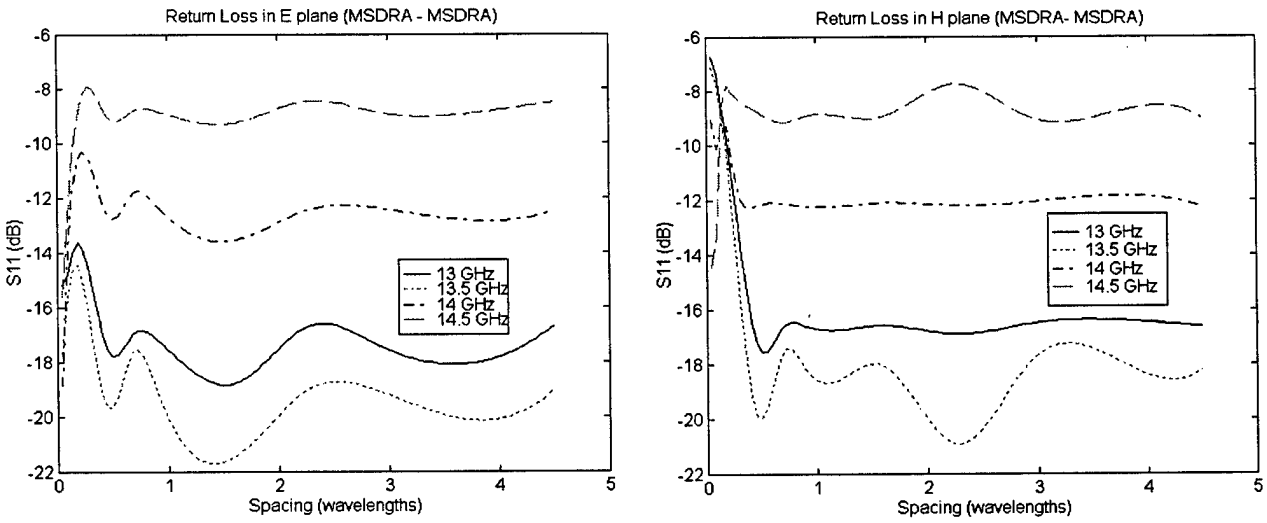

Figure 27: E and H Plane Reflection Comparisons vs. Spacing at various Frequencies

The following characteristics are worth noting:

a. The return loss plots indicate that the coupling interaction in the E plane increases the bandwidth, whereas the H plane coupling interaction shifts the resonant frequency upward significantly at close spacing distances. The effect here is that "loading" has a beneficial effect in the E plane, providing good impedance matching characteristics for a larger frequency range. The effect in the H plane is to cause an impedance mismatch and a shift in resonant frequency, which has detrimental effects on the radiation characteristics of the antenna. Examinations of the simulated S_{11} graphs presented in Annex C show this variation in resonant frequency.

b. The oscillatory nature of destructive and constructive interference can be seen in figure 27. The plots show a sinusoidal variation in return loss with increasing spacing distances. This is due to the impedance changes as a result of the field patterns either adding to each other or cancelling each other out. The spacing distances dictate whether the field values are in phase or out of phase, thus whether they are destructive or constructive. Once again, this is more pronounced in the E plane due to the higher coupling levels encountered.

4.7 Sources of Error

Errors are inevitable in the conduct of any research. The goal is to minimize the potential sources in order to prevent errors from occurring at the outset, or, failing this to explain the discrepancies in the resultant data. There are some results, however, for which valid explanations cannot be provided. The following sections deal with the potential sources of error and the effects of these errors. The potential errors induced through the simulation process are included, however general comments on the trials and tribulations encountered in the simulation software are provided in Annex D.

4.7.1 Experimental Error

Usually the first scapegoat, experimental error only plays a small part in the results, and does not affect the overall outcome or findings. The errors found in the experimental data come from two potential sources.

a) The coaxial connectors with which the antenna arrangement was connected to the network analyzer for scattering parameter measurements attributed reflection oscillations to the resulting plots. This error can be seen as the 2 GHz ringing frequency most evident in the Line – Line coupling relationships, or in the other plots at large spacing distances. This evidence is due to the low level of coupling achieved, which makes the noise level and this ringing the more dominant characteristic.

b) The second source of potential error comes from the silicon sealant that is used to fix the DRA to the microstrip line. Since it was desired to change the configurations of the antenna structure in order to measure all aspects and configurations, (Line – Line, MSDRA – Line and MSDRA – MSDRA), there was a requirement to temporarily fix and remove the DRA to the microstrip line

without causing any damage. The silicon sealant used however exhibits some dielectric properties that are not part of the design. The effect of the sealant, which has a permittivity of around 2 – 4 would be to alter the resonant frequency. A simulation was conducted to determine the return loss for the single MSDRA as compared to simulations without the sealant, as well as experimental results. This is the same comparison conducted in section 4.5.1, with the addition of the simulation results taking into account the sealant. The results are presented in Figure 28.

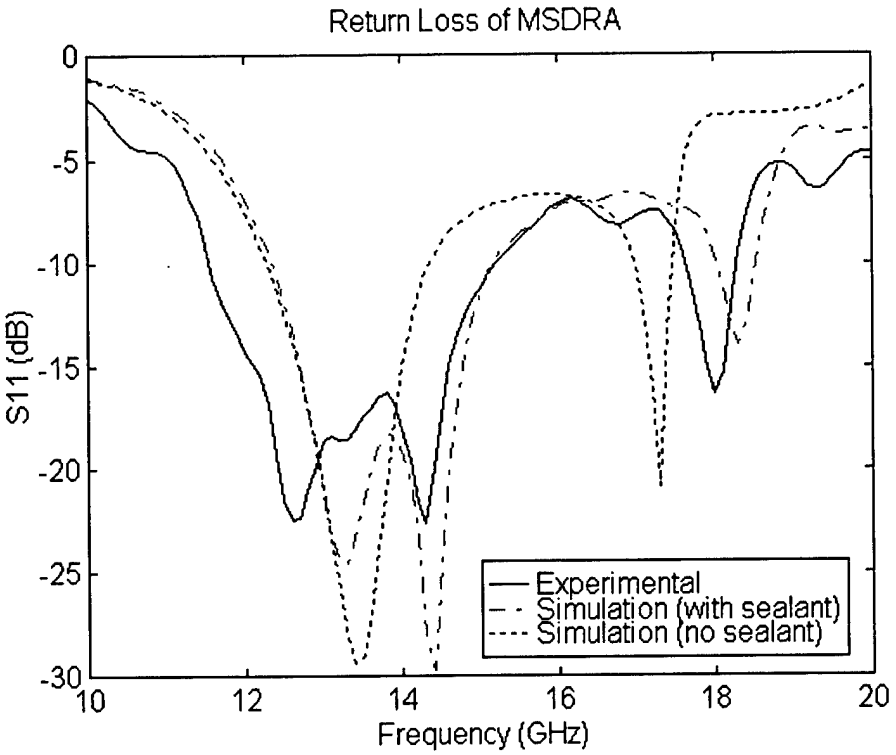

Figure 28: Comparisons Showing Effect of Silicon Sealant

The effect of the sealant appears significant, with the simulation that takes into account the sealant achieving much closer agreement to the experimental measurements. However, this glue layer could not be taken into account in all simulations because of the requirement for extremely small meshes to include this 0.02 mm thick layer. The simulation conducted to create this single curve took over 100 hours of CPU time and 60 Mbytes of RAM. Since exact frequencies are not overly significant at

this stage of the research activity, this potential error is only mentioned as a possible reason for some of the frequency shifts observed between experimental data and that achieved through numerical simulations. A smaller potential error that could not be simulated, and is considered to be negligible is the glue used to hold together the DRA and the insert. Since this is applied under pressure during the manufacturing process, its thickness is much less than the sealant and should not affect the results.

4.7.2 Tolerance Errors

Another source of error is the tolerance ranges of the materials used. In the case of the dimensional tolerances of the DRAs, the resonant frequencies and electromagnetic response of the DRA are very stable, while the fabrication tolerances are very precise. Thus dimensional data is not considered as a source of error. The tolerances in the dielectric permittivity however, are not as lenient and can be up to 10 % for higher values of ε. Figure 29 shows the effect of a small change in ε_r.

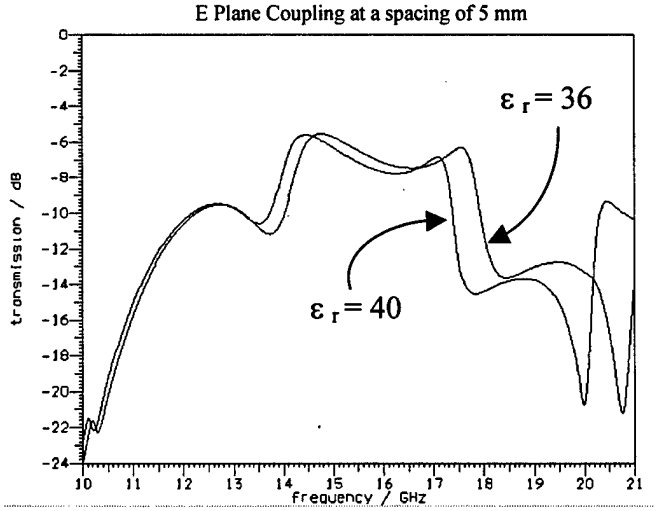

Figure 29: The effect of a 10% change in the permittivity of insert

The calculated parameter is the coupling characteristic for a spacing of 5 mm, and the only difference between the two curves is a 10% decrease in the permittivity of the insert. (From $\varepsilon_r = 40$ to 36) As can be seen this results in fairly significant differences in the frequency response, especially at increased frequencies. This difference provides good insight into a potential reason for the frequency shift exhibited between experimentation and simulation results, and also helps explain the frequency dependency of the shift. The high permittivity of this insert allows a 10% change to be significant. Permittivities of the remainder of the dielectric substances, being substantially lower, do not change significantly with the same tolerance level. Thus, for high permittivity materials, tolerances must be made as small as possible, or large discrepancies could occur.

4.7.4 Simulation Errors

The simulation process can be fraught with errors, as the user does not fully follow closely what is occurring during the computations. It is for this reason that rigorous comparisons were carried out throughout this research. Without the measuring stick of experimental data or theoretical approximations, there would be no yardstick available with which to analyze the simulated data.

There were many difficulties encountered during the simulations, however, through the use of these comparisons, any anomalous results were examined and the simulation input data confirmed for accuracy. Virtually all of the causes of simulation data disagreeing with experimental or theoretical results were a result of incorrect inputting of data. The adage of garbage in, garbage out is definitely true. Once corrected, the simulations provided data with good agreement. Annex D is devoted to some of the "learning steps" taken in mastering the use of the software.

4.7.5 Other Possible Error Sources

An unexplainable error is the cause of the significant difference between the simulation and experimental coupling response for frequencies higher than 15 GHz. No matter how many different simulations were attempted, either through using a finer mesh size, or simulating the structure over a larger ground plane, the cause of this disagreement could not be determined. Also, experimentation was repeated to eliminate that as a potential cause. It is thought that the nature of the field interaction between MSDRAs might be a cause. This hypothesis is based on the fact that the parasitic coupling measurements, detailed in the next chapter, exhibit a closer frequency agreement. The case of the H plane directional parasitic coupling example is very close to that measured in this mutual coupling determination, with the major difference being that the coupled element is simply a DRA, and does not contain the higher permittivity insert. The frequency agreement between experimentation and simulation is much greater in that case. The significant discrepancy found through including the silicon sealant could also help explain this error. Nevertheless, this discrepancy is one area for further research.

4.8 Summary

The above investigation demonstrates the close agreement achieved through numerical simulations using Micro-Stripes™. The S_{11} and S_{21} scattering parameters clearly demonstrate the field interactions of the two elements with respect to spacing distances. The coupling levels at a typical array spacing distance of $\lambda/2$ are small, however, they should not be completely discounted. The configurations utilized also demonstrate that the feed network of a direct microstrip coupled array must be carefully designed due to the amount of coupling produced from microstrip-DRA or even microstrip-microstrip proximities. E plane coupling appears well behaved, in that the resonant frequency is maintained constant at all spacings. H plane coupling however has the effect of altering resonant frequency for small ($< \lambda/4$) spacings.

It is apparent that for standard array environments in which elements are typically positioned at greater than $\lambda/2$ spacing distances, inter-element coupling will not play a significant factor, but cannot be discounted.

It was initially intended to expand this analysis of inter-element coupling to linear or planar arrays, however, based on the results obtained so far, as well as the limited capability of the simulation software, the investigation into mutual coupling focussed on potential positive practical purposes. Parasitic coupling uses the principle of mutual coupling to allow the excitation of a single normally fed element to excite subsequent elements, with the effect being enhanced radiation characteristics, either through radiation pattern manipulation, bandwidth enhancements or resonant frequency changes.

One such application is the Yagi-Uda antenna, which employs a single element parasitically coupled to a series of directors and reflectors, with numbers dependent on the gain and radiation pattern desired. Further research uncovered two papers that investigated the use of parasitically coupled DRAs to create antennas with wide bandwidth or dual frequency operation. [F,A,I&P 96] [F&A 97] It was decided to investigate these features and to provide simulation configurations in which parasitically coupled microstrip coupled DRA geometries are investigated, with the goal of achieving wide bandwidths, dual frequency operation, or squint angles in the antenna radiation pattern.

CHAPTER 5

5.1 Parasitic Coupling Analysis

In the continuing examination of mutual coupling, the concept of parasitic coupling was investigated. Parasitic coupling uses the principle of mutual coupling in order to excite subsequent antenna elements from one fed through conventional methods. Probably the first, and most assuredly the most common parasitic antenna is the Yagi-Uda Antenna [Yagi 28]. This antenna consists of a number of linear dipoles, only one of which is energized. The others act as parasitic directors whose currents are induced through mutual coupling. This antenna could be found on the roofs of most homes, as television reception antennas, until the advent of cable, and more recently satellite dishes. The key aspect in this antenna style was the fact that the passive radiators were positioned within $\lambda/2$ wavelengths of the fed element in order to make use of the mutual coupling effects in altering the radiation beam pattern.

This basis provided a starting point in exploiting the mutual coupling characteristics of the DRA. Three parameters that can be manipulated through mutual coupling interactions are bandwidth, frequency of operation and radiation pattern manipulation. All three of these will be examined in the following sections, with the majority of the analysis centered on radiation pattern manipulation.

5.2 Wideband or Dual Frequency Operation

Preliminary experimental research has already been conducted using parasitically coupled DRAs, [S&L 94] who examined aperture coupled cylindrical DRAs for circularly polarized CP applications, and [F,A,I&P 96] [F&A 97], who used slot coupled rectangular DRAs to achieve wide bandwidth as well as dual frequency operation. The latter two of these papers were examined closely, since the configuration is very close to that already analyzed, and the applications fit into this research on mutual coupling.

The basic principle employed by both works is the use of rectangular DRAs of slightly different dimensions fed through the same aperture coupled feedline. Due to the dimensional differences, the resonant frequencies exhibited will be different. Selecting elements with resonant frequencies close to one another will result in wideband operation, while frequencies selected further apart will result in dual frequency operation. The critical factor in the extent of frequency range available is the capability of coupling sufficient energy to each of the radiators

Once again, to confirm the simulation capabilities of the TLM software, one of the configurations presented in [F&A 97] was simulated. The configuration chosen is shown in Figure 30.

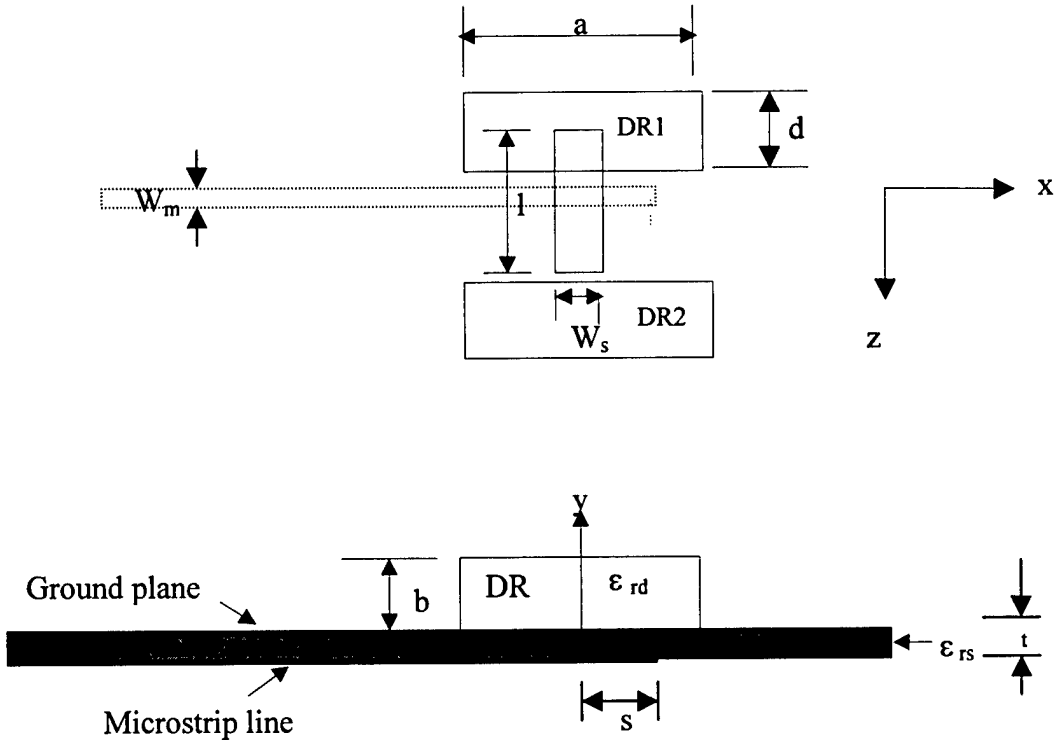

Figure 30: Top and Side views of two element aperture coupled rectangular DRA

Two dielectric resonators of permittivity $\varepsilon_{rd} = 20$ are excited through the aperture. DR1, centred –5.7 mm in the z direction, has dimensions of a = 12 mm, b = 6 mm and d = 8 mm, and DR2, centred 5.1 mm in the z direction, has a = 12 mm, b= 4 mm and d = 8 mm. The substrate has t = 0.635 mm and $\varepsilon_{rs} = 10.2$, S = 4.2 mm, $w_m = 0.6$ mm, and $w_s = 1.3$ mm. Using the modified DWM model approximations, this should yield isolated resonant frequencies of 4.73 and 5.43 GHz respectively. The measured resonances when the elements are excited individually are 5.10 and 6.15 GHz respectively, which compares adequately with the modified DWM. When excited together, the outcome is dual frequency operation at 5.06 GHz and 6.26 GHz. Their return loss plot is reproduced here in Figure 31.

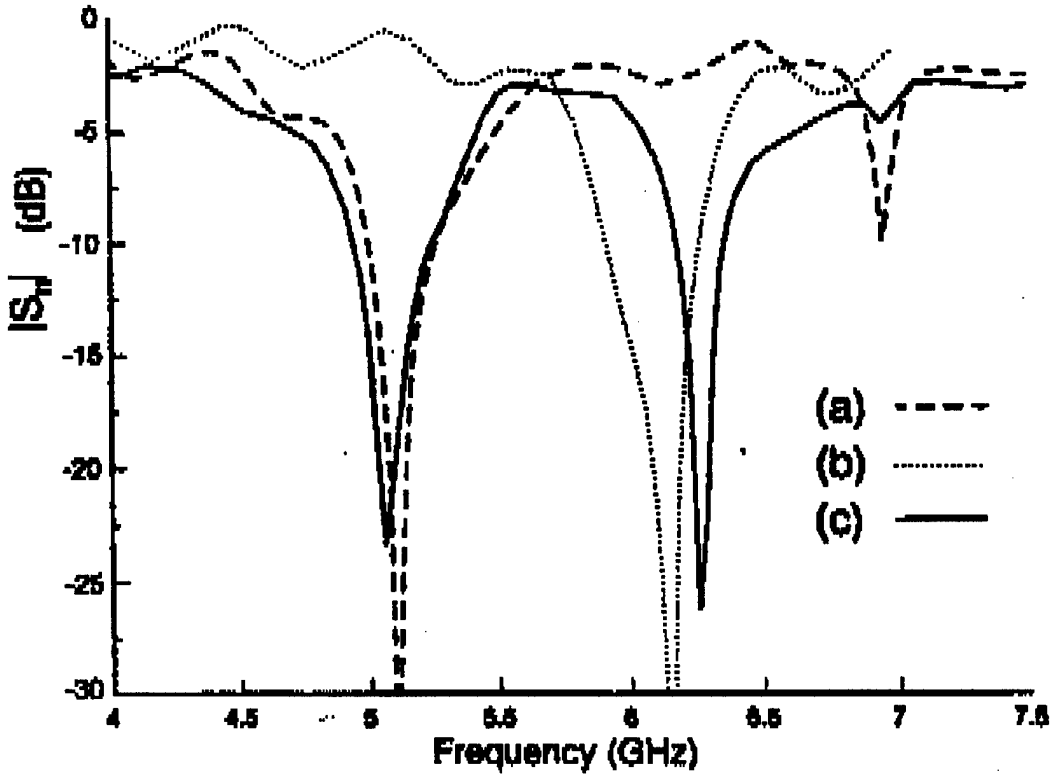

Return loss against frequency for (a) one element: DR1 with $y_c = -5.7$ mm, (b) one element: DR2 with $y_c = -6.0$ mm, (c) two elements: DR1 with $y_{c1} = -5.7$ mm, DR2 with $y_{c2} = 5.1$ mm.

Figure 31: Experimental Return Loss against Frequency

Examinations of the experimental return loss show a frequency shift for both resonant frequencies, with the lower resonance shifted downward and the higher resonance shifted upward slightly. This shift follows from the results shown in the mutual coupling determinations of Chapter 4. Mutual coupling interaction in the H plane, as is the case here, causes a change in the impedance characteristics, which causes a shift in resonant frequency. The simulations conducted provide similar results, as can be seen from Figure 32. Isolated resonances of 4.79 and 5.77 GHz are transformed slightly into dual frequency operation at 4.77 and 5.85 GHz, when excited together. Thus, the same trend is apparent, with the resonances shifting away from each other when mutually coupled.

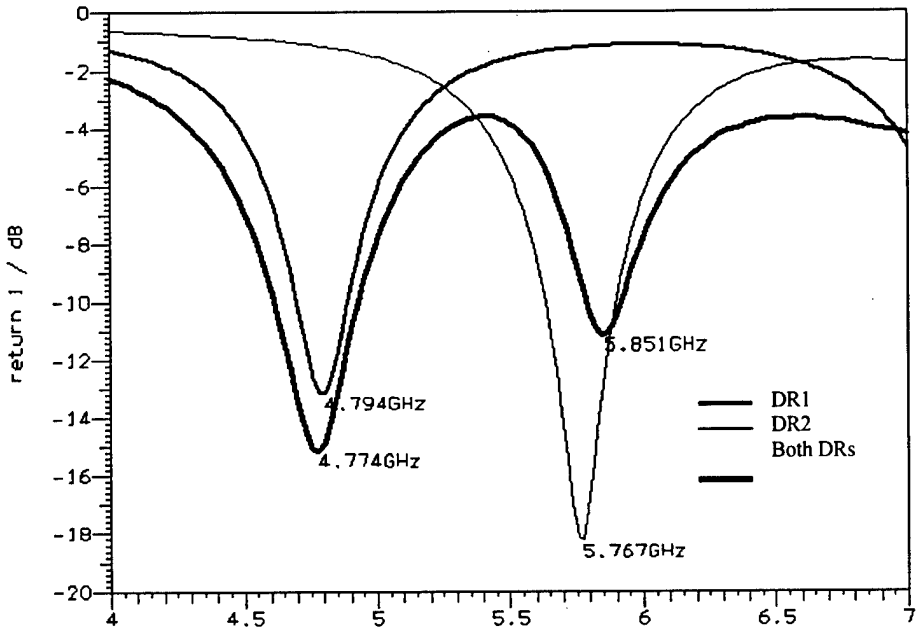

Figure 32: Return Loss for Simulated Dual Frequency Example

With the close agreement achieved in this comparison of practical uses for mutual coupling, the next step is to blaze new trails and apply the principles obtained in further exploitations of this phenomenon. The selected application is the use of mutual coupling in achieving antenna pattern manipulation. Like the Yagi-Uda antenna, which uses parasitic dipoles to produce an endfire array pattern, parasitic DRAs are experimented with, with the intent to achieve a similar goal. Radiation pattern manipulation through the use of parasitic elements was also investigated in [P,M,I&W 95] and [C,P,I&W 96].

5.2.1 Radiation Pattern Manipulation

The DRA element and feed structure to be used in this analysis continue to be the MSDRA with a direct microstrip coupled feedline. The difference comes in the parasitic elements. Since there is no need to couple the energy from the DRA to a second or subsequent feed lines, there should be no requirement for the higher permittivity insert. Recall, this insert was only necessary to match impedances with the microstrip line. Thus a simple DRA was used to fulfil the role of parasitic elements.

Three positional configurations were examined as shown in Figure 33.

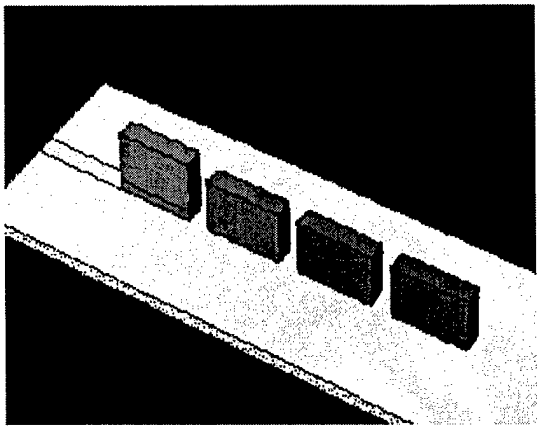

a) E Plane Directional Configuration

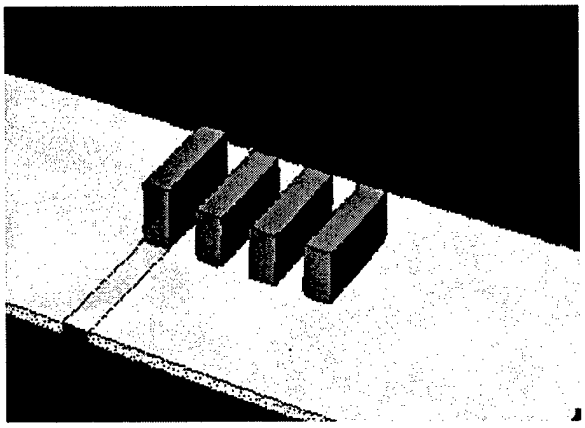

b) H Plane Directional Configuration

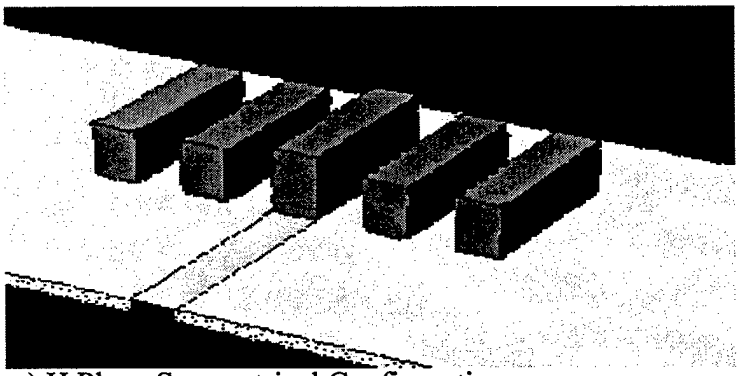

c) H Plane Symmetrical Configuration

Figure 33: Parasitic Coupling Configurations

The exact number of parasitic elements to achieve the desired goal was originally unknown, therefore simulations were carried out with up to four parasitic elements, and in the case of the H plane symmetrical case, 3 pairs of elements. Simple array theory was used to predict the expected radiation patterns without considering mutual coupling. It was expected that the directional E plane configuration shown in Figure 33a would produce an endfire pattern much like that of the Yagi-Uda antenna. The directional H plane configuration of Figure 33b is expected to produce an H plane pattern squinted in the direction of the radiators. The symmetrical H plane configuration of Figure 33c is expected to produce a uniform pattern in the E plane with a very directional boresight H plane pattern.

Simulations of each of these configurations were conducted, starting with only one, or in the case of the symmetrical H plane configuration one pair, of parasitic DRAs placed with a spacing distance of 1 mm. This process was repeated with a 2 mm spacing distance. These spacing distances were chosen based on the high coupling levels achieved in the results of chapter 4. Similar coupling trends are expected, with the E plane parasitic coupling expected to exhibit a stable resonant frequency, while the H plane coupling should exhibit an upward frequency shift.

The scattering parameters, as well as the far field radiation pattern were determined for each case. Experimental data is presented for one example of each configuration for the purpose of corroboration. Each of the 3 orientation configurations will be discussed separately in the following sections.

5.3 E Plane Directional Configuration

5.3.1 E Plane Directional Antenna Results

The return loss (S_{11}) for the MSDRA with 1 parasitic element is presented in Figure 34 for both of the spacing considerations, while Figures 35 and 36 show the same characteristics for 2 and 3 parasitic elements respectively. Examinations of these figures show that the resonant frequency remains very close to 13.5 GHz and in fact widens considerably compared to the isolated resonator. This characteristic agrees with that determined from the mutual coupling measurements of chapter 4.

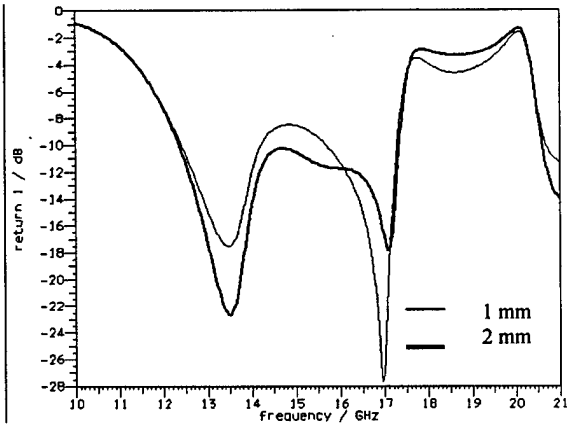

Figure 34: Return Loss for One Parasitic Element (1 & 2 mm)

The far field radiation patterns at a frequency of 13.5 GHz are presented in Figures 37 through 39. The analysis of these results will be conducted in the next section.

The return loss measurement for the 2 mm spacing configuration with 2 parasitic elements is compared with experimental data in Figure 40. Return Loss comparisons with the other configurations are included in Annex E.

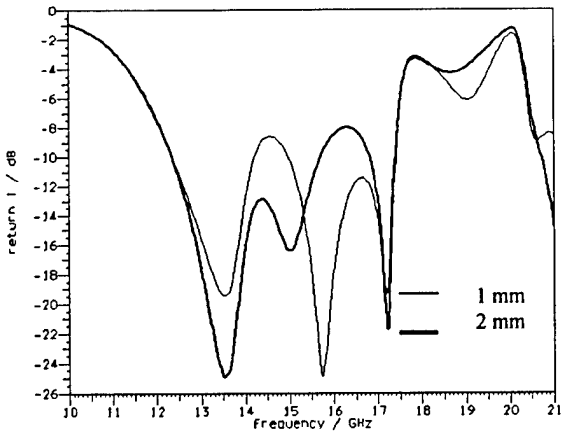

Figure 35: Return Loss for two parasitic elements (1 & 2 mm)

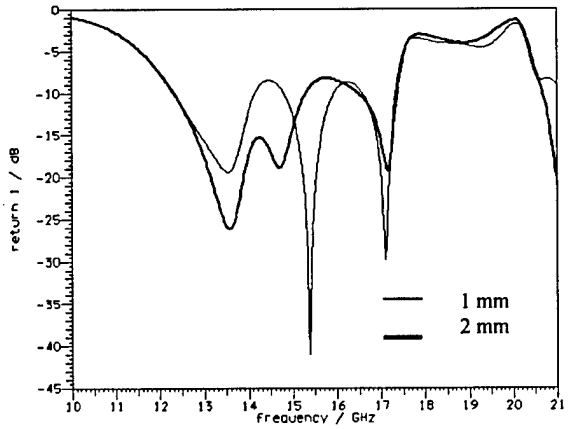

Figure 36: Return Loss for three parasitic elements (1 & 2 mm)

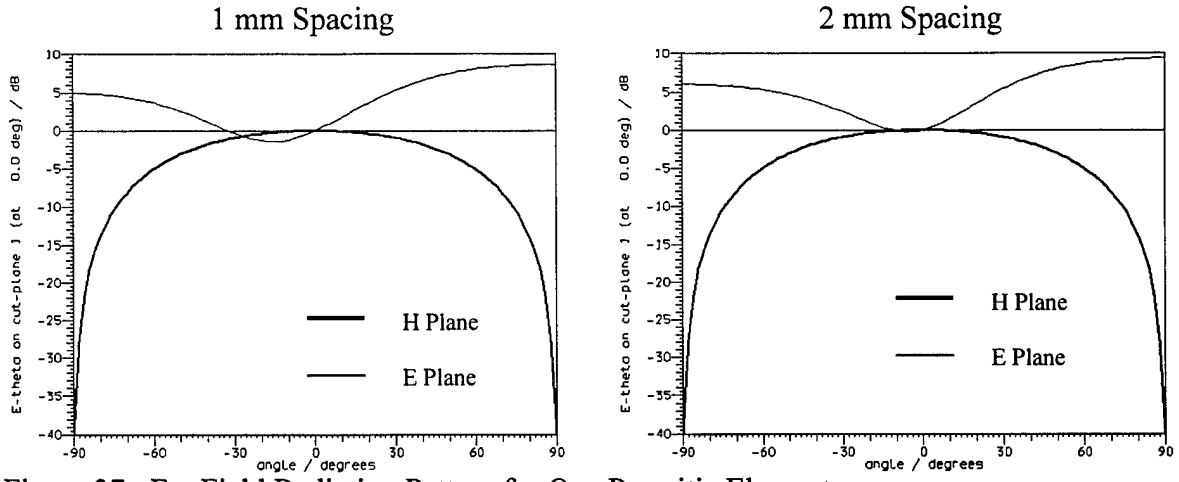

Figure 37: Far Field Radiation Pattern for One Parasitic Element

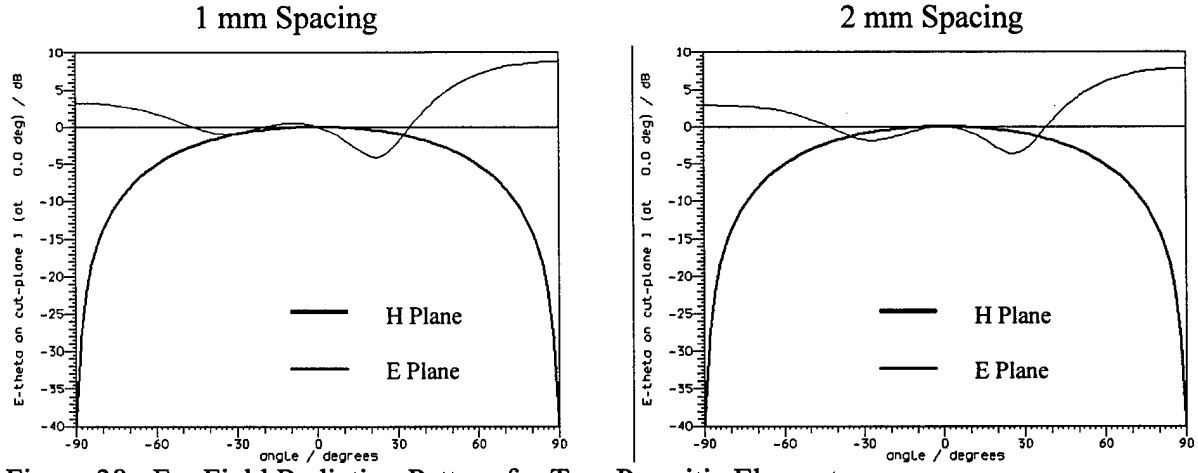

Figure 38: Far Field Radiation Pattern for Two Parasitic Elements

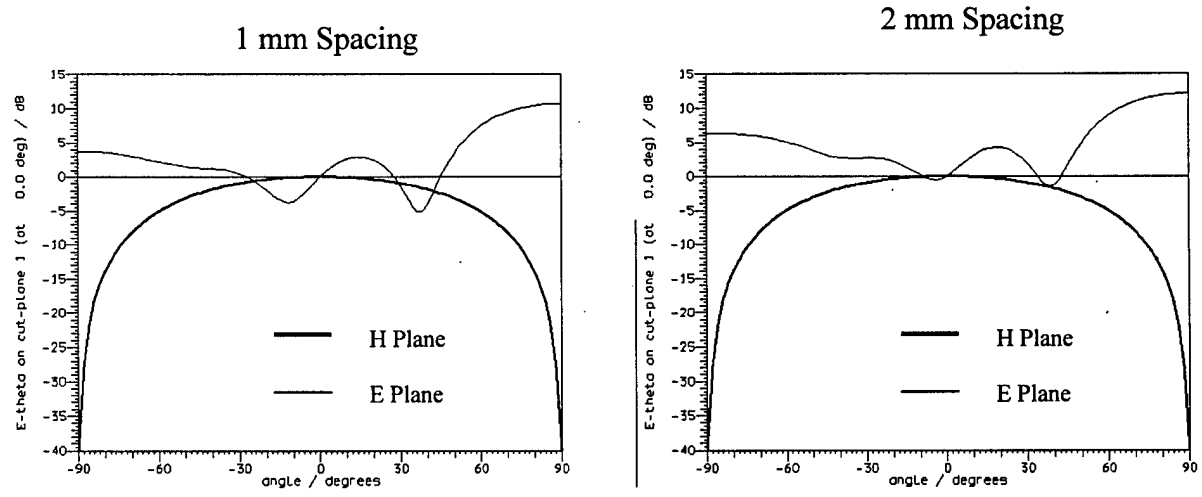

Figure 39: Far Field Radiation Pattern for Three Parasitic Elements

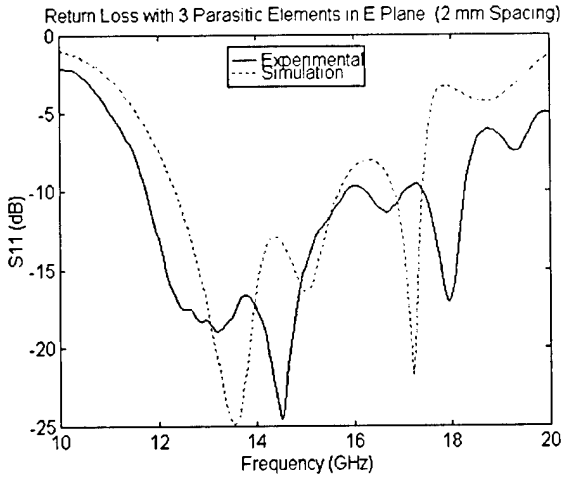

Figure 40: Experimental vs. Simulated Results for 3 parasitic elements (2 mm)

5.3.2 E Plane Directional Antenna Discussion

The simulation results obtained agree closely with expectations as well as with experimental data. The far field radiation pattern exhibits a squint in the E plane pattern, and with 3 parasitic elements at a spacing of 2 mm an end fire directional beamwidth of 60 degrees with a normalized gain of 12 dB is produced. Using a greater number of elements increases the directional characteristics of this structure, however the sidelobes begin to be prominent, therefore the simulations were stopped at this configuration. No attempt to optimize the radiation pattern was attempted at this stage.

The nature of parasitic coupling in the E plane shows the same characteristics as determined for the MSDRA - MSDRA coupling of Chapter 4, in that the return loss at the resonant frequency of 13.5 GHz remains relatively stable. There appear to be some higher order modes or additional excitations that influence the return loss characteristics with an increase in the number of parasitic elements. This serves to increase the bandwidth phenomenally. Spacing distance also affects the bandwidth characteristics, with a spacing of 2 mm providing a significantly better impedance match, and thus reducing the return loss considerably more than for 1 mm. Simulations for frequencies up to 14.5 GHz exhibit similar radiation patterns, thus exploitation of this wide bandwidth would be possible.

5.4 H Plane Directional Configuration

5.4.1 H Plane Directional Antenna Results

The return loss (S_{11}) for the MSDRA with 1 parasitic element is shown in Figure 41 for both of the spacing considerations. Figure 42 shows the same characteristics for 2 parasitic elements. The return loss for the configuration with 2 parasitic elements spaced 1 mm apart is compared with experimental data in Figure 45. Return Loss comparisons with the other configurations are included in Annex E.

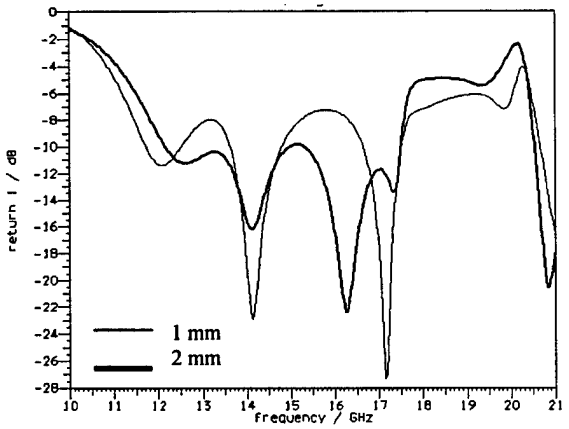

Figure 41: Return Loss for H Plane Directional Coupling with 1 Parasitic Element

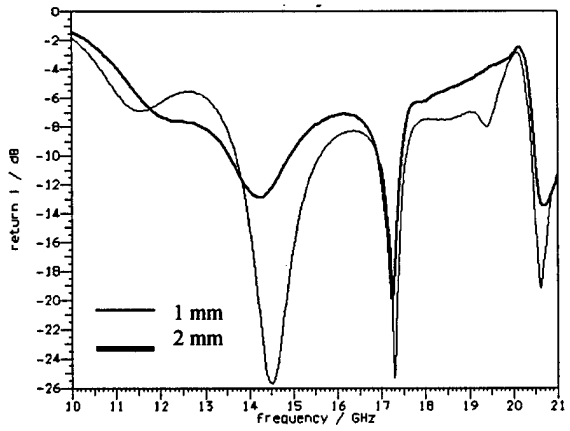

Figure 42: Return Loss for H Plane Directional Coupling with 2 Parasitic Elements

Similarly, the far field radiation patterns are presented in Figures 43 and 44. A frequency of 14 GHz for the radiation pattern plot for 1 element and 14.5 GHz for two elements was used based on the return loss plots shown in Figures 41 and 42. This shift in resonant frequency was predicted, since the H plane coupling determination from chapter 4 also exhibited significant shifts in resonant frequency at small spacing distances.

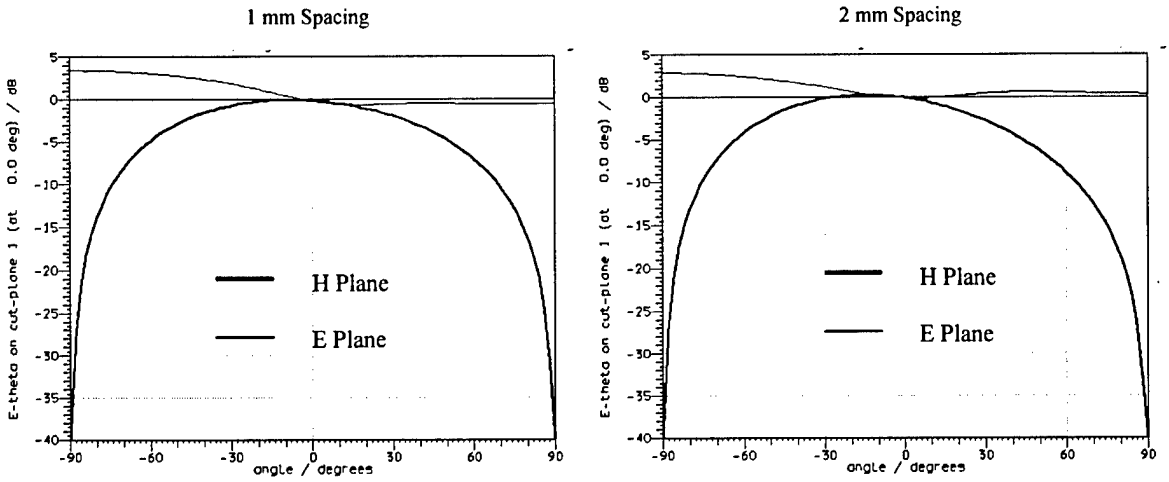

Figure 43: Far Field Patterns for 1 Parasitic Element in the H Plane (f = 14 GHz)

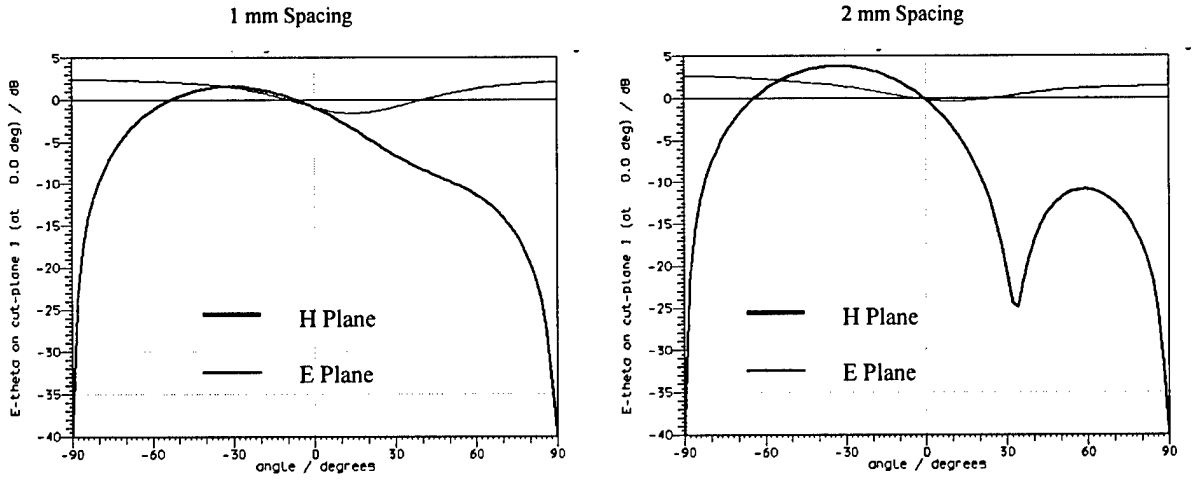

Figure 44: Far Field Patterns for 2 Parasitic Element in the H Plane (f=14.5 GHz)

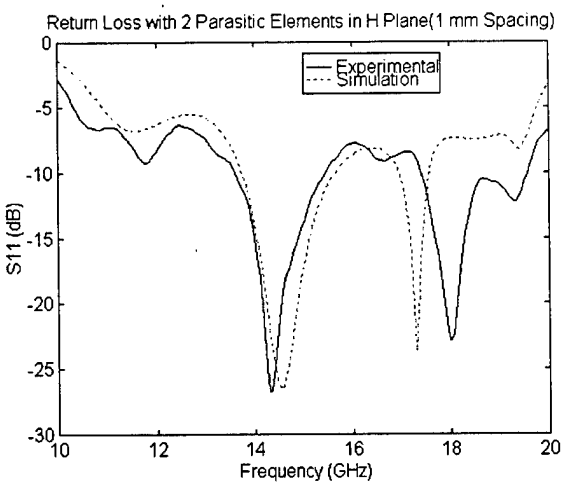

Figure 45: Experimental and Simulated Return Loss Comparisons

5.4.2 H Plane Directional Antenna Discussion

Again, simulation results agree with both expectations and experimental results. The far field radiation pattern exhibits the expected squint, while the return loss curve shows that the mutual coupling effects cause an increase in the resonant frequency. The far field radiation patterns at frequencies of 13.5, 14 and 14.5 GHz were determined, with all three frequencies exhibiting the same pattern. The difference however is the amount of energy coupled to the antenna. Unless the selected frequency matches the resonant frequency, there will be very little energy transmitted. As can be readily seen, the pattern is still controlled primarily by the dominant first order mode, however it appears that other modes are beginning to have an effect. The radiation pattern at 14.5 GHz using 2 parasitic elements positioned 2 mm apart is centered at 35 ^{o} off boresight, has a beamwidth of 50 ^{o} and a normalized gain of 4 dB. The E plane radiation pattern however, does not resemble the expected pattern. It was expected to achieve either a constant 0 dB level, or at least to have the maximum value at boresight (directly overhead at 0 ^{o}). The reason for this discrepancy is still under investigation, however it is believed that the error lies in the simulation of the structure. The equivalent surface definition required for the simulation geometry appears to be very sensitive. Small changes in its location result in significant changes to the E plane pattern, however the H plane pattern remains stable.

An interesting feature is the closer agreement to experimentation at higher frequencies than that achieved through the MSDRA – MSDRA coupling presented in Chapter 4. The difference between this configuration and that used in Chapter 4 is the lack of the higher permittivity insert in the parasitic elements. Thus, a potential reason for the discrepancies between experimentation and simulation is the effect of this insert. As mentioned in the sources of error section in Chapter 4, more research must be conducted on this to obtain conclusive information.

5.5 H Plane Symmetrical Configuration

5.5.1 H Plane Symmetrical Results

The return loss (S_{11}) for the MSDRA with 1 pair of parasitic elements is shown in Figure 46 for both 1 and 2 mm spacing considerations. Figure 47 shows the same characteristic for 2 pairs of parasitic elements. 14 GHz was chosen as the resonant frequency, based on the return loss plots of figures 46 and 47, with the far field radiation patterns presented in figures 48 and 49. The 2 mm spacing configuration with 2 pairs of parasitic elements is compared with experimental data in Figure 50. Return Loss comparisons with the other configurations are included in Annex E.

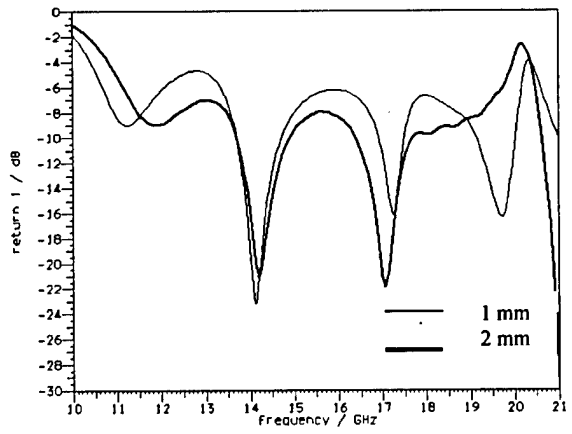

Figure 46: S_{11} for H Plane Symmetrical Coupling (1 pair Parasitic Elements)

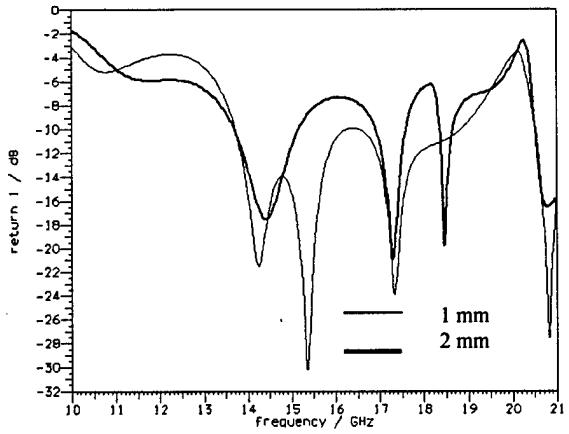

Figure 47: S_{11} for H Plane Symmetrical Coupling (2 pair Parasitic Elements)

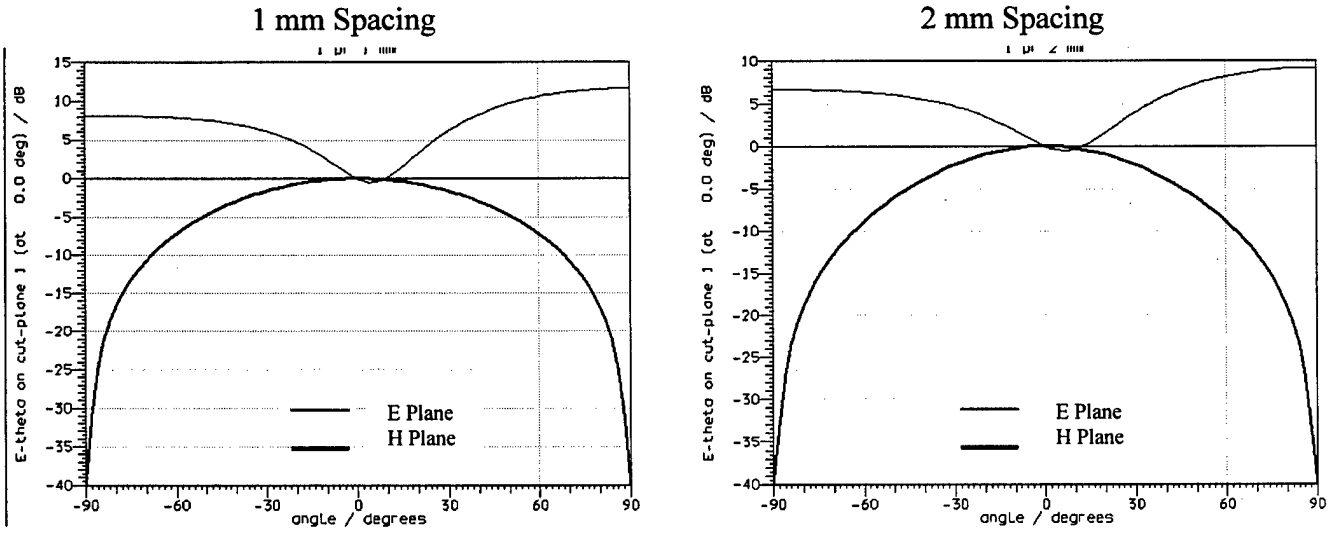

Figure 48: Radiation Pattern with 1 Pair of Parasitic Elements (f = 14 GHz)

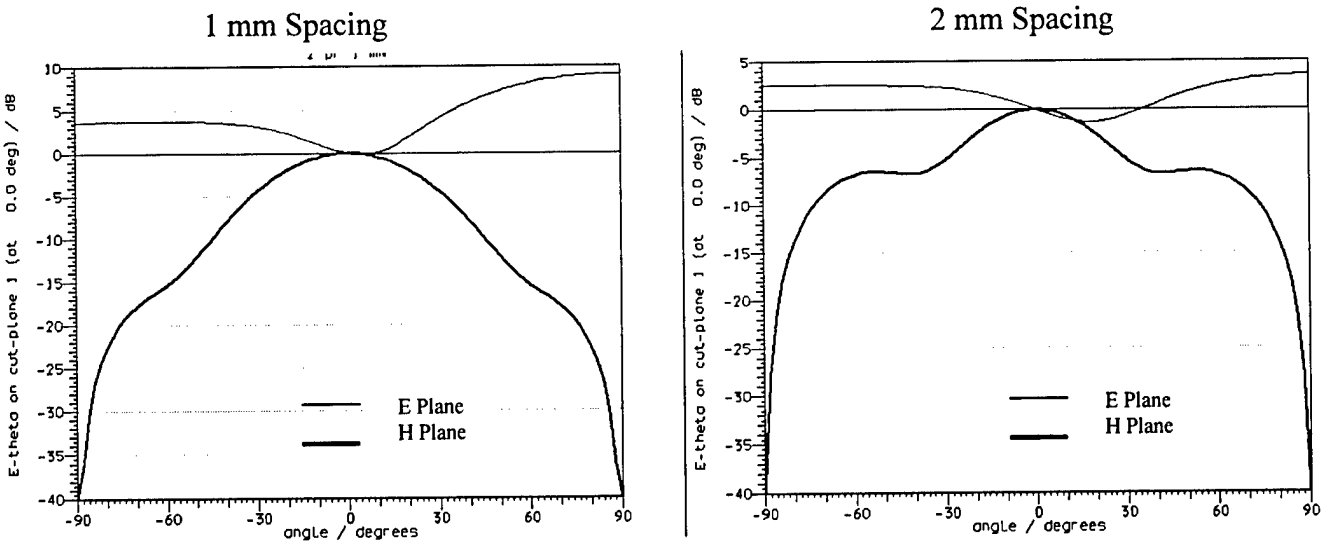

Figure 49: Radiation Pattern with 2 Pairs of Parasitic Elements (f = 14 GHz)

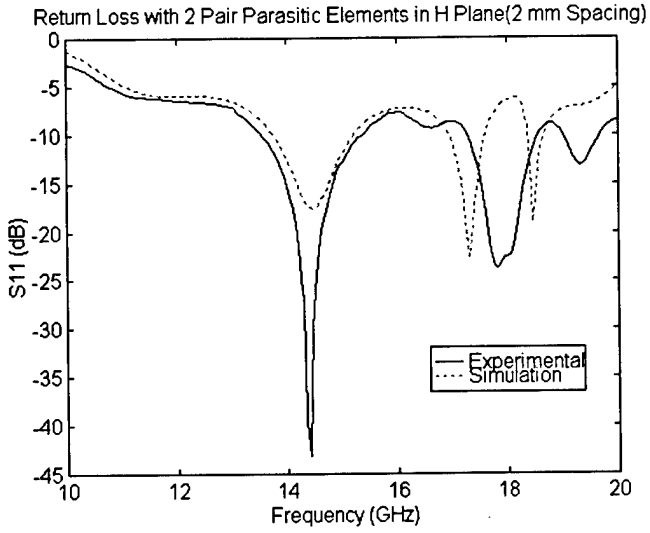

Figure 50: Return Loss Comparison (2 pairs Parasitic Elements)

5.5.2 H Plane Symmetrical Antenna Discussion

This configuration continues to demonstrate the expected results in the H plane radiation pattern characteristics, however the E plane results show the same discrepancies as in the H plane directional case. The reason for this is considered to be for the same equivalent surface definition difficulties. Also, return loss comparisons do not exhibit the same large frequency shifts as were evident in the directional H plane coupling case. The

resonant frequency shift is not as significant, with both configurations exhibiting resonance close to 14 GHz. This is potentially due to the canceling effect that the pair of elements would have on impedance matching, over the asymmetrical case of the previous section.

Examination of the radiation patterns shows a significant narrowing of the beamwidth in the H plane, as expected. The beamwidth narrows from almost 80 ° with one pair of elements to 40 ° with two pair. In this case, the spacing of 1 mm exhibits better radiation characteristics. Although the sidelobes of the curves shown in Figure 49 are significantly different, the beamwidths are virtually the same. Since the goal was to narrow the beamwidth, the choice of the sharper drop in power would be more beneficial, therefore the 1 mm spacing configuration would be preferred. The bandwidth at 1 mm is also significantly greater.

5.6 Summary

The analysis of parasitic coupling presented in this chapter exhibits very beneficial results through the exploitation of the mutual coupling phenomenon. The expected results of wider bandwidths, dual frequency operation and radiation pattern manipulation were all achieved. The small number of elements required to induce a significant change to the radiation pattern is also worthy of note. Having gained confidence in the methodology developed in this study, the analysis could have continued to higher numbers of elements to determine whether the beneficial effects would continue to improve, however this is left for further study. In addition, useful array design information for other applications can be generated using this methodology. The close comparison between experimentation and simulation results also provides a high level of confidence in the analysis developed here using the TLM commercial software.

CHAPTER 6

6.1 Concluding Remarks

The initial step of a basic theoretical review of dielectric resonators was required to set the conditions, and show the necessity of the ensuing investigation into the modal structures of the DRA. Once begun it became quickly apparent that the entire report could have been based on a thorough analysis of this structure, in terms of the behaviour of the electric and magnetic fields within an isolated DRA. A cursory examination was undertaken, but only to confirm that the approximations generally accepted were reasonably accurate, and that the TLM simulations used to analyze these DRAs provided valid results. A brief examination of the internal field structure showed good promise in using the TLM simulations, or any other method of examining the field structure of the DRA, to determine equivalent wavelength, and thus resonant frequency, based on the obtained field structure. Although this seemed promising, the initial desire of examining mutual coupling took over, and further analysis of modal structures was left uncompleted.

The analysis of the modal fields, as well as the resonant frequency comparisons between the values determined by the modified DWM with MMWs, experimentation and TLM simulation provided a good validation process for the TLM software. This instilled the confidence to push on to the analysis of mutual coupling between two similarly fed DRAs. Mutual coupling between DRAs has been previously investigated experimentally, however for different shapes and/or feed mechanisms. As well, all previous analysis commenced with an initial spacing distance of $\lambda/2$. As is evident from the results presented in this report, the analysis of coupling interaction at spacings less than $\lambda/2$ was necessary, not only for element-element interaction in array environments, but also for element-feedline interactions. The rigorous comparison between simulation and experimentation also ensured the accuracy and validity of the conclusions presented. This thorough analysis of mutual coupling led directly into the investigation of practical uses through which the coupling mechanism could be exploited.

Parasitic coupling, which uses the principle of mutual coupling to couple energy from an element fed through normal mechanisms to another "parasitic" element was examined for these practical applications. Previous research has examined bandwidth enhancement and dual frequency applications through the use of parasitically coupled DRAs with different dimensions. The concept of radiation pattern manipulation was proposed as a new application, with very good results obtained. The small number of parasitic elements required indicates a very promising and simple method of producing the desired patterns. The agreement in coupling behaviour between the parasitic configurations examined and the initial mutual coupling analysis help corroborate and emphasize useful practical applications of a phenomenon normally thought of as being strictly detrimental and to be avoided.

6.2 Accomplishments

The accomplishments achieved with respect to the goals initially set out are summarized as follows:

a. The verification of the numerical TLM software, Micro-Stripes ™ was completed. This verification was conducted, not only at the outset, but at every configuration examined. Experimental data was compared, as was results previously published. The close agreement achieved instils a high level of confidence in the ability of this software, and would allow future research to be conducted to a further level without the safety net of experimental confirmation until a much later stage.

b. The dominant mode of a single DRA was thoroughly examined from a resonant frequency perspective, as well as a moderate investigation of the internal field structure. The more complex MSDRA was also examined from both perspectives, with close agreement achieved between the commonly accepted approximations as well as experimental measurement. Both the aperture coupling technique and the direct microstrip coupling

technique was investigated, with each exhibiting expected results. The choice of coupling method is predominantly dependent on feed complexity and is therefore application intended.

c. The mutual coupling effect between two rectangular MSDRAs was completely characterized, from spacings of 1 mm through to 100 mm (4.5 λ). The results obtained provide a good representation of the effects of element proximities, and even characterized the effects of microstrip feed line proximities.

d. This analysis of mutual coupling culminated in an investigation of positive, practical applications. Parasitic coupling was successfully utilized between a very few number of elements in manipulating radiation patterns to produce E and H plane beam patterns with significant squint angles, to the extent of an endfire application in the E plane. Beamwidth reduction was also accomplished with an H plane initial beamwidth of some 85 degrees reduced to 40 degrees. Success in achieving increased bandwidths was also achieved.

6.3 Future Work

There are very few research activities that either meet all their initial goals in the time frame allotted, or do not raise more research areas during the process. This is certainly not one of those. Some of the more interesting topics are mentioned here for areas that require further investigation;

a. As mentioned in the accomplishments, modal analysis was not pursued further. The simulations conducted indicate that there is a wealth of data available with which the internal modal structure of a DRA can be completely analyzed. Higher order modes are an additional aspect that has yet to be examined.

b. The analysis of mutual coupling examined one specific MSDRA configuration. Although comparisons were made to probe fed cylindrical as well as aperture fed rectangular DRAs, the complete characterization of mutual coupling for other dielectric resonator shapes is yet to be conducted.

c. The examination of parasitic coupling, although novel, once again only examined one specific rectangular configuration, and two uniform spacing distances. It is assumed that the mutual coupling effects would be similar for other shapes or even similar shapes with different dimensions, however due to the lack of closed form solutions, and the requirement for approximation methods or numerical method simulations, complete characterization of the effect is not possible without examinations of each and every case. The advantages of utilizing a simulation process become quickly apparent from this analysis. Further investigation into additional spacing considerations and number of parasitic elements could be combined with experimental confirmation of the final design.

d. The radiation pattern simulations for H plane parasitic coupling must also be re-examined. The results obtained for the E plane patterns do not agree with expectations, and simulations using different equivalent surface locations do not produce consistent results. The problem appears to be in the E plane only, since consistent results remain in the H plane patterns.

6.5 Summary

The results presented in this report confirm the validity of the approximation methods currently used, as well as the accuracy of the TLM software used for the simulation of the DRA structures. The effects of mutual coupling between two microstrip fed MSDRAs are presented. A novel method of manipulating radiation patterns through the exploitation of mutual coupling is presented.

REFERENCES

[A&F 96] Y.M.M. Antar & Z. Fan, Theoretical Investigation of Aperture Coupled Rectangular Dielectric Resonator, *IEE Proceedings Microwave Antenna Propagation,* Vol. 143, No 2, April 1996, pp 113-118.

[A,C,S,H&K98] Y.M.M. Antar, D. Cheng, G Seguin, B. Henry & M. Keller, Modified Waveguide Model For Rectangular Dielectric Resonator Antenna, submitted to Microwave and Optical Technology Letters

[Bala 82] C.A. Balanis, Antenna Theory, John Wiley and Sons, New York, 1982

[B&G 81] M.T. Birand & R.V. Gelsthorpe, Experimental Millimetric Array Using Dielectric Resonators Fed by means of a Dielectric Waveguide, *Electronic Letters*, 3 Sept 1981, Vol 17, No 18, pp 633-635.

[C,P,I&W 96] M. Cooper, A. Petosa, A. Ittipiboon, & J.S. Wight, Investigation of Dielectric Resonator Antennas for L-Band Communications, ANTEM-96, Montreal, 1996, pp 167-170.

[F&A 97] Z. Fan and Y.M.M. Antar, Slot Coupled DR Antenna for Dual Frequency Operation, *IEEE Transactions on Antennas and Propagation*, Vol 45, No 2, February 1997, pp 306-308.

[F,A,I&P 96] Z Fan, Y.M.M. Antar, A. Ittipiboon, and A. Petosa, Parasitic coplanar three-element dielectric resonator antenna subarray, *Electronic Letters*, 25 April 1996, Vol 32, No 9, pp 789-790.

[G&G 77] P Guillon, Y. Garault, Accurate Resonant Frequencies of Dielectric Resonators, *MTT-25*, No 11, Nov 1977, pp 916-922.

[Hawe 96] I.D. Hawes, A New Dielectric Archimedean Spiral Travelling Wave Antenna. M.Eng Thesis, Royal Military College of Canada, Kingston 1996.

[I,C,M,B&A 93]A Ittipiboon, M Cuhaci, R.K. Mongia, P. Bhartia, Y.M.M. Antar, Aperture Fed Rectangular and Triangular Dielectric Resonators for use as Magnetic Dipoole Antennas, *Electronic Letters,* 11 Nov 1993, Vol 29, No 23, pp 2001-2002.

[Itoh 89] T. Itoh,ed. Numerical Techniques for Microwave and Millimeter-Wave Passive Structures, John Wiley and Sons, New York, 1989.

[J&B 68] E.C Jordan and K.G. Balmain, Electromagnetic Waves and Radiating Systems, Prentice-Hall, New Jersey, 1968, pp 188.

[J,P&C 81] R.P. Jedlinka, M.T. Poe & K.R. Carver, "Measured Mutual Coupling Between Microstrip Antennas", *IEEE Transactions on Antennas and Propagation*, Jan 81, Vol AP-29, No 1, pp 147-149.

[KCC 97] Kimberley Communication Systems, Micro-Stripes User's Manual, Nottingham, U.K., 1997.

[K,R,A&I 95] M.G. Keller, D. Roscoe, Y.M.M. Antar, A. Ittipiboon, Active Millimetre-Wave Aperture Coupled Microstrip Patch Antenna Array, *Electronic Letters*, 5 Jan 1995, Vol 31, No 1, pp 2-3.

[K,A&K 89] A.A. Kishk, B. Ahn, D. Kajfez, Broadband Stacked Dielectric Resonator Antennas, *Electronic Letters*, 17 Mar 1989, Vol 25, No 18, pp 1232-1233.

[K,I,A&C 93] A.A. Kishk, A. Ittipiboon, Y.M.M. Antar, M. Cuhaci, Dielectric Resonator Antenna Fed by a Slot in the Ground Plane of a Microstrip Line, *Proc. Eight Int. Conf. On Antennas and Propagation ICAP '93*, April 1993, Part 1, pp 540-543.

[L&A 94] G.D. Loos & Y.M.M. Antar, A New Aperture-coupled Rectangular Dielectric Resonator Antenna Array, Microwave and Optical Technology Letters, Vol 7, No 14, October 5 1994, pp 677-678

[L,K,T&C 80] J.F. Legier, P. Kennis, S. Toutain, J. Citerne, Resonant Frequencies of Rectangular Dielectric Resonators, *MTT-28,* No 9, Sept 1980, pp 1031-1034.

[Loos 94] G.D. Loos, Investigation of a Novel Aperture Coupled Rectangular Dielectric Resonator Antenna Array, M.Eng Thesis, Royal Military College of Canada, Kingston, 1994.

[L,L&L 94] K.M.Luk, W.K. Leung and K.W. Leung, Mutual Impedance of Hemispherical Dielectric Resonator Antennas, *IEEE Transactions on Antennas and Propagation*, Vol 42, No 12, December 1994.

[Marc 69] E.A.J. Marcatili, Dielectric Rectangular Waveguide and Directional Coupler for Integrated Optics, *Bell Systems Technical Journal,* Vol 48 September 1969, pp 2071-2102.

[Mart 90] J.T.H. St. Martin, Aperture Coupling of Circular Cylindrical Dielectric Resonator Antennas, M Eng Thesis, Royal Military College of Canada, 1990.

[M,A,K,I&C 90]J.T.H. St Martin, Y.M.M. Antar, A.A. Kishk, A. Ittipiboon, M. Cuhachi, Dielectric Resonator Antenna Using Aperture Coupling, *Electronic Letters*, Vol 26, 1990, pp 2015-2016.

[M&B 94] R.K. Mongia & P Bhartia, A Review and General Design Relations for Resonant Frequency and Bandwidth, *International Journal of Microwave and Millimeter-Wave Computer Aided Engineering,* Vol 4, No 3, 1994, pp 230-247.

[M&I 97] R.K. Mongia and A. Ittipiboon, Theoretical and Experimental Investigations on Rectangular Dielectric Resonator Antennas, *IEEE Transactions on Antennas and Propagation,* Vol 45, No 9, September 1997, pp 1348-1356.

[M,I&C 94a] R.K. Mongia, A. Ittipiboon, M. Cuhaci, Measurement of Radiation Efficiency of Dielectric Resonator, *IEEE Microwave and Guided Wave Letters*, Vol 4, No 3, March 1994, pp 80-82.

[M,I&C 94b] R.K. Mongia, A. Ittipiboon, M. Cuhaci, Low Profile Dielectric Resonator Antennas using a Very High Permittivity Material, *Electronic Letters*, 18 August 1994, Vol 30, No 17, pp 1362-1363.

[M,I,C&R 94]R.K. Mongia, A. Ittipiboon, M. Cuhaci, D. Roscoe, Circularly Polarized Dielectric Resonator Antenna, *Electronic Letters*, 18 August 1994, Vol 30, No 17, pp 1361-1362.

[M,L&C 83] M.W. McAllister, S.A. Long, G.L. Conway, Rectangular Dielectric Resonator Antenna, *Electronic Letters*, 17 Mar 1983, Vol 19, No 6, pp 218-219.

[Mong 88] R.K. Mongia, Theoretical and Experimental Investigations on Dielectric Resonators. Ph.D Thesis, Centre for Applied Research in Electronics, Indian Institute of Technology, Delhi, 1988.

[Mong 92] R.K. Mongia, Theoretical and Experimental Resonant Frequencies of Rectangular Dielectric Resonators, *IEE Proceedings* – H, Vol 139, No 1, February 1992, pp 98-104.

[O&B 62] A.K. Okaya & L.F. Barash, The Dielectric Microwave Resonator, *IRE Proceedings,* Vol 50, October 1962, pp 2081-2092.

[Oliv 95] M.B. Oliver, Circularly Polarized Rectangular Dielectric Resonator Antenna using a Single Feed. M.Eng Thesis, Royal Military College of Canada, Kingston, 1996.

[P&H 69] D.T. Paris, F.K. Hurd, Basic Electromagnetic Theory, McGraw-Hill, New York, 1969, p 166.

[P&R 81] J.K. Plourde, Chung-Li Ren, Application of Dielectric Resonators in Microwave Components, *MTT-29*, No 8, Aug 1981, pp 754-770.

[P,C,S,I&R 96] A Petosa, M Cuhaci, N.R.S. Simon, A Ittipiboon, R. Larose, Microstrip-Fed Stacked Dielectric Resonator Antenna, *ANTEM-96*, pp 705-708.

[P,I,C&R 96] A. Petosa, A. Ittipiboon, M. Cuhaci, R. Larose, Bandwidth Improvements for a Microstrip-Fed Series Array of Dielectric Resonator Antennas, *Electronic Letters*, Vol 32, No 7, March 96, pp 608-609.

[P,L,I&C 97] A. Petosa, R. Larose, A. Ittipiboon, M. Cuhaci, Active Phased Array of Dielectric Resonator Antennas, IEEE AP-S 1997, Vol 2, pp 690 – 693.

[P,M,I&W 95] A. Petosa, R.K. Mongia, A. Ittipiboon, J.S. Wight, Design of Microstrip-fed Series Array of Dielectric Resonator Antennas, *Electronic Letters*, 3 Aug 1995, Vol 31, No 16, pp 1306-1307.

[P,M,I&W 95] A. Petosa, R.K. Mongia, A. Ittipiboon, & J.S. Wight, Investigation of Various Feed Structures for Linear Arrays of Dielectric resonator Antennas, *IEEE AP-S 95,* Newport Beach, June 1995, pp 1982-1985.

[P,S,S,I&M 98] A Petosa, N.R.S. Simon, R Siushansian, A Ittipiboon, M Cuhaci, Design and Analysis of Multi-Segment Dielectric Resonator Antennas, Submitted to MTT.

[Poza 82] D.M. Pozar, Input Impedance and Mutual Coupling of Rectangular Microstrip Antennas, *AP-30,* No 6, Nov 1982, pp 1191-1193.

[Poza 83] D.M. Pozar, Considerations for Millimeter Wave Printed Antennas, *IEEE Transactions on Antennas and Propagation*, AP-31, No 5, September 1983, pp 740-747.

[Poza 85] D.M. Pozar, Microstrip Antenna Aperture Coupled to a Microstripline, *Electronic Letters*, 17 January 1985, Vol 21, No 2, pp 49-50.

[Poza 90] D.M. Pozar, Microwave Engineering, Addison-Wesley Publishing Co, New York, 1990, pp 267-276.

[Rich 39] R.D. Richtmyer, Dielectric Resonators, *Journal of Applied Physics,* Vol 10, June 1939, pp 391-398.

[S&L 94] S.M. Shum, K.M. Luk, Analysis of Aperture Coupled Rectangular Dielectric Resonator Antenna, *Electronic Letters*, 13 Oct 1994, Vol 30, No 21, pp 1726-1727.

[S&N 66] J.C. Sethares, S.J. Naumann, Design of Microwave Dielectric Resonators, *MTT-14,* No 1, Jan 1966, pp 2-7.

[VanB 75b] J. Van Bladel, The Excitation of Dielectric Resonators of Very High Permittivity, *MTT-23,* No 2, February 1975, pp 208-218.

[VanB 75a] J. Van Bladel, On the Resonances of a Dielectric Resonator of Very High Permittivity, *MTT-23,* No 2, February 1975, pp 199-208.

[Yagi 28] H. Yagi, Beam Transmission of Ultra Short Waves, *Proc IEEE*, Vol 72, No 5, May 1984, pp 634-645.

[Yee 65] H.Y. Yee, Natural Resonant Frequencies of Microwave Dielectric Resonators, *MTT-13*, March 1965, pp 256.

ANNEX A

Micro-Stripes Geometric Code Representative Examples

This annex contains the MicroStripes™ geometric code input files for three representative configurations. The first configuration is a single aperture coupled rectangular DRA, while the second and third configurations are two direct microstrip fed MSDRAs located 5 mm apart, and oriented for measurements of their mutual coupling levels.

A1.1 Sample A: Aperture Coupled Rectangular DRA

```
data_id  Dielectric Radiator

work_space
  brick
    corner; coords       -10m      -3.5m       -10m
    corner; coords        10m        10m        10m


# Microstrip feed line
metal
  colour 250 230  10
  brick
    corner; coords       -10m          0      -300u
    corner; coords       2.7m          0       300u

# Termination of line
metal
  surface_impedance 95
  colour 250   0   0
  brick
    corner; coords       -10m          0      -300u
    corner; coords       -10m       640u       300u

# Substrate
medium
  epsr  10.2
  colour 100 230 250
  brick
    corner; coords         -1          0         -1
    corner; coords          1       640u          1

# Ground Plane
metal
  colour 200 150  10
  intersectnot
    brick
      corner; coords         -1       640u         -1
      corner; coords          1       640u          1
    brick
      corner; coords       -600u       640u      -3.05m
      corner; coords        600u       640u       3.05m

# Dielectric Resonator
medium
  epsr  37.84
  colour 150 150 150
  brick
    corner; coords    -7.385m       640u    -4.385m
    corner; coords     1.385m      4.15m     4.385m

output
```

```
  time_domain
    # Outer port
    point
      coords      -9.5m       320u          0
      field Ey Hz
    # Inner port
    point
      coords      -5.5m       320u          0
      field Ey Hz

space_domain
    frequency 5.244G 6.855G 7.473G
    brick
      corner; coords    -7.5m       -300u    -4.5m
      corner; coords     1.5m      4.5m     4.5m
      field Er Ei Hr Hi Kr Ki partial_equivalent_surface
initial_mode
  brick
    corner; coords     -9.99m      -3.5m       -10m
    corner; coords     -9.99m        10m        10m

  initial
    brick
      corner; coords     -9.99m          0      -300u
      corner; coords     -9.99m       640u       300u
    E          0         -1          0
  frequency 0

mesh
  cubic
    cell_size 500u
    work_space
      brick
        corner; coords       -10m      -3.5m       -10m
        corner; coords        10m        10m        10m
    boundaries
      xmin  absorbing
      xmax  absorbing
      ymin  absorbing
      ymax  absorbing
      zmin  absorbing
      zmax  absorbing
    duration_times_c 1
    x
      cell_face 0
    y
      cell_face 0
    z
      cell_face 0
  rectangular
    cell_size 300u
    work_space
      brick
        corner; coords       -10m      -3.5m          0
        corner; coords        10m        10m        10m
    boundaries
      xmin  absorbing
```

```
  xmax  absorbing
  ymin  absorbing
  ymax  absorbing
  zmin  magnetic_wall
  zmax  absorbing
  space_truncation  unchecked
duration_times_c 2
x
  cell_face -10m
  cells     9
  cell_face -7.385m
  cells     23
  cell_face -600u
  cells     4
  cell_face 600u
  cells     3
  cell_face 1.385m
  cells     5
  cell_face 2.7m
  cells     25
  cell_face 10m
y
  cell_face -3.5m
  cells     12
  cell_face 0
  cells     3
  cell_face 640u
  cells     10
  cell_face 4.15m
  cells     19
  cell_face 10m
z
  cell_face -10m
  cells     26
  cell_face -4.385m
  cells     5
  cell_face -3.05m
  cells     10
  cell_face -300u
  cells     2
  cell_face 300u
  cells     10
  cell_face 3.05m
  cells     5
  cell_face 4.385m
  cells     26
  cell_face 10m
```

A2.1 E Plane MSDRA - MSDRA Mutual Coupling (5 mm)

```
data_id  E Plane Coupling of Dielectric Radiators over microstrip line

work_space
  brick
    corner; coords      -17.5m       -500u       -15m
    corner; coords       17.5m         10m        15m


# Ground Plane
metal
  colour 200 150  10
  brick
    corner; coords          -1           0         -1
    corner; coords           1           0          1

# Substrate
medium
  epsr  3
  colour 230 230 250
  brick
    corner; coords          -1           0         -1
    corner; coords           1        762u          1

# PORT 1
# Microstrip feed line
metal
  colour 250 230  10
  brick
    corner; coords      -17.5m        762u       -950u
    corner; coords       -2.5m        762u        950u

# End termination
metal
  surface_impedance 249
  colour 250   0   0
  brick
    corner; coords      -17.5m           0       -950u
    corner; coords      -17.5m        762u        950u

# Dielectric Resonator
# Insert
medium
  epsr  40
  colour 150 150 150
  brick
    corner; coords    -10.375m        762u       -950u
    corner; coords       -2.5m     1.397m        950u

# Top
medium
```

```
  epsr  10
  colour 150 150 150
  brick
    corner; coords   -10.375m      1.397m       -950u
    corner; coords      -2.5m      4.572m        950u

# PORT 2
# Microstrip feed line
metal
  colour 250 230  10
  brick
    corner; coords       2.5m       762u       -950u
    corner; coords      17.5m       762u        950u

# End termination
metal
  surface_impedance 249
  colour 250   0   0
  brick
    corner; coords      17.5m         0       -950u
    corner; coords      17.5m       762u        950u

# Dielectric Resonator
# Insert
medium
  epsr  40
  colour 150 150 150
  brick
    corner; coords       2.5m       762u       -950u
    corner; coords    10.375m      1.397m        950u

# Top
medium
  epsr  10
  colour 150 150 150
  brick
    corner; coords       2.5m      1.397m       -950u
    corner; coords    10.375m      4.572m        950u

output
  time_domain
    # Port 1
    point
      coords       -15m       350u          0
      field Ey Hz
    point
      coords       -12m       350u          0
      field Ey Hz
    # Port 2
    point
      coords        16m       350u          0
      field Ey Hz
    point
      coords        13m       350u          0
      field Ey Hz

initial_mode
```

```
  brick
    corner; coords    -17.49m       -500u        -15m
    corner; coords    -17.49m         10m         15m

  initial
    brick
      corner; coords    -17.49m          0       -950u
      corner; coords    -17.49m        762u       950u
    E          0          1          0
  frequency 0

mesh
  cubic
    cell_size 200u
    work_space
      brick
        corner; coords     -17.5m       -500u        -15m
        corner; coords      17.5m         10m         15m
    boundaries
      xmin  absorbing
      xmax  absorbing
      ymin  absorbing
      ymax  absorbing
      zmin  absorbing
      zmax  absorbing
    duration_times_c 500m
    x
      cell_face 0
    y
      cell_face 0
    z
      cell_face 0
  rectangular
    cell_size 200u
    work_space
      brick
        corner; coords     -17.5m          0           0
        corner; coords      17.5m         10m         15m
    boundaries
      xmin  absorbing
      xmax  absorbing
      ymin  electric_wall
      ymax  absorbing
      zmin  magnetic_wall
      zmax  absorbing
      space_truncation  unchecked
    duration_times_c 2
    x
      cell_face -17.5m
      cells     10
      cell_face -10.375m
      cells     40
      cell_face -2.5m
      cells     10
      cell_face 2.5m
      cells     40
      cell_face 10.375m
```

```
  cells      10
  cell_face 17.5m
y
  cell_face -500u
  cells      3
  cell_face 0
  cells      3
  cell_face 762u
  cells      4
  cell_face 1.397m
  cells      10
  cell_face 4.572m
  cells      10
  cell_face 10m
z
  cell_face -15m
  cells      20
  cell_face -950u
  cells      5
  cell_face 0
  cells      5
  cell_face 950u
  cells      20
  cell_face 15m
```

A3.1 H Plane MSDRA - MSDRA Mutual Coupling (5 mm)

```
data_id  H Plane Coupling of Dielectric Radiators over microstrip line

work_space
  brick
    corner; coords      -19.4m       -500u        -11m
    corner; coords       19.4m         10m         11m


# Ground Plane
metal
  colour 200 150  10
  brick
    corner; coords          -1           0          -1
    corner; coords           1           0           1

# Substrate
medium
  epsr  3
  colour 230 230 250
  brick
    corner; coords          -1           0          -1
    corner; coords           1        762u           1

# PORT 1
# Microstrip feed line
metal
  colour 250 230  10
  brick
    corner; coords       -4.4m        762u        -11m
    corner; coords       -2.5m        762u     3.9375m

# End termination
metal
  surface_impedance 249
  colour 250   0   0
  brick
    corner; coords       -4.4m           0        -11m
    corner; coords       -2.5m        762u        -11m

# Dielectric Resonator
# Insert
medium
  epsr  40
  colour 150 150 150
  brick
    corner; coords       -4.4m        762u    -3.9375m
    corner; coords       -2.5m     1.397m     3.9375m

# Top
medium
  epsr  10
```

```
  colour 150 150 150
  brick
    corner; coords      -4.4m     1.397m   -3.9375m
    corner; coords      -2.5m     4.572m    3.9375m

# PORT 2
# Microstrip feed line
metal
  colour 250 230  10
  brick
    corner; coords       2.5m       762u   -3.9375m
    corner; coords       4.4m       762u        11m

# End termination
metal
  surface_impedance 249
  colour 250   0   0
  brick
    corner; coords       2.5m         0         11m
    corner; coords       4.4m       762u        11m

# Dielectric Resonator
# Insert
medium
  epsr  40
  colour 150 150 150
  brick
    corner; coords       2.5m       762u   -3.9375m
    corner; coords       4.4m     1.397m    3.9375m

# Top
medium
  epsr  10
  colour 150 150 150
  brick
    corner; coords       2.5m     1.397m   -3.9375m
    corner; coords       4.4m     4.572m    3.9375m

output
  time_domain
    # Port 1
    point
      coords     -3.45m       350u       -9m
      field Ey Hx
    point
      coords     -3.45m       350u       -6m
      field Ey Hx
    # Port 2
    point
      coords      3.45m       350u       10m
      field Ey Hx
    point
      coords      3.45m       350u        7m
      field Ey Hx

initial_mode
  brick
```

```
    corner; coords      -19.4m       -500u     -10.99m
    corner; coords       19.4m         10m     -10.99m

  initial
    brick
      corner; coords       -4.4m           0     -10.99m
      corner; coords       -2.5m        762u     -10.99m
    E          0           1           0
  frequency 0

mesh
  cubic
    cell_size 200u
    work_space
      brick
        corner; coords      -19.4m       -500u        -11m
        corner; coords       19.4m         10m         11m
    boundaries
      xmin  absorbing
      xmax  absorbing
      ymin  absorbing
      ymax  absorbing
      zmin  absorbing
      zmax  absorbing
    duration_times_c 500m
    x
      cell_face 0
    y
      cell_face 0
    z
      cell_face 0
  rectangular
    cell_size 200u
    work_space
      brick
        corner; coords      -19.4m           0        -11m
        corner; coords       19.4m         10m         11m
    boundaries
      xmin  absorbing
      xmax  absorbing
      ymin  electric_wall
      ymax  absorbing
      zmin  absorbing
      zmax  absorbing
      space_truncation  unchecked
    duration_times_c 2
    x
      cell_face -19.4m
      cells     20
      cell_face -4.4m
      cells     10
      cell_face -2.5m
      cells     10
      cell_face 2.5m
      cells     10
      cell_face 4.4m
      cells     20
```

```
  cell_face 19.4m
y
  cell_face -500u
  cells     2
  cell_face 0
  cells     3
  cell_face 762u
  cells     4
  cell_face 1.397m
  cells     10
  cell_face 4.572m
  cells     10
  cell_face 10m
z
  cell_face -11m
  cells     10
  cell_face -3.9375m
  cells     40
  cell_face 3.9375m
  cells     10
  cell_face 11m
```

ANNEX B

Mutual Coupling Comparisons of Experimental and Simulation data

This Annex contains the plots that show the comparisons between experimentation and simulation results. The curves are the coupling characteristics (S_{21}) for all three (MSDRA –MSDRA, MSDRA – Line, and Line – Line) configurations. Plots are presented for the coupling in both planes at various spacing distances.

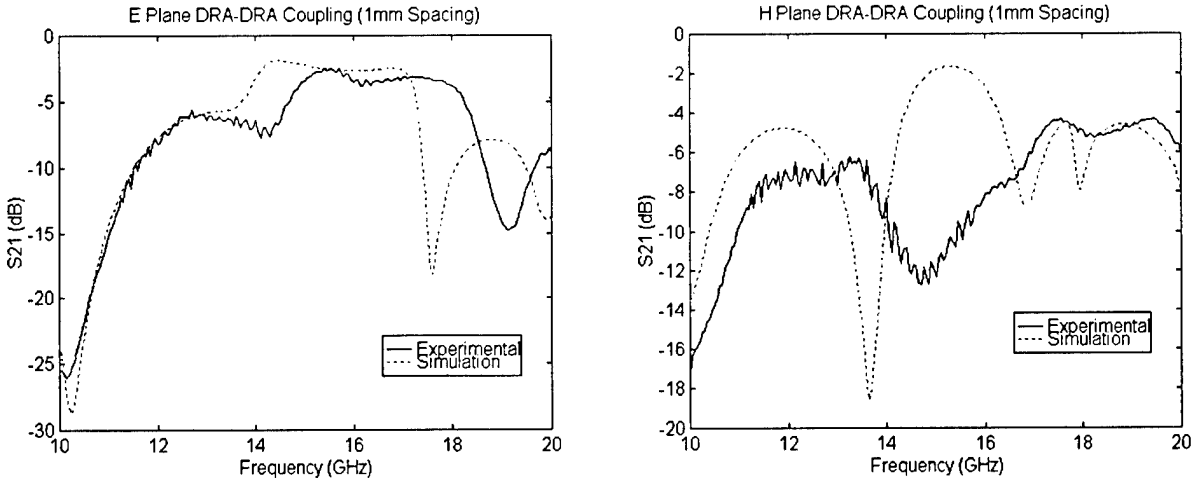

Figure B1: MSDRA-MSDRA Coupling Comparisons (1 mm)

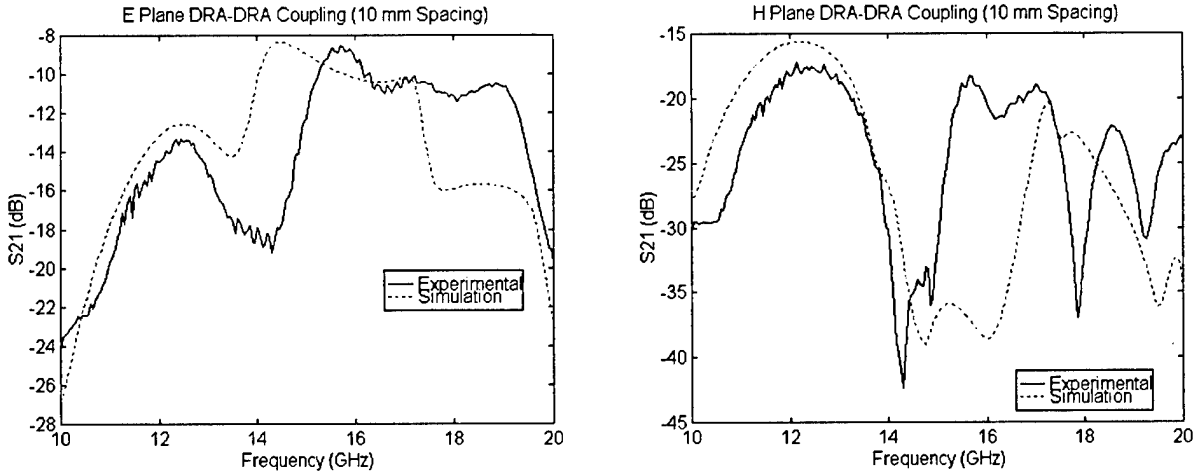

Figure B2: MSDRA-MSDRA Coupling Comparisons (10 mm)

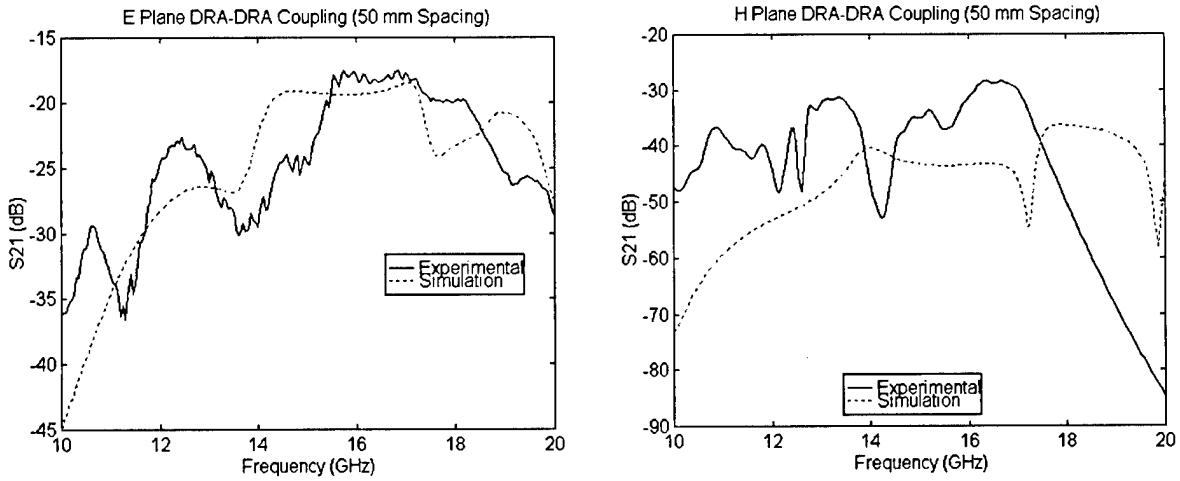

Figure B3: MSDRA-MSDRA Coupling Comparisons (50 mm)

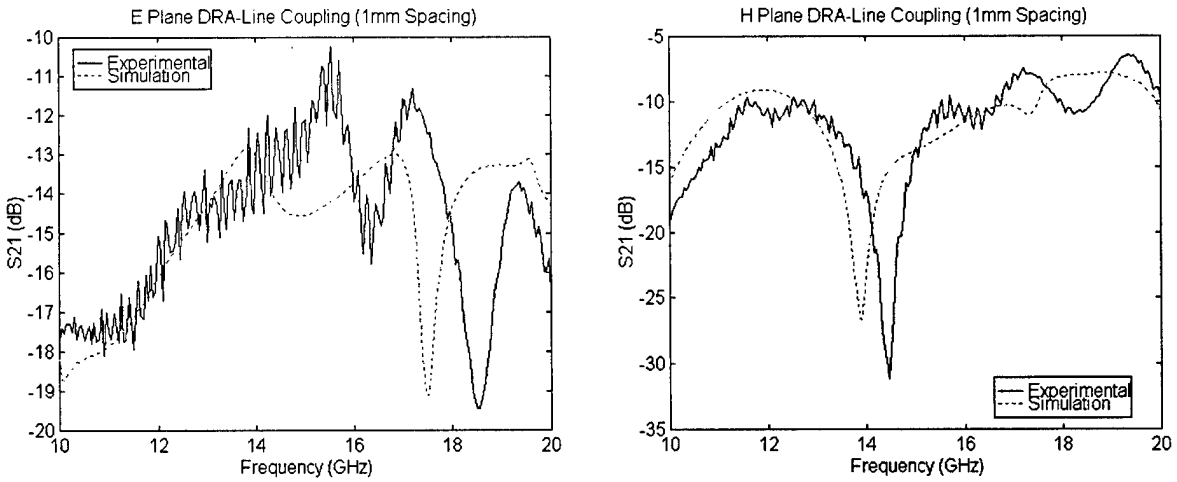

Figure B4: MSDRA-Line Coupling Comparisons (1 mm)

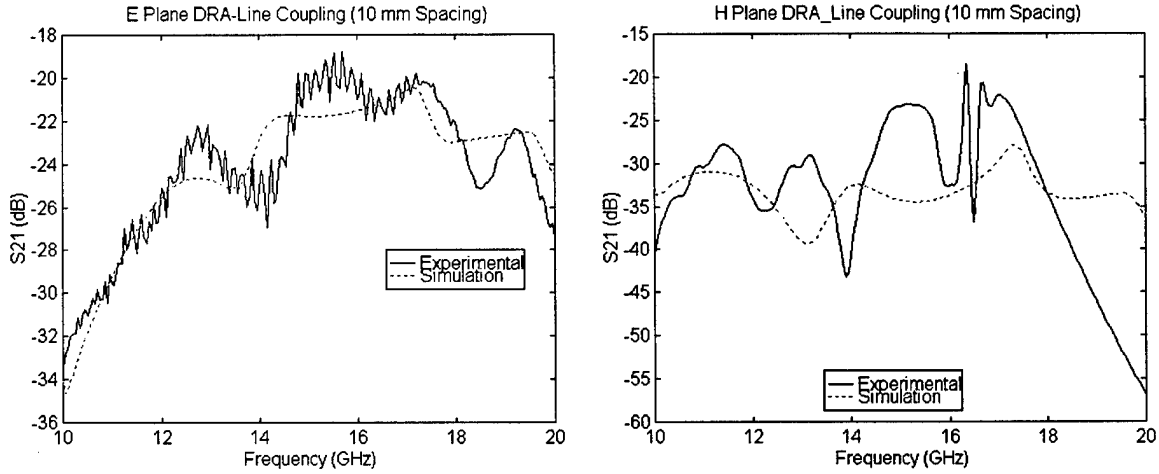

Figure B5: MSDRA-Line Coupling Comparisons (10 mm)

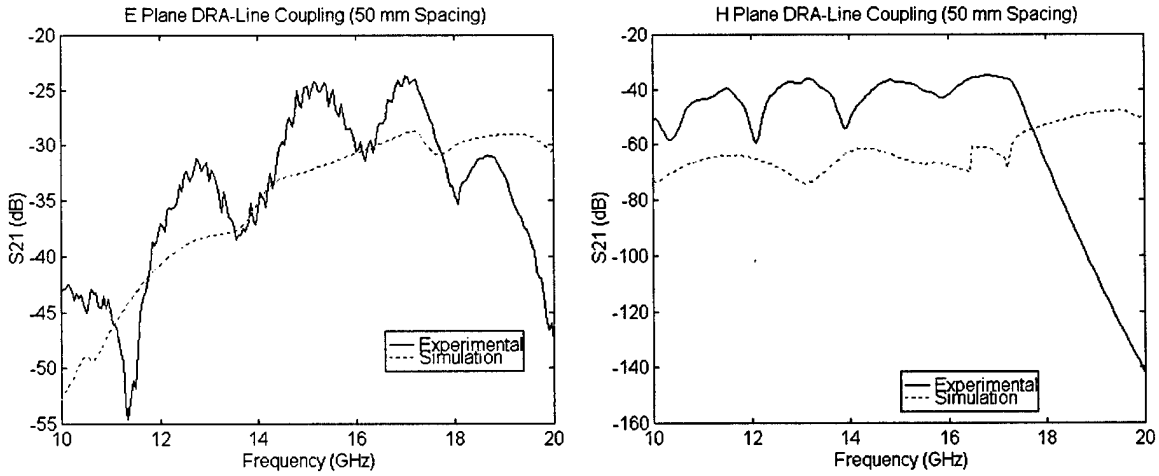

Figure B6: MSDRA-Line Coupling Comparisons (50 mm)

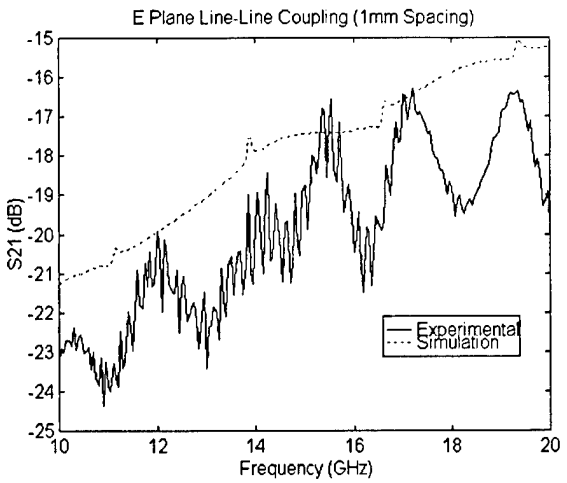

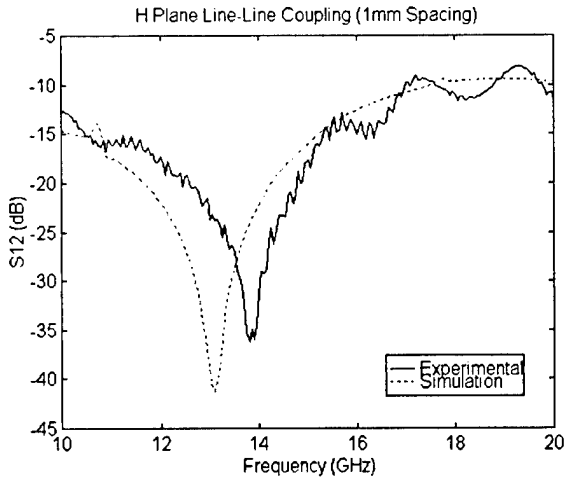

Figure B7: Line-Line Coupling Comparisons (1 mm)

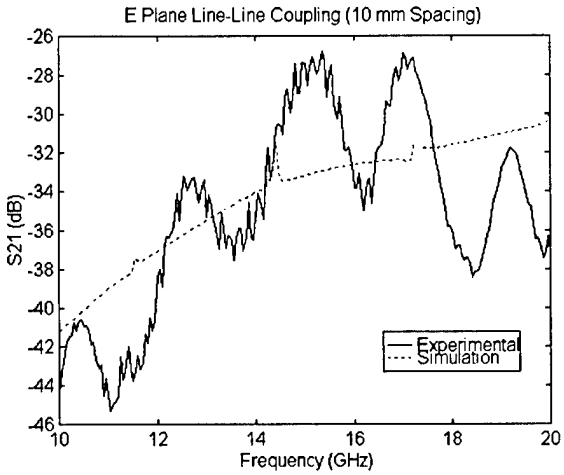

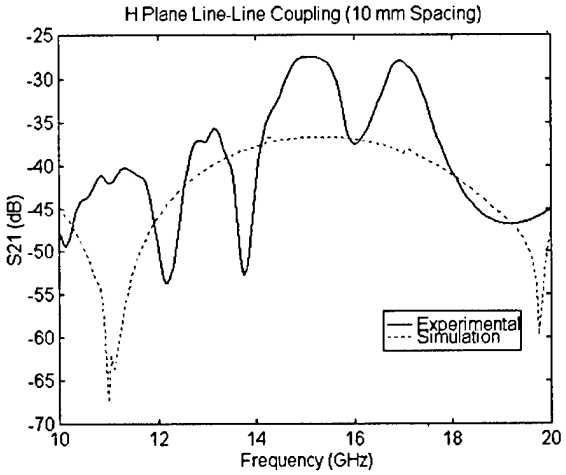

Figure B8: Line-Line Coupling Comparisons (10 mm)

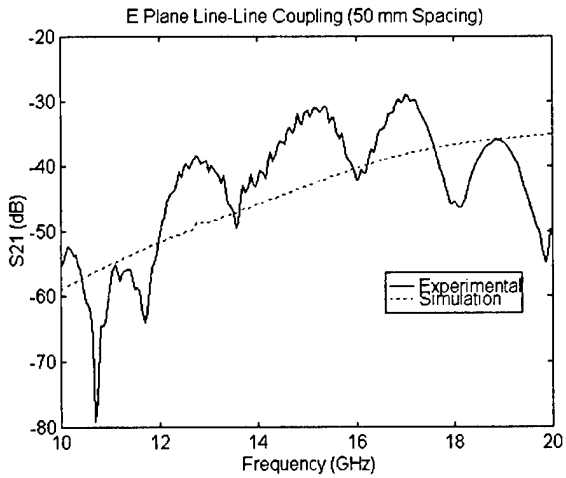

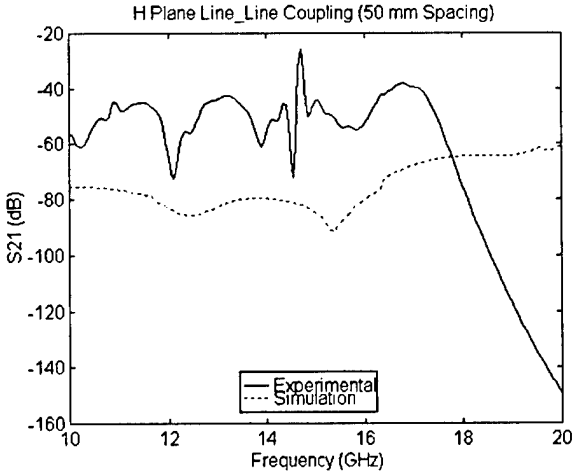

Figure B9: Line-Line Coupling Comparisons (50 mm)

ANNEX C

Mutual Coupling Simulation Data

This Annex contains the plots that show the mutual coupling configuration scattering parameters of the simulation data. The curves are the return (S_{11}) and coupling characteristics (S_{21}) for all three (MSDRA –MSDRA, MSDRA – Line, and Line – Line) configurations. Plots are presented for the coupling in both planes at all simulated spacing distances.

E Plane

H Plane

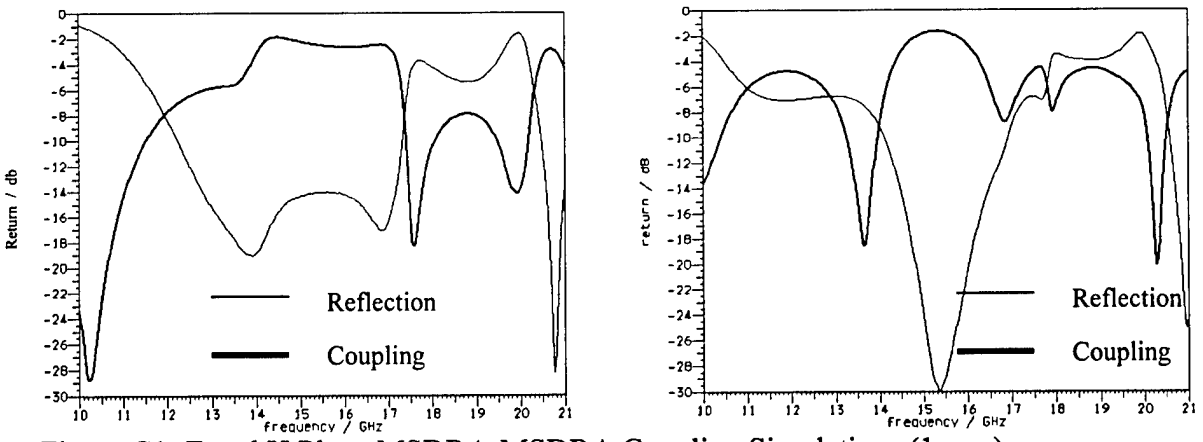

Figure C1: E and H Plane MSDRA-MSDRA Coupling Simulations (1 mm)

E Plane

H Plane

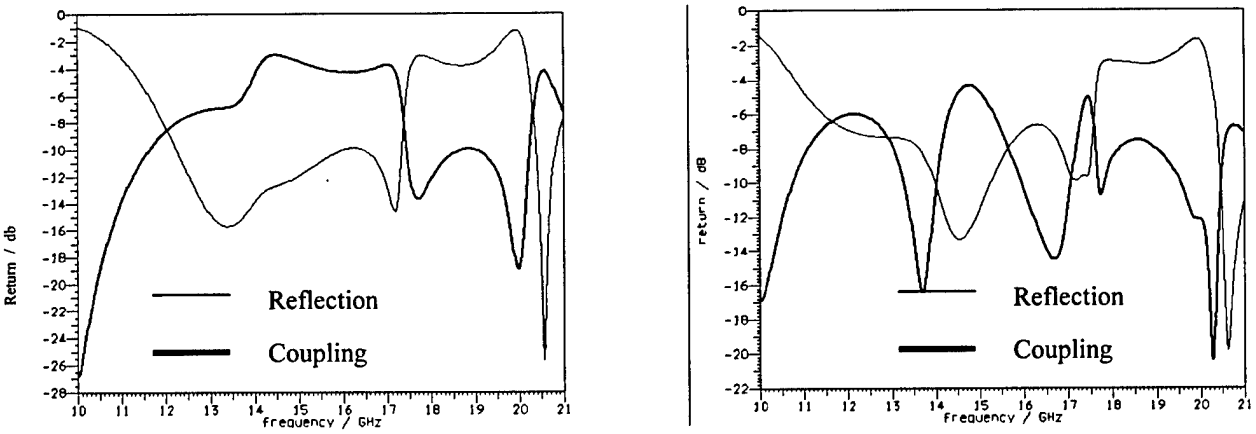

Figure C2: E and H Plane MSDRA-MSDRA Coupling Simulations (2 mm)

E Plane

H Plane

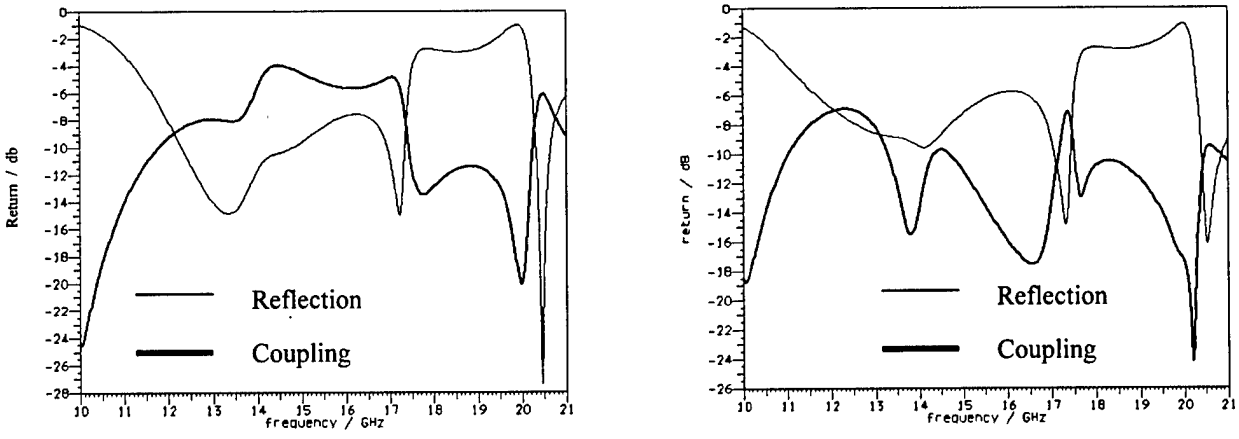

Figure C3: E and H Plane MSDRA-MSDRA Coupling Simulations (3 mm)

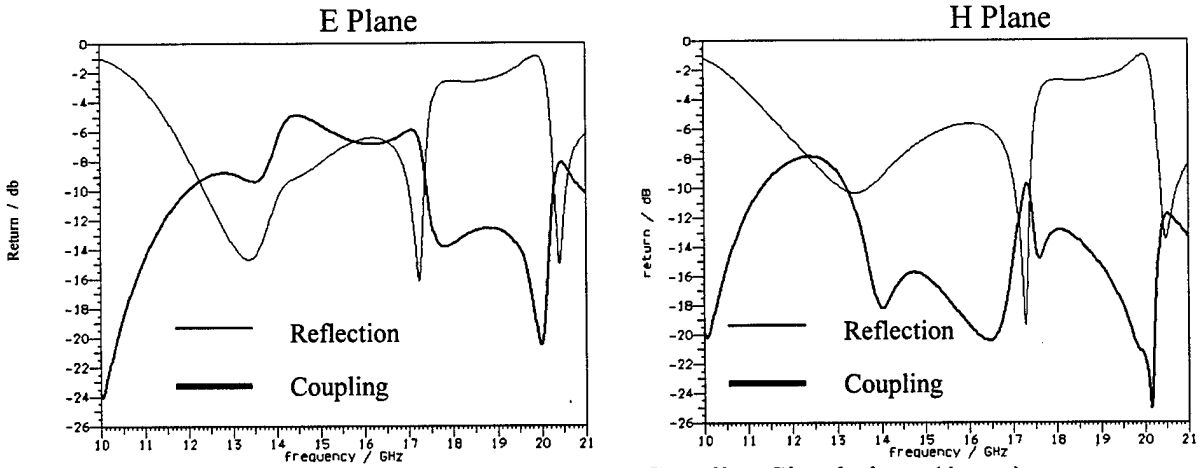

Figure C4: E and H Plane MSDRA-MSDRA Coupling Simulations (4 mm)

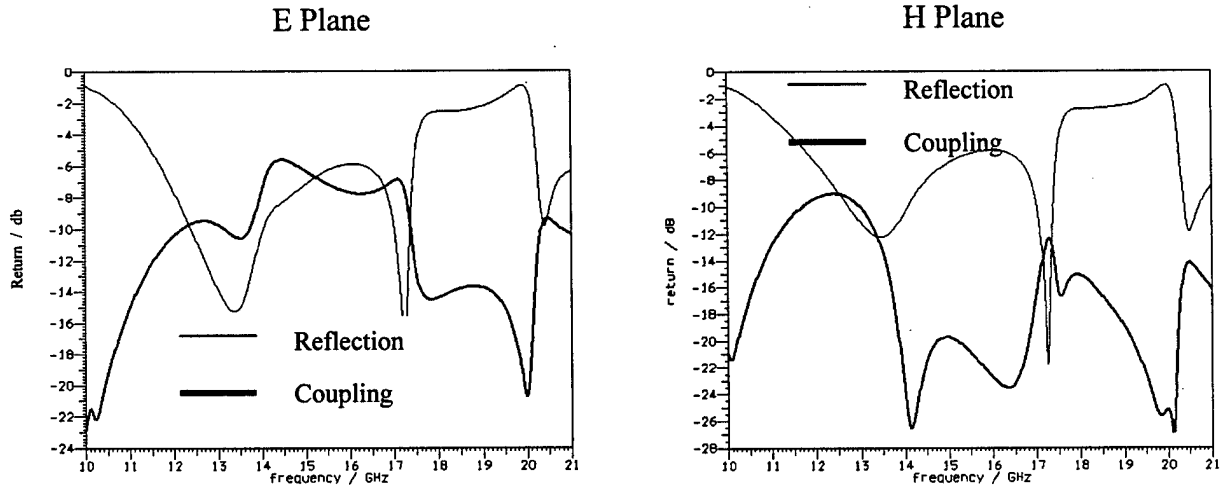

Figure C5: E and H Plane MSDRA-MSDRA Coupling Simulations (5 mm)

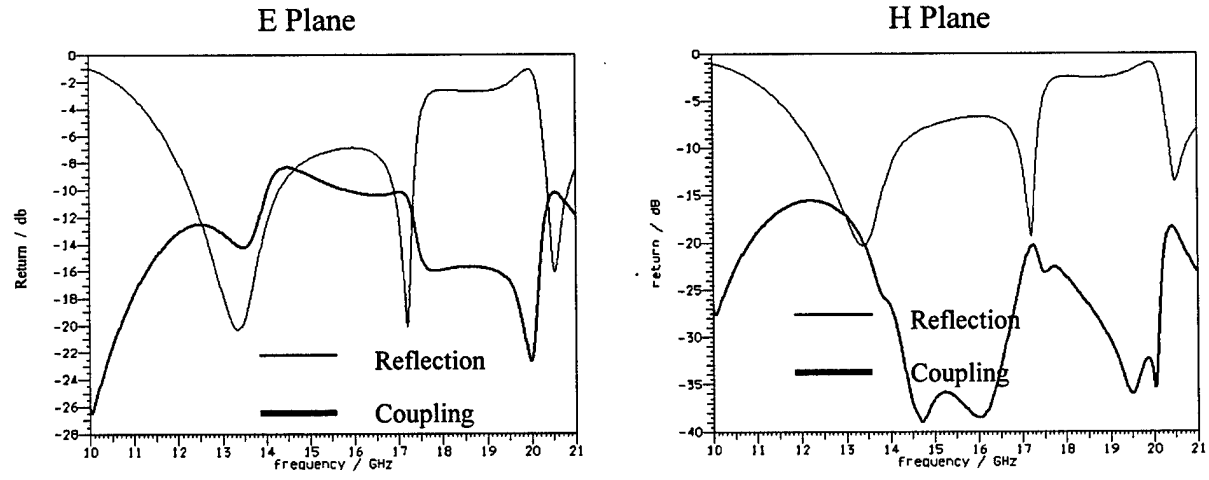

Figure C6: E and H Plane MSDRA-MSDRA Coupling Simulations (10 mm)

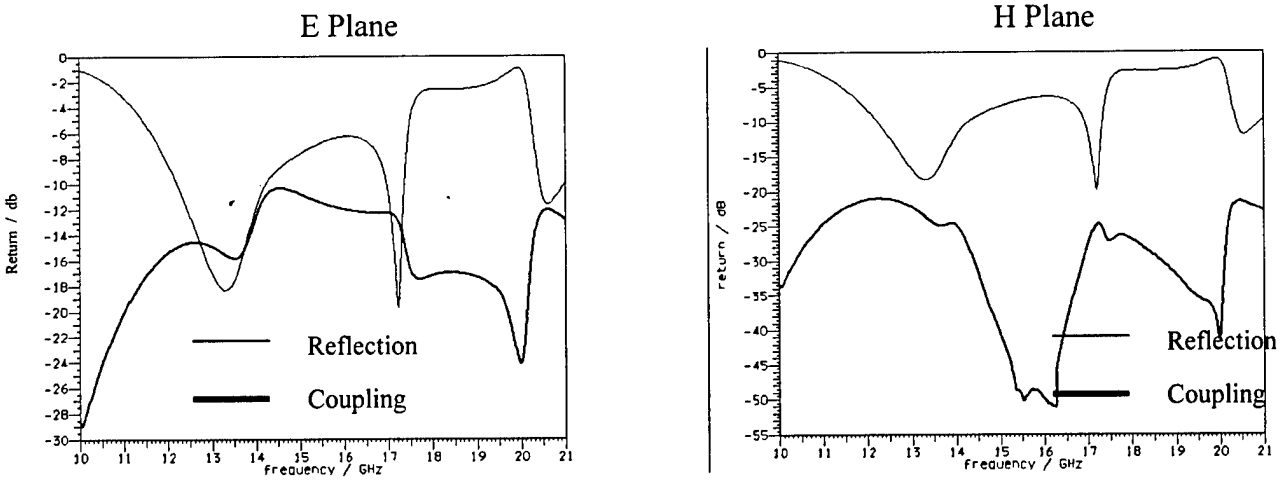

Figure C7: E and H Plane MSDRA-MSDRA Coupling Simulations (15 mm)

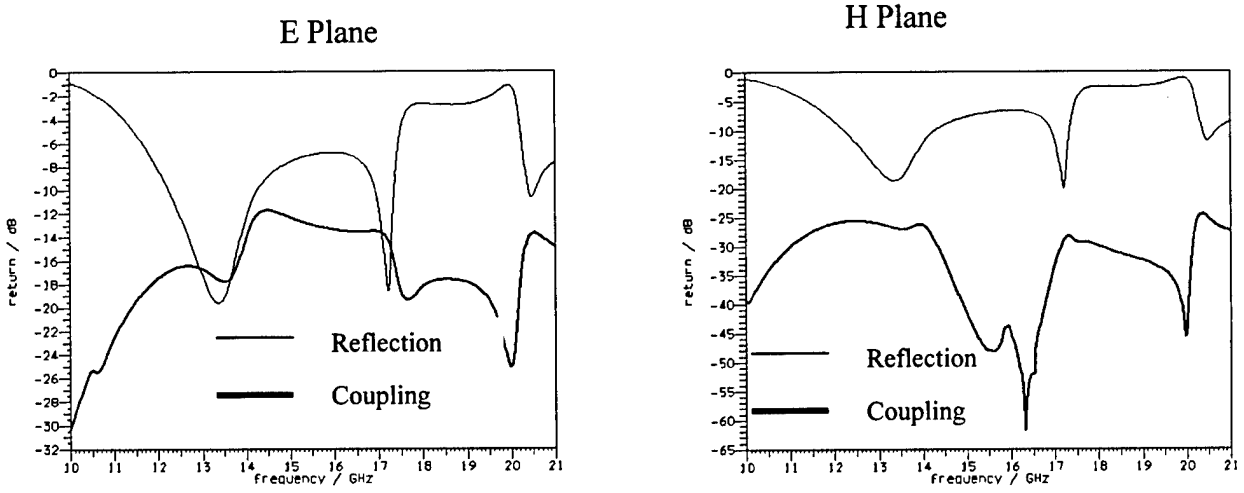

Figure C8: E and H Plane MSDRA-MSDRA Coupling Simulations (20 mm)

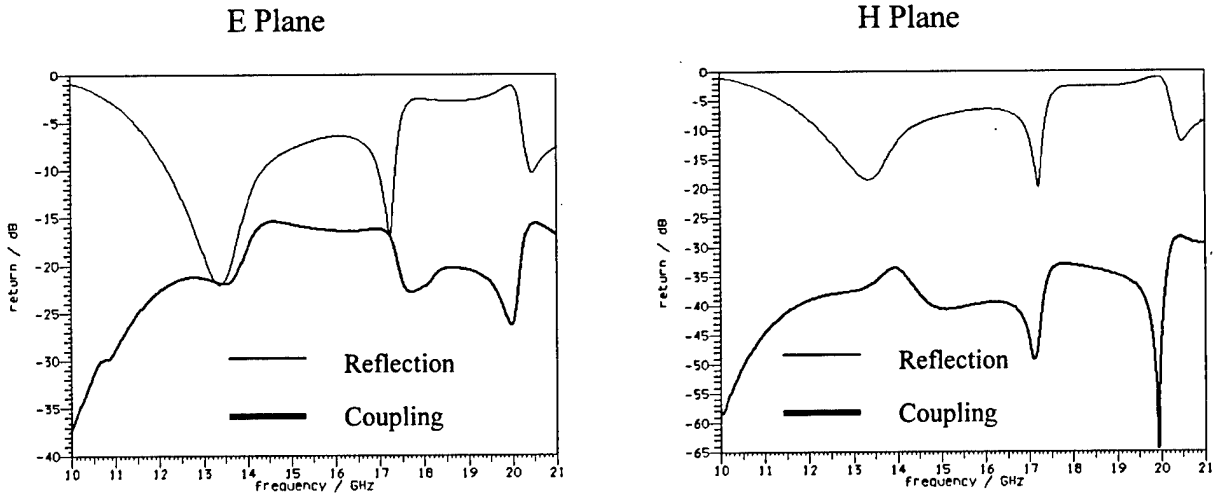

Figure C9: E and H Plane MSDRA-MSDRA Coupling Simulations (35 mm)

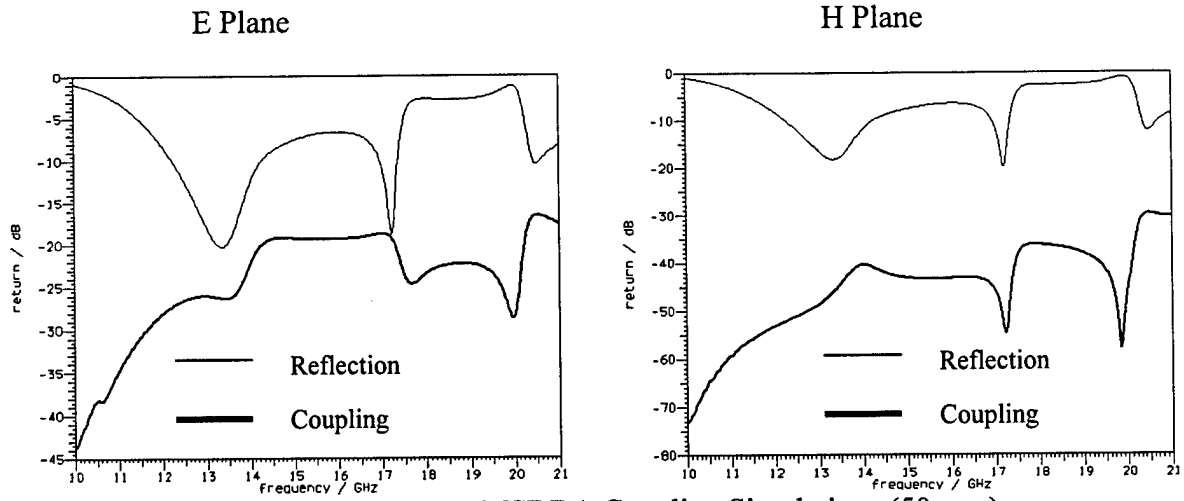

Figure C10: E and H Plane MSDRA-MSDRA Coupling Simulations (50 mm)

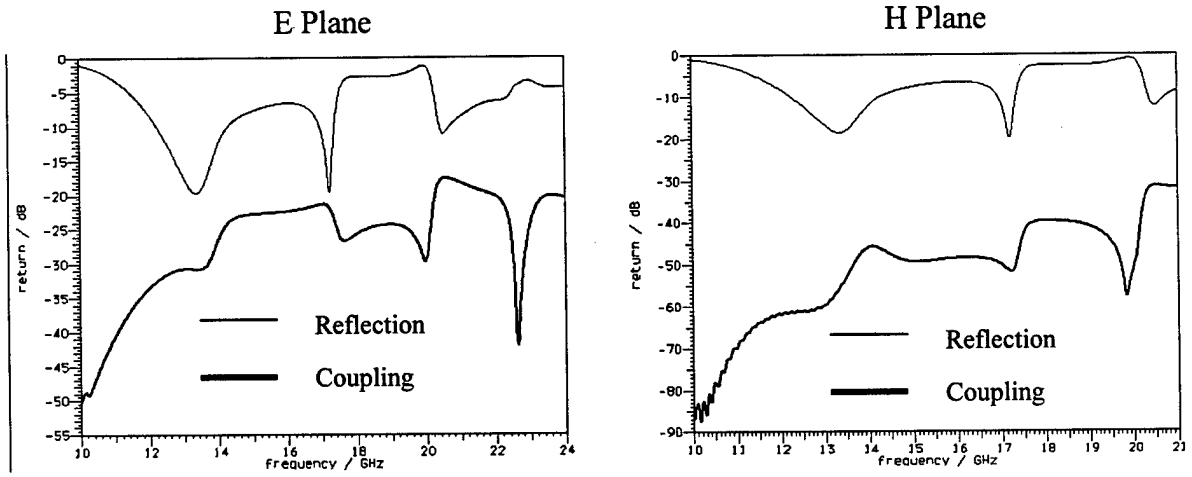

Figure C11: E and H Plane MSDRA-MSDRA Coupling Simulations (65 mm)

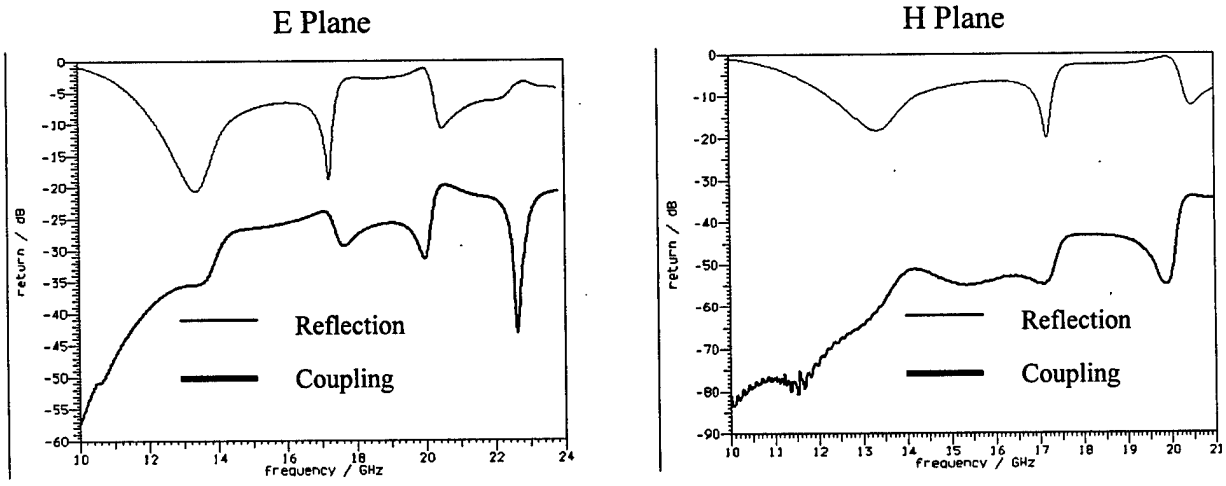

Figure C12: E and H Plane MSDRA-MSDRA Coupling Simulations (80 mm)

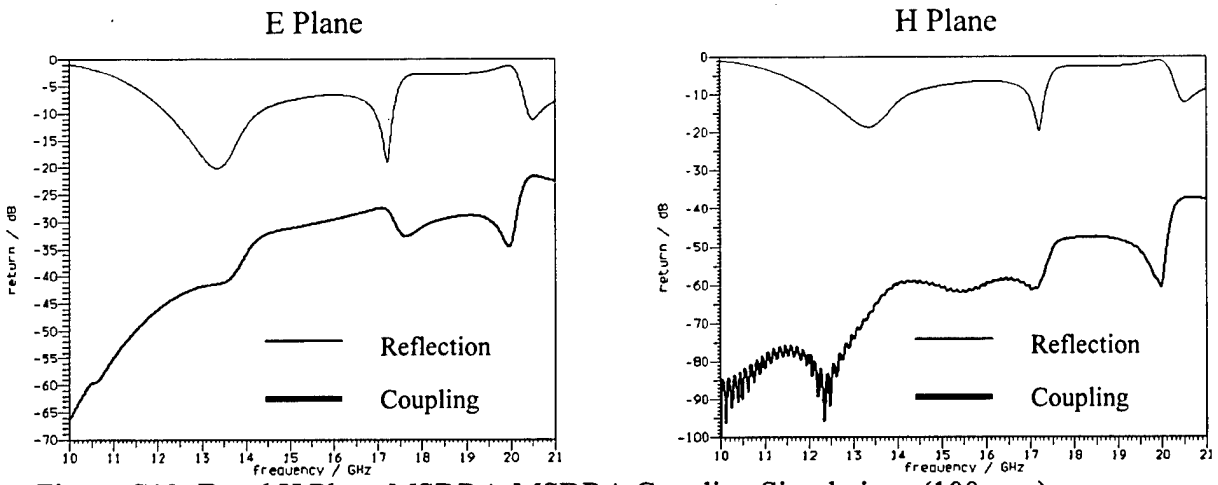

Figure C13: E and H Plane MSDRA-MSDRA Coupling Simulations (100 mm)

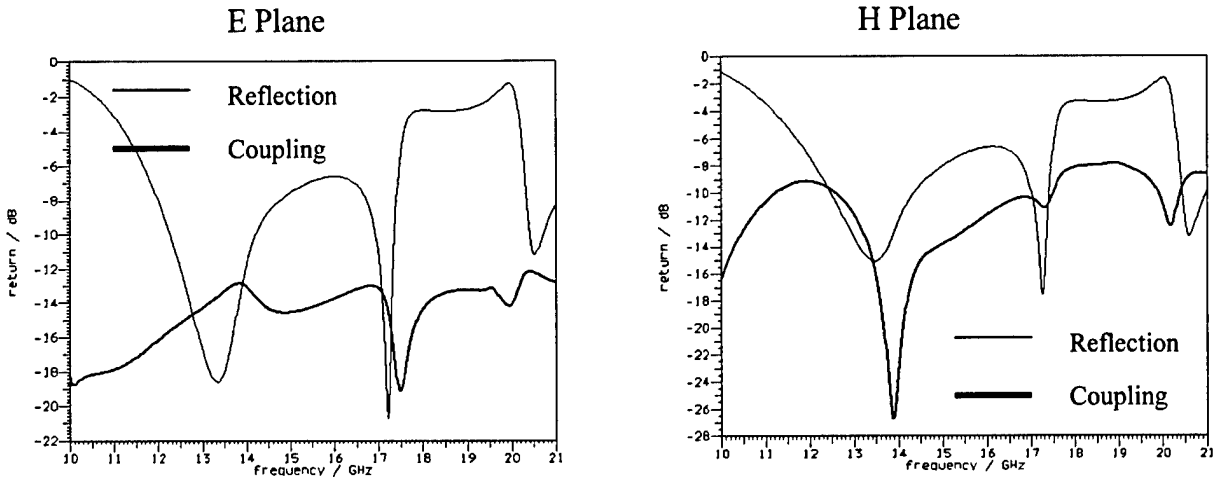

Figure C14: E and H Plane MSDRA-Line Mutual Coupling Simulations (1 mm)

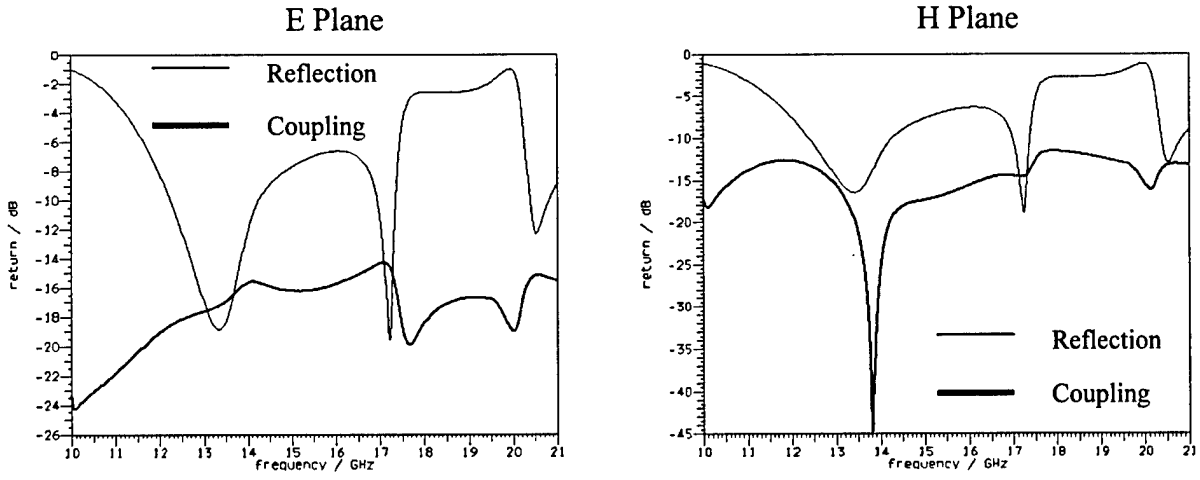

Figure C15: E and H Plane MSDRA-Line Mutual Coupling Simulations (2 mm)

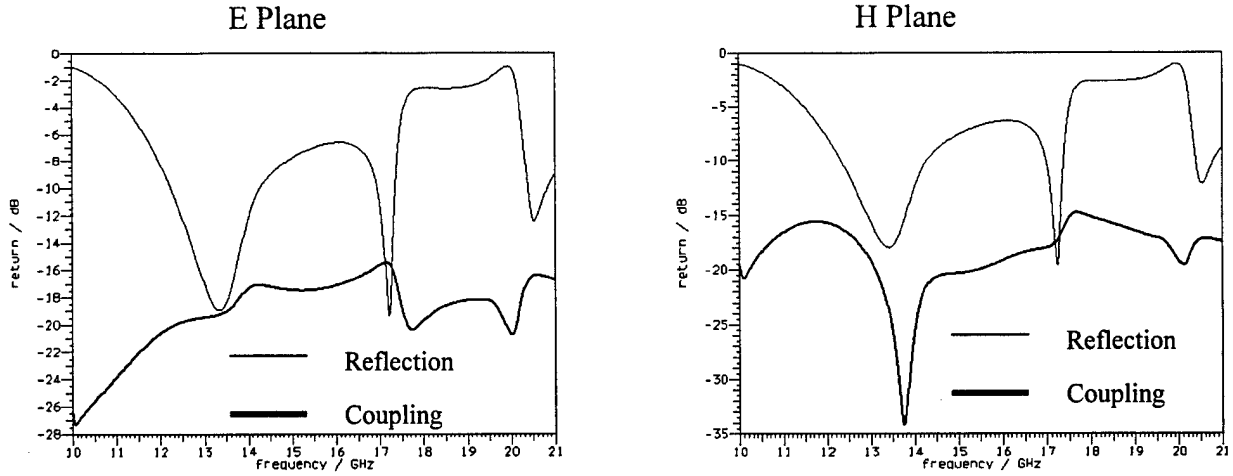

Figure C16: E and H Plane MSDRA-Line Mutual Coupling Simulations (3 mm)

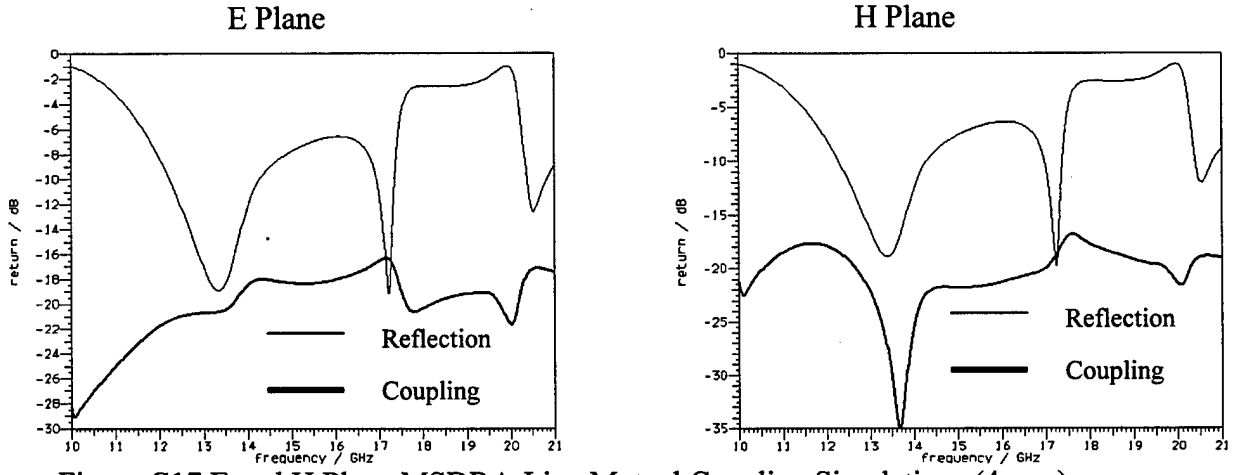

Figure C17 E and H Plane MSDRA-Line Mutual Coupling Simulations (4 mm)

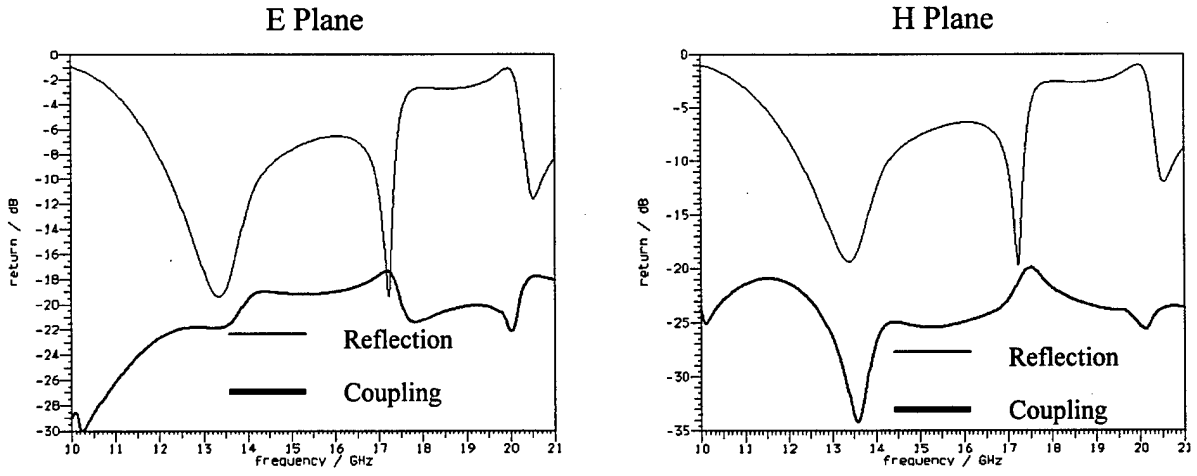

Figure C18: E and H Plane MSDRA-Line Mutual Coupling Simulations (5 mm)

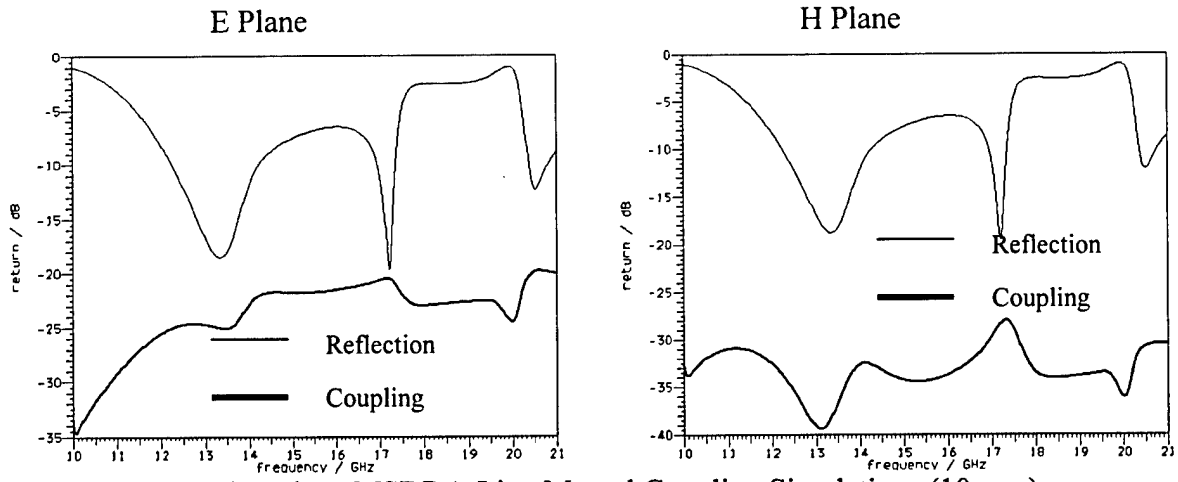

Figure C19: E and H Plane MSDRA-Line Mutual Coupling Simulations (10 mm)

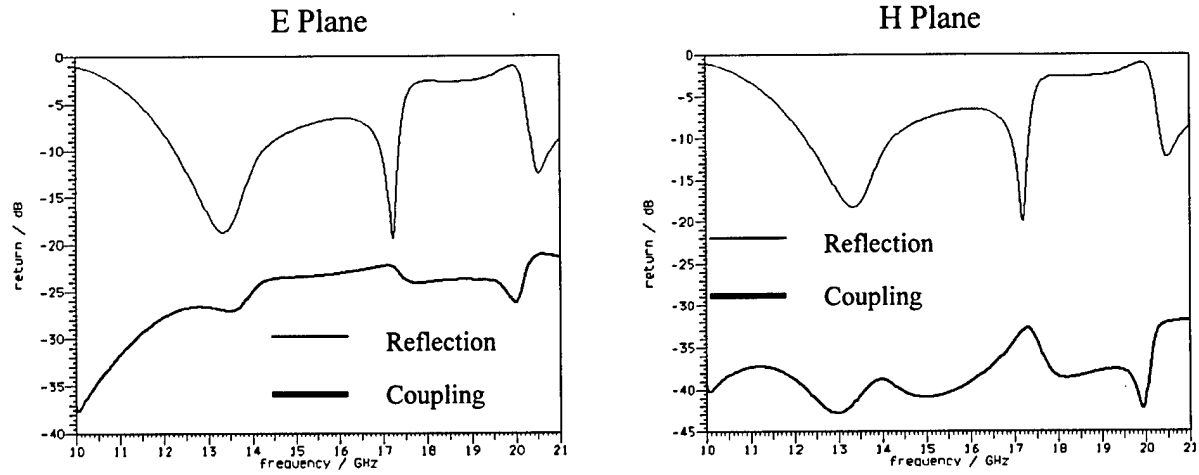

Figure C20: E and H Plane MSDRA-Line Mutual Coupling Simulations (15 mm)

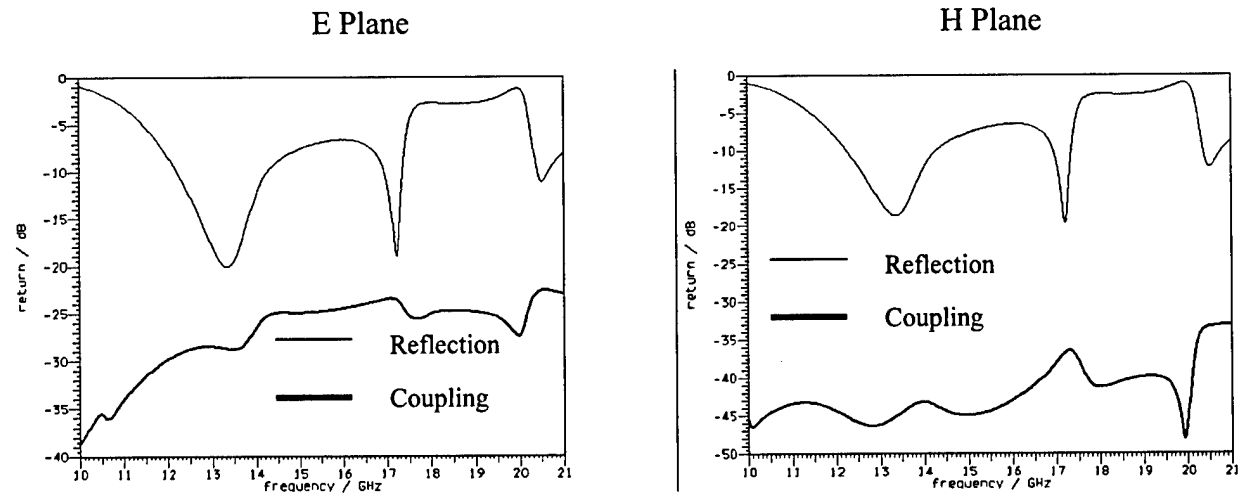

Figure C21: E and H Plane MSDRA-Line Mutual Coupling Simulations (20 mm)

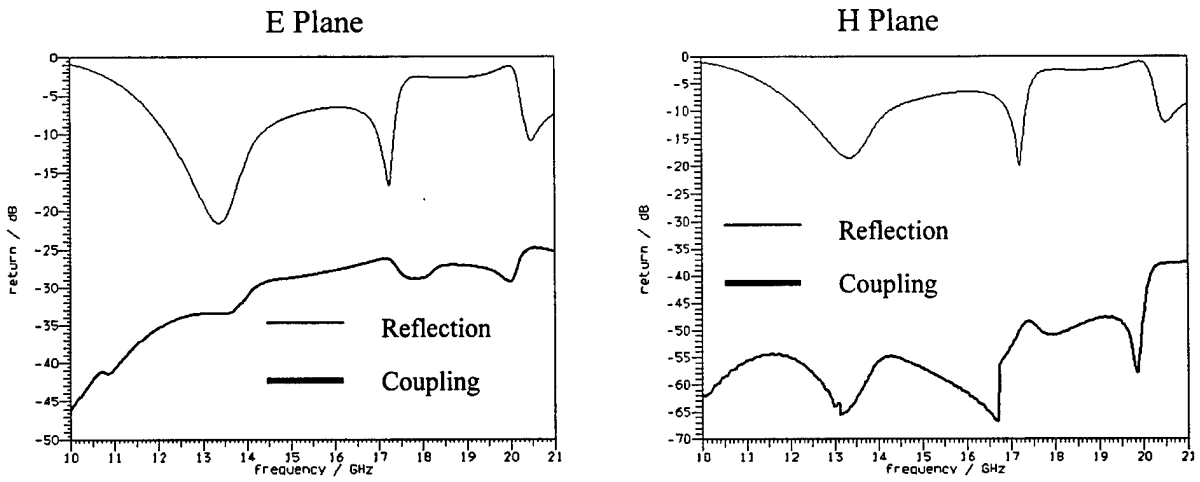

Figure C22: E and H Plane MSDRA-Line Mutual Coupling Simulations (35 mm)

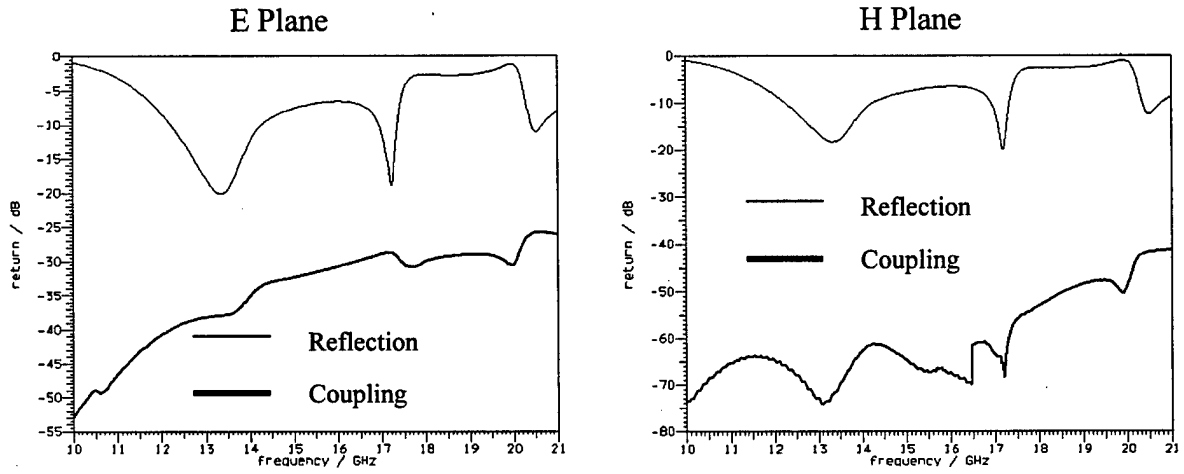

Figure C23: E and H Plane MSDRA-Line Mutual Coupling Simulations (50 mm)

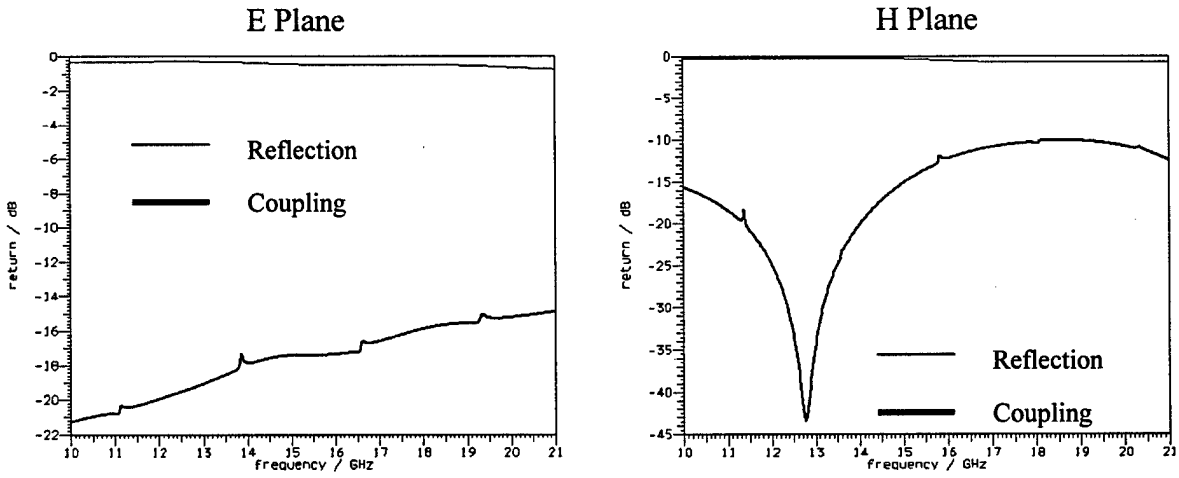

Figure C24: E and H Plane Line-Line Mutual Coupling Simulations (1 mm)

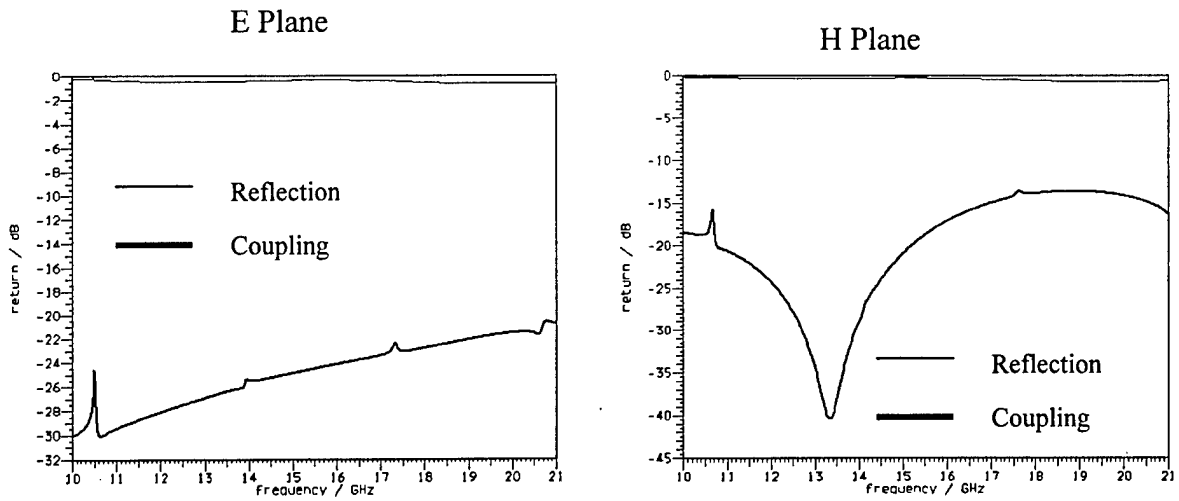

Figure C25: E and H Plane Line-Line Mutual Coupling Simulations (2 mm)

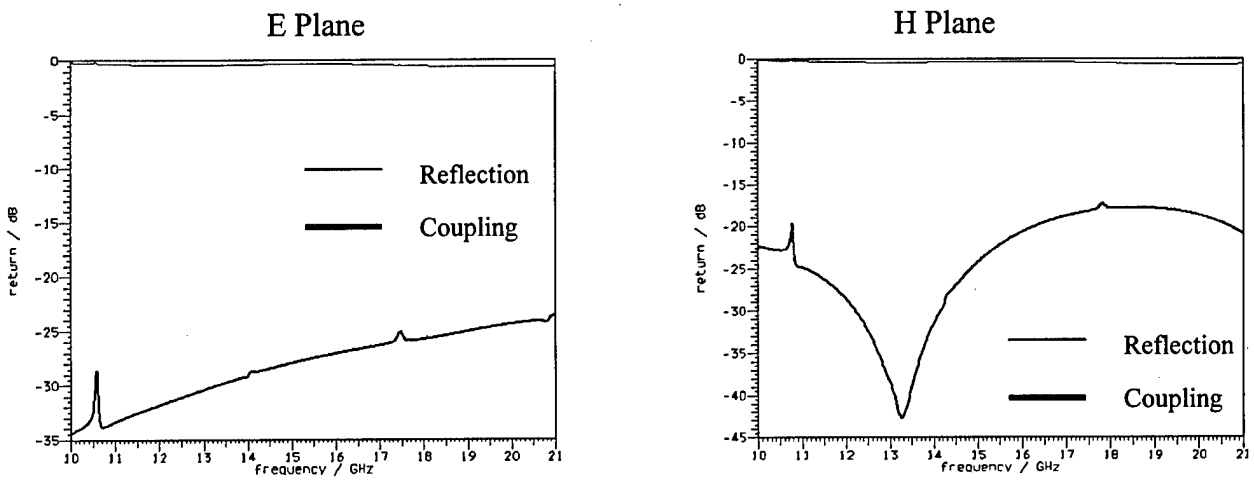

Figure C26: E and H Plane Line-Line Mutual Coupling Simulations (3 mm)

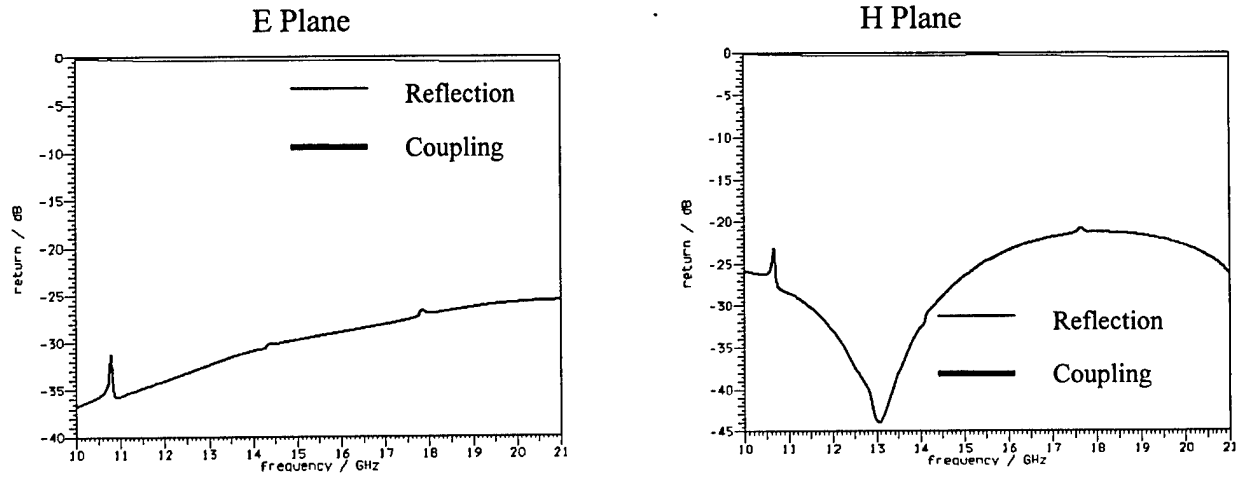

Figure C27: E and H Plane Line-Line Mutual Coupling Simulations (4 mm)

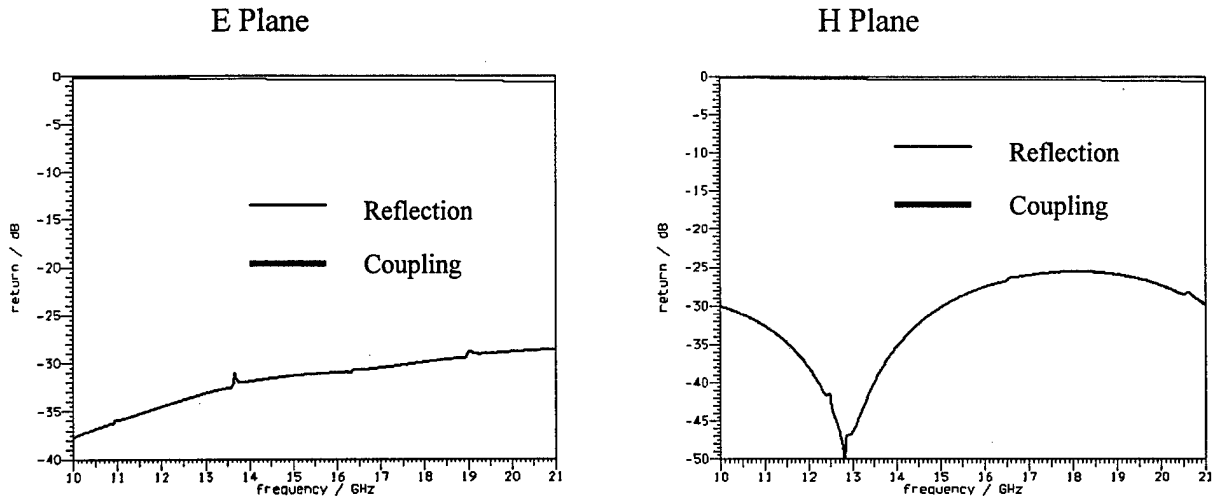

Figure C28: E and H Plane Line-Line Mutual Coupling Simulations (5 mm)

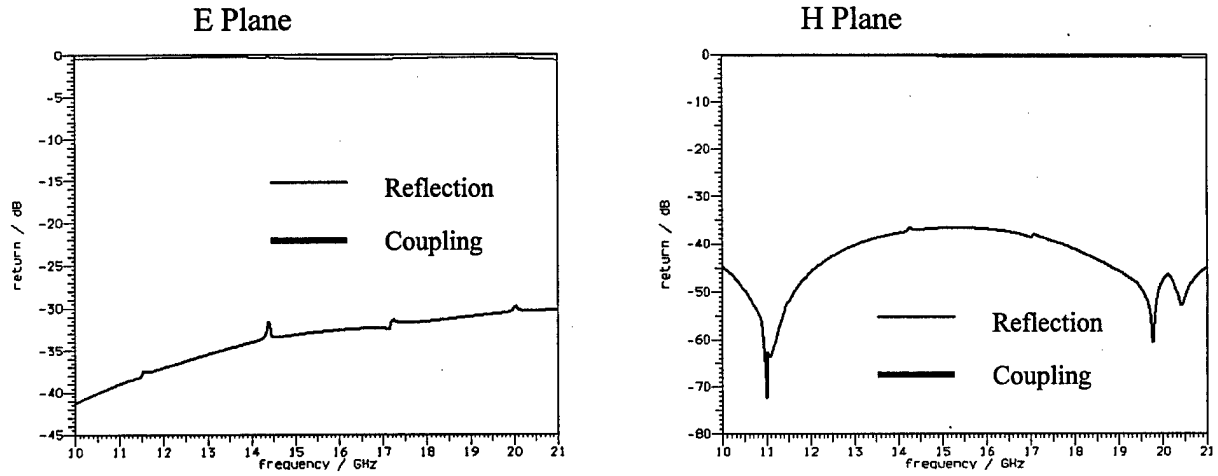

Figure C29: E and H Plane Line-Line Mutual Coupling Simulations (10 mm)

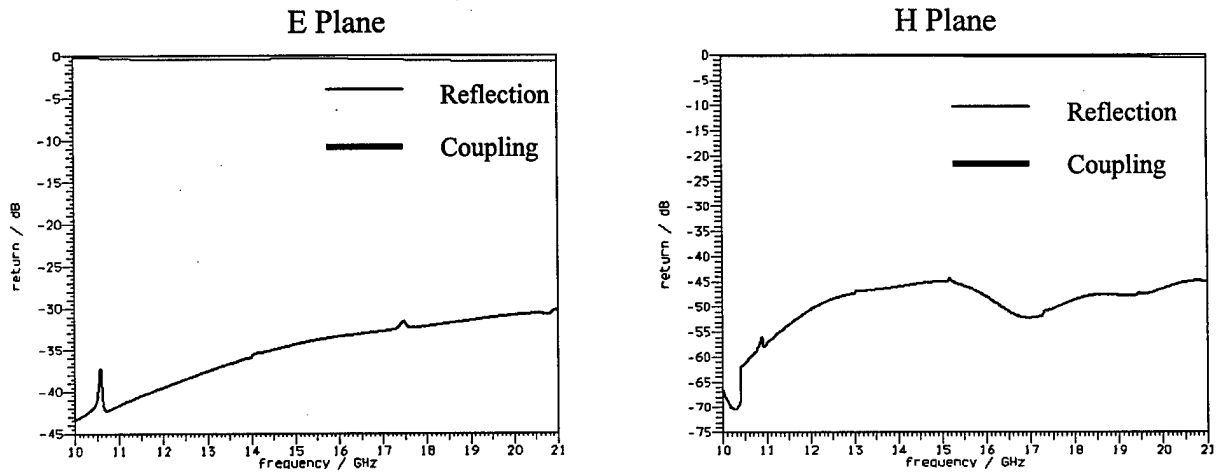

Figure C30: E and H Plane Line-Line Mutual Coupling Simulations (15 mm)

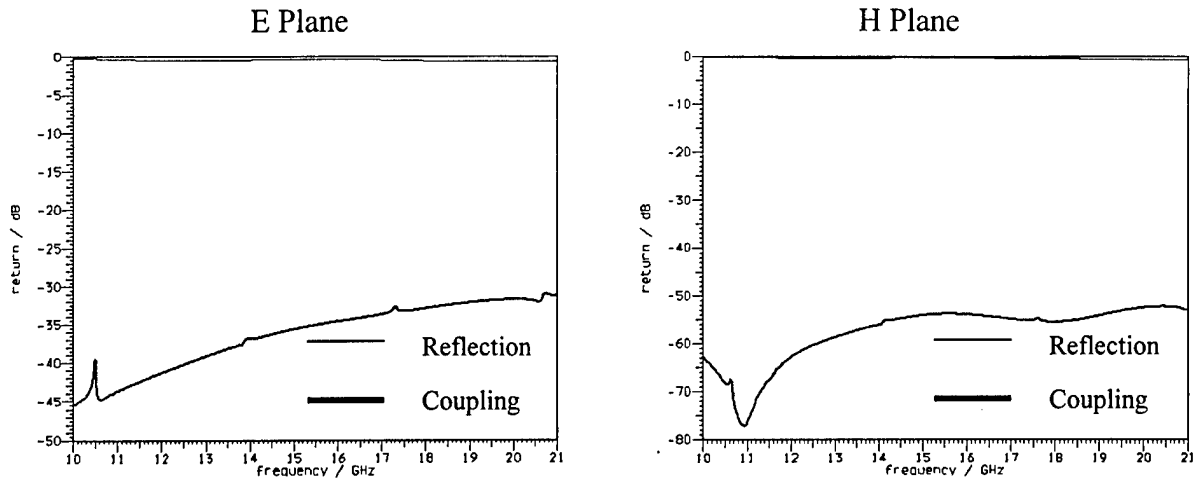

Figure C31: E and H Plane Line-Line Mutual Coupling Simulations (20 mm)

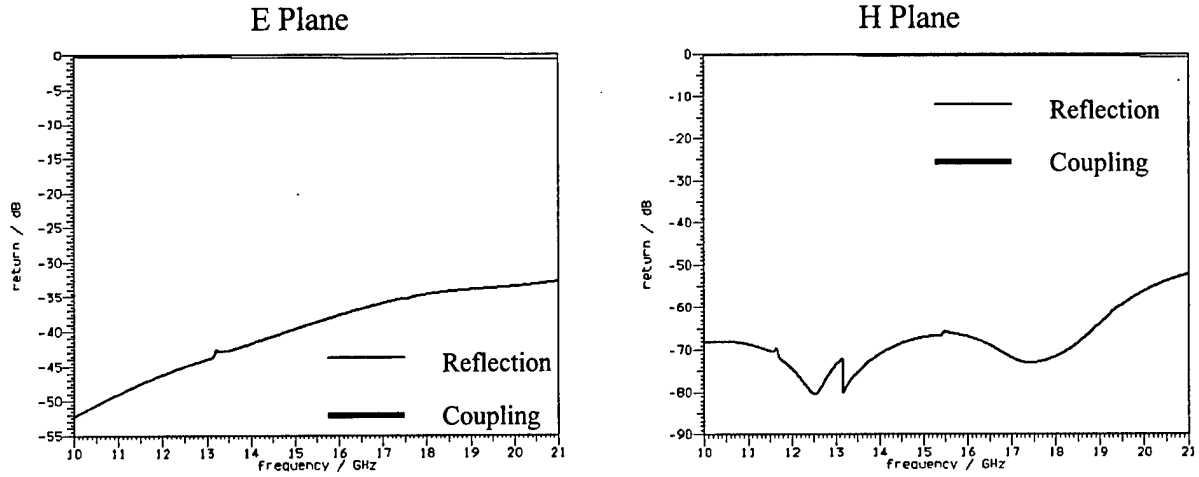

Figure C32: E and H Plane Line-Line Mutual Coupling Simulations (35 mm)

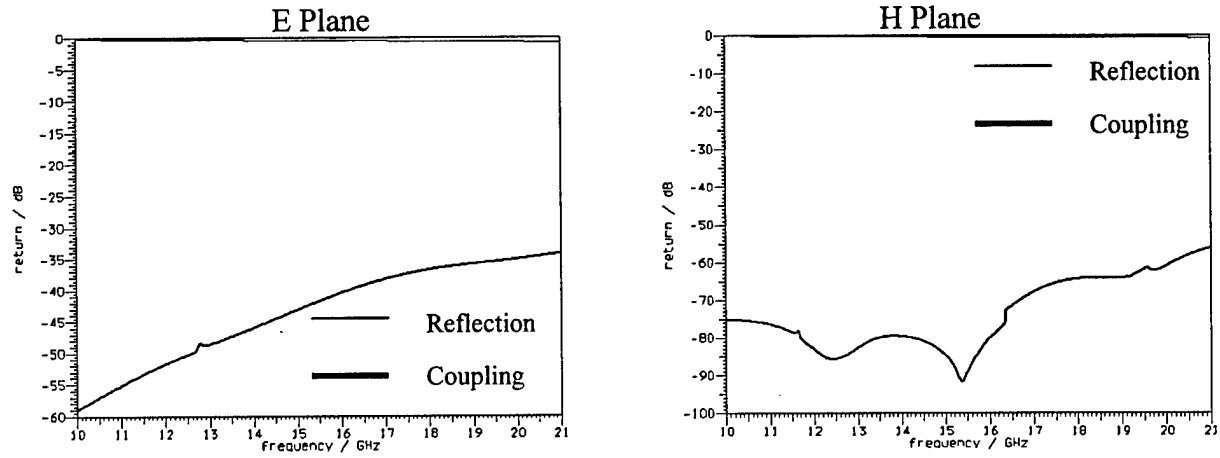

Figure C33: E and H Plane Line-Line Mutual Coupling Simulations (50 mm)

ANNEX D

Comments on Simulation Software

Like any new tool, the user must become familiar with its intricacies and nuances to fully appreciate its capabilities and limitations. Hindsight, being 20/20, allows the following comments to more correctly reflect the method with which the Micro-Stripes™ simulation software could have been used to avoid some of the many problems encountered.

First and foremost, the user should attempt simulations for which the outcome is explicitly known. In this way, seemingly small insignificant bumps or shifts in the obtained scattering parameters or field structures can be explained and corrected for. This step was not conducted until well into the research, which led to a great deal of frustration and extra work along the way. Once brought back on track the simulation process proceeded in a much more predictable fashion. The important problem areas are explained as follows:

a. A great deal of time was spent in determining the appropriate surface impedance value used for the match terminations of the simulations at the structure's boundary. It was also found that this characteristic was probably the most crucial factor in providing the expected results. It was not until simple simulations of the microstrip line itself were conducted to realize that the incorrect value had been chosen. Once correctly used, many previously unexplainable bumps and dips were eliminated.

b. Another problem area was in the location of this end termination along with the source excitation point. It was found that displacing the source into the structure to leave at least one empty cell between the source and the termination provided a smoother response curve in the scattering

parameters. Initial simulations positioned these two features at the same point in order to keep the simulated structure's size at a reasonable level. One additional row of cells however makes an insignificant difference in the run time, but a great deal of difference in the final outcome.

c. On the issue of cell size and number of cells, the TLM analysis method is based on the discretization of the modelling space. Small cell size allows for higher frequency response, but also increase the simulation run time. Cell size is also dependent on the material's permittivity itself. The higher the permittivity, the smaller the cell size requirement, since the spatial resolution should be smaller than $\lambda/10$ for accurate results. Micro-Stripes allows for a graded mesh, such that different mesh sizes are possible in the different materials, provided the minimum spatial resolution criterion is met. This greatly reduces the number of cells and thus the computer run time and memory requirements. It was found that a discretization of $\lambda/10$ was appropriate for scattering parameter measurements, however, for field pattern determination, a finer mesh provided a much smoother representation of the fields within the structures. The increased CPU time for finer meshing was not overly significant.

d. The requirement to generate the near and far field parameters was the significant cause for large simulation run times. As well, unless the resonant frequency of the structure is known before hand, two simulations must be conducted to create the field structure. The first simulation is used to determine the return loss, and thus the resonant frequency, while the fields can be determined from the second simulation, once the resonant frequency has been input.

ANNEX E

Parasitic Coupling Comparisons of Experimental and Simulation Data

This Annex contains the simulation and experimentation comparisons for the three parasitic configuration (E Plane Directional, H Plane Directional and H Plane Symmetrical). The comparisons are made of the return loss (S_{11}) characteristic.

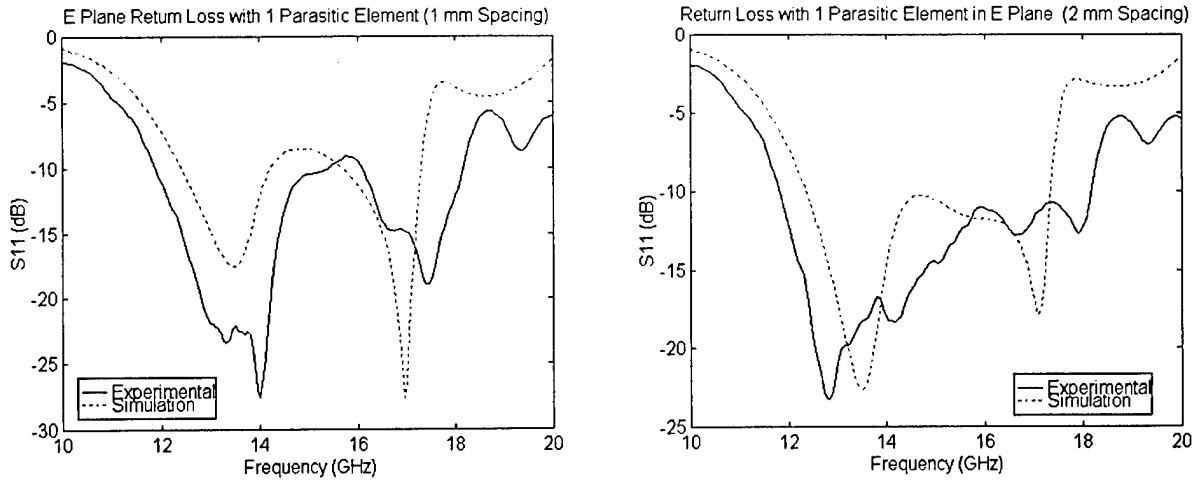

Figure E1: Return Loss for Directional E Plane Parasitic Coupling (1 element)

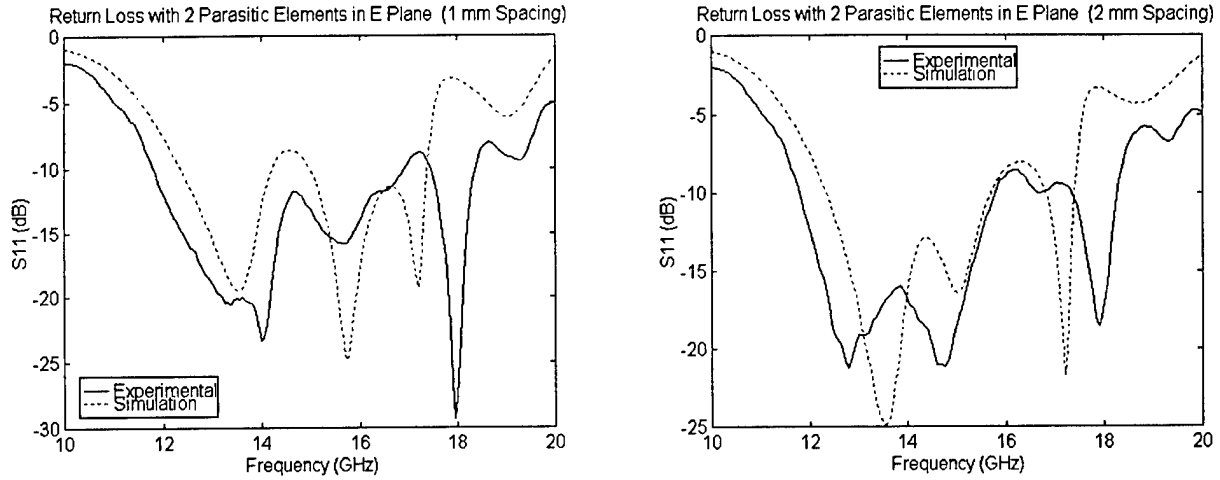

Figure E2: Return Loss for Directional E Plane Parasitic Coupling (2 elements)

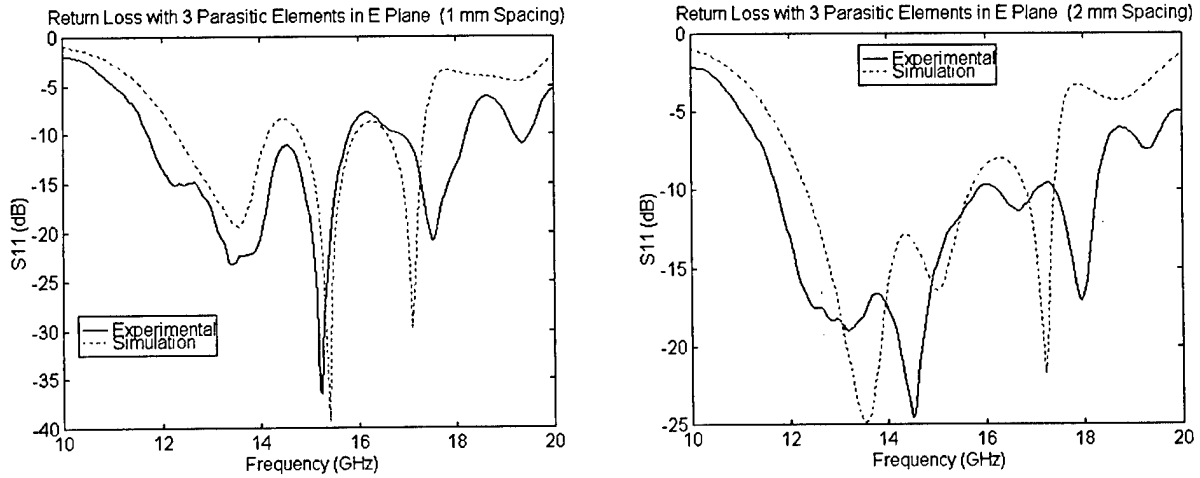

Figure E3: Return Loss for Directional E Plane Parasitic Coupling (3 elements)

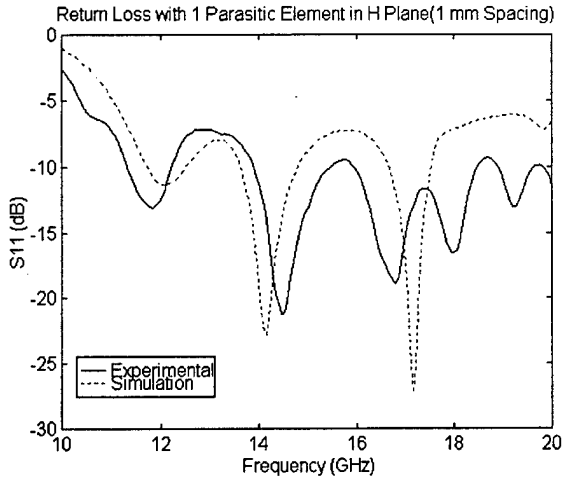

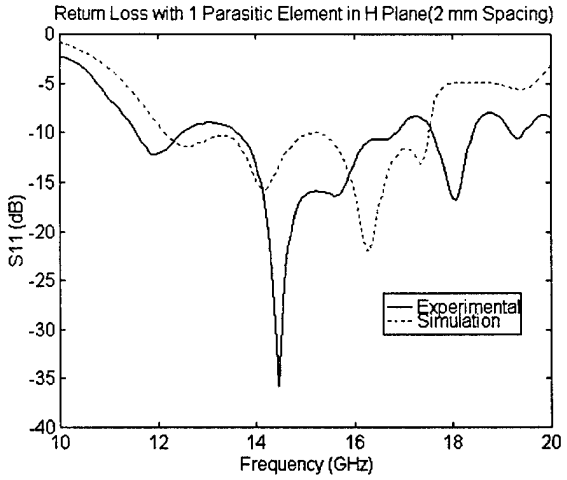

Figure E4: Return Loss for Directional H Plane Parasitic Coupling (1 element)

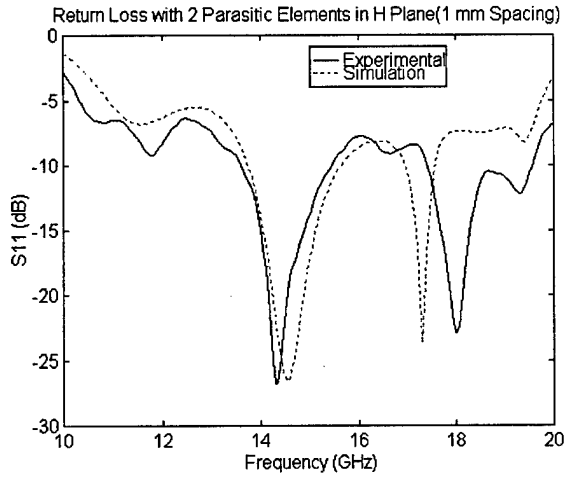

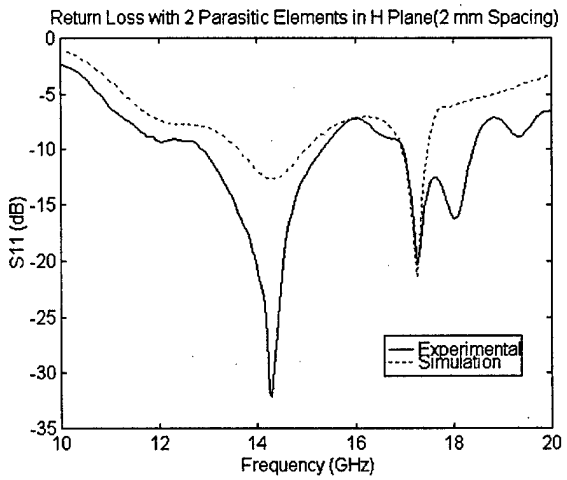

Figure E5: Return Loss for Directional H Plane Parasitic Coupling (2 elements)

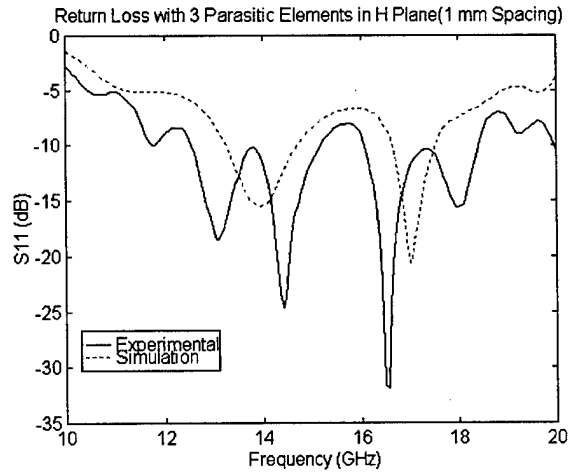

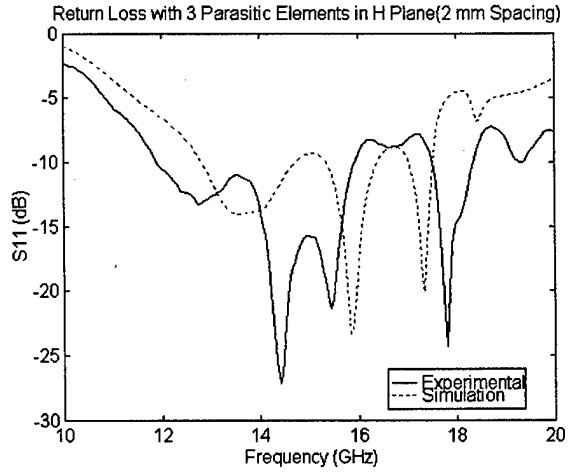

Figure E6: Return Loss for Directional H Plane Parasitic Coupling (3 elements)

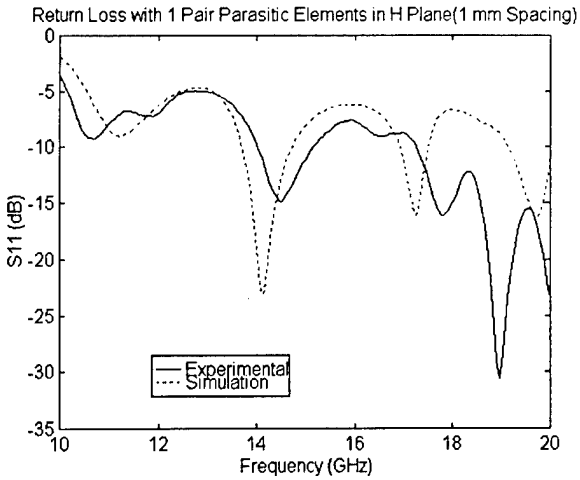

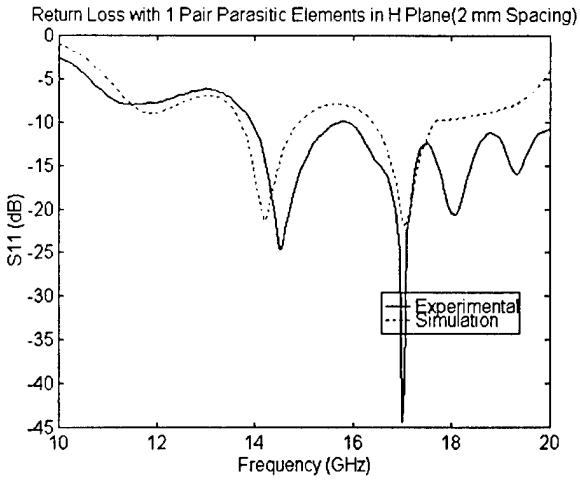

Figure E7: Return Loss for H Plane Symmetrical Coupling (1 pair of elements)

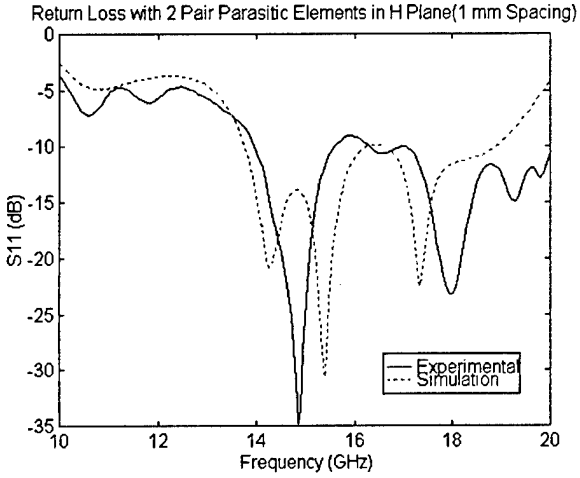

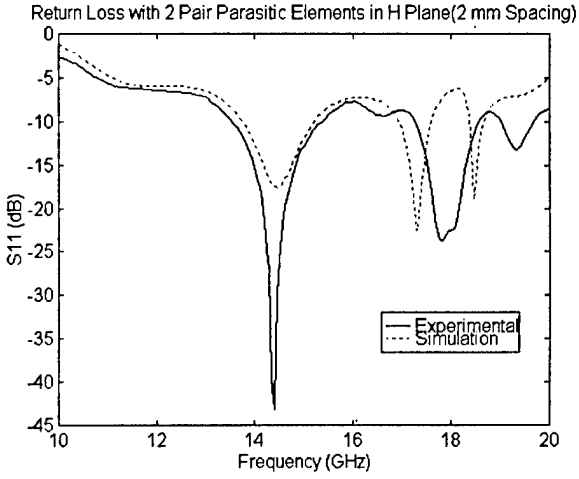

Figure E8: Return Loss for H Plane Symmetrical Coupling (2 pairs of elements)

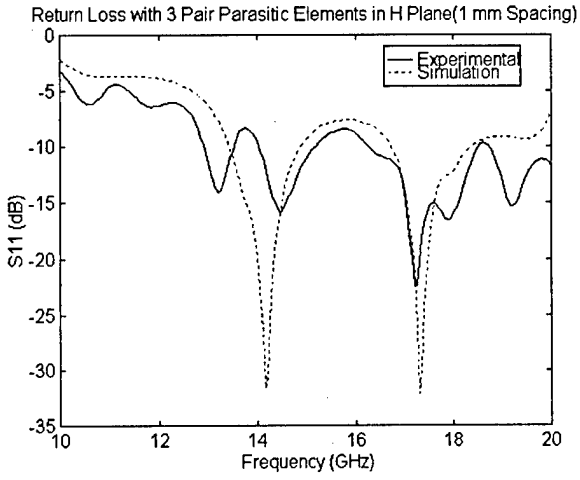

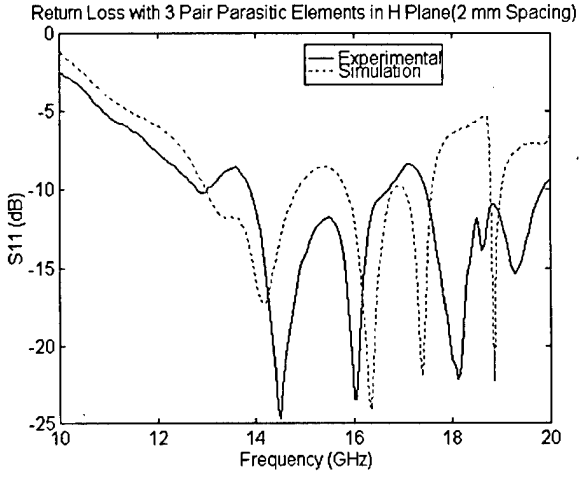

Figure E9: Return Loss for H Plane Symmetrical Coupling (3 pairs of elements)

UNCLASSIFIED

SECURITY CLASSIFICATION OF FORM
(highest classification of Title, Abstract, Keywords)

DOCUMENT CONTROL DATA

(Security classification of title, body of abstract and indexing annotation must be entered when the overall document is classified)

1. ORIGINATOR (the name and address of the organization preparing the document. Organizations for whom the document was prepared, e.g. Establishment sponsoring a contractor's report, or tasking agency, are entered in section 8.)

Defence Research Establishment Ottawa
Ottawa, Ontario
K1A 0Z4

2. SECURITY CLASSIFICATION (overall security classification of the document including special warning terms if applicable)

UNCLASSIFIED

3. TITLE (the complete document title as indicated on the title page. Its classification should be indicated by the appropriate abbreviation (S,C or U) in parentheses after the title.)

Mutual Coupling Between Rectangular Dielectric Resonator Antenna Elements (U)

4. AUTHORS (Last name, first name, middle initial)

B. Henry (RMC), A. Petosa (CRC), Y.M.M. Antar (RMC), G.A. Morin (DREO)

5. DATE OF PUBLICATION (month and year of publication of document)

May 1998

6a. NO. OF PAGES (total containing information. Include Annexes, Appendices, etc.)

xvii + 126

6b. NO. OF REFS (total cited in document)

53

7. DESCRIPTIVE NOTES (the category of the document, e.g. technical report, technical note or memorandum. If appropriate, enter the type of report, e.g. interim, progress, summary, annual or final. Give the inclusive dates when a specific reporting period is covered.

DREO Report

8. SPONSORING ACTIVITY (the name of the department project office or laboratory sponsoring the research and development. Include the address.

Defence Research Establishment Ottawa
Ottawa, Ontario, K1A 0Z4

9a. PROJECT OR GRANT NO. (if appropriate, the applicable research and development project or grant number under which the document was written. Please specify whether project or grant)

5ca12

9b. CONTRACT NO. (if appropriate, the applicable number under which the document was written)

10a. ORIGINATOR'S DOCUMENT NUMBER (the official document number by which the document is identified by the originating activity. This number must be unique to this document.)

DREO REPORT 1333

10b. OTHER DOCUMENT NOS. (Any other numbers which may be assigned this document either by the originator or by the sponsor)

11. DOCUMENT AVAILABILITY (any limitations on further dissemination of the document, other than those imposed by security classification)

(X) Unlimited distribution
( ) Distribution limited to defence departments and defence contractors; further distribution only as approved
( ) Distribution limited to defence departments and Canadian defence contractors; further distribution only as approved
( ) Distribution limited to government departments and agencies; further distribution only as approved
( ) Distribution limited to defence departments; further distribution only as approved
( ) Other (please specify):

12. DOCUMENT ANNOUNCEMENT (any limitation to the bibliographic announcement of this document. This will normally correspond to the Document Availability (11). however, where further distribution (beyond the audience specified in 11) is possible, a wider announcement audience may be selected.)

Unlimited Announcement

13. **ABSTRACT** (a brief and factual summary of the document. It may also appear elsewhere in the body of the document itself. It is highly desirable that the abstract of classified documents be unclassified. Each paragraph of the abstract shall begin with an indication of the security classification of the information in the paragraph (unless the document itself is unclassified) represented as (S), (C), or (U). It is not necessary to include here abstracts in both official languages unless the text is bilingual).

Dielectric resonator antennas (DRAs) have been suggested as a potentially efficient antenna for use in Personal Communication Systems, Global Positioning Systems and wireless computer networks. They offer several advantages, such as high efficiency, large bandwidth, low profile, small size, ease of fabrication, and low production cost.

This paper examines characteristics of the rectangular DRA, both as individual radiating elements as well as elements in array environments. Numerical methods are used to obtain detailed information with respect to the resonant frequency, bandwidth, scattering parameters, input impedance, field structures and radiation patterns on which DRA design is based. This obtained information is then used to help in understanding and quantizing the interaction between elements in close proximity, i.e. mutual coupling. This coupling analysis provides important information for the array design process, as well as the necessary information required to positively exploit these coupling characteristics.

The simulation software provides data that very closely matches both experimentation and the theoretical models. Mutual coupling measurements indicate that, beyond a spacing of one half-wavelength, there is very little mutual interaction. This mutual coupling was exploited at lesser distances however with parasitically coupled dielectric elements used to create novel single feed multi-element antennas with altered resonant frequencies, increased bandwidth and enhanced radiation patterns, as compared to a single element.

14. **KEYWORDS, DESCRIPTORS or IDENTIFIERS** (technically meaningful terms or short phrases that characterize a document and could be helpful in cataloguing the document. They should be selected so that no security classification is required. Identifiers, such as equipment model designation, trade name, military project code name, geographic location may also be included. If possible keywords should be selected from a published thesaurus. e.g. Thesaurus of Engineering and Scientific Terms (TEST) and that thesaurus-identified. If it is not possible to select indexing terms which are Unclassified, the classification of each should be indicated as with the title.)

dielectric resonator antenna
phased array antenna
mutual coupling